Universität Stuttgart

Institut für Wasser- und Umweltsystemmodellierung

Mitteilungen

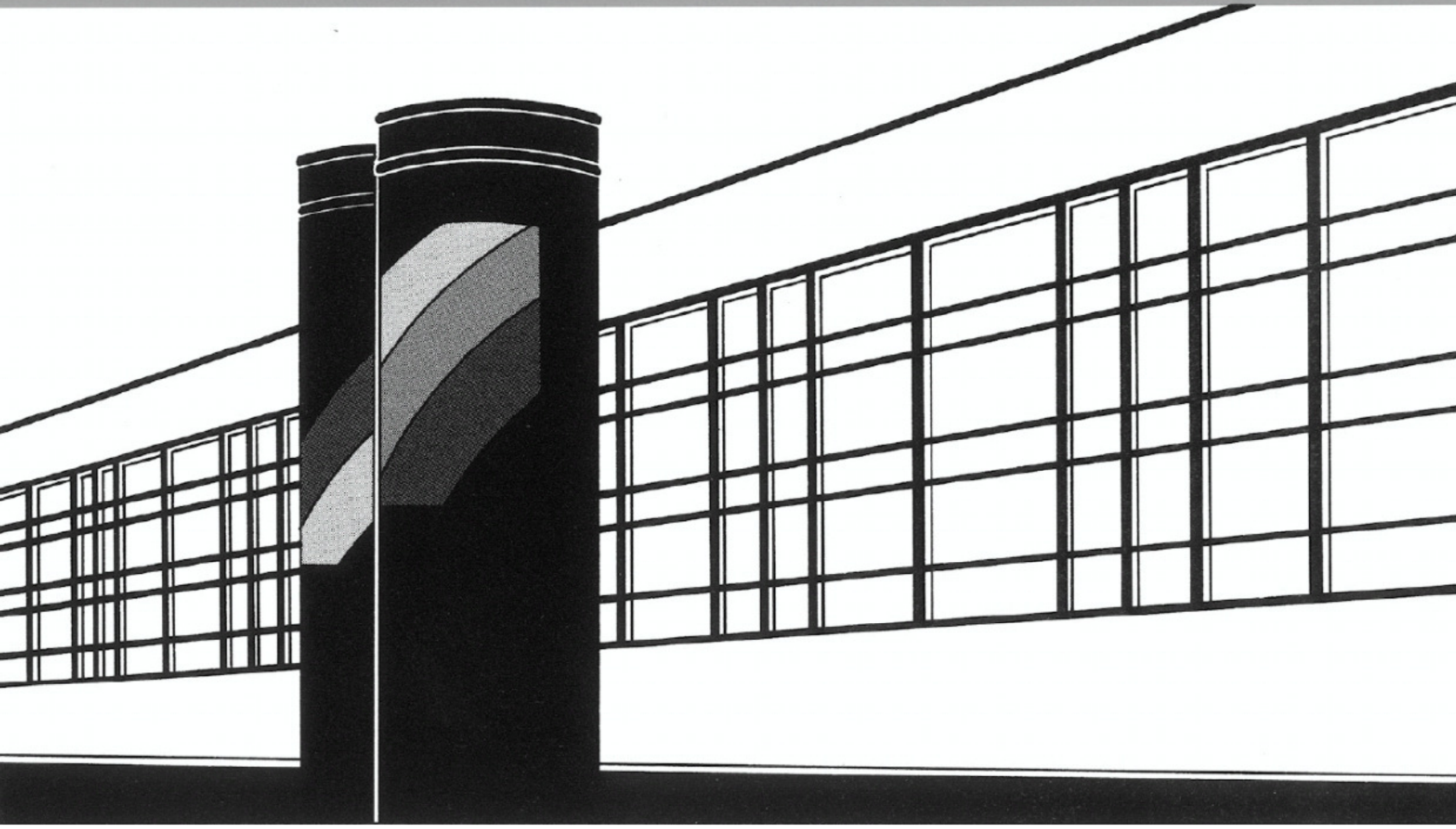

Heft 228

Andreas Lauser

Theory and Numerical Applications of Compositional Multi-Phase Flow in Porous Media

Theory and Numerical Applications of Compositional Multi-Phase Flow in Porous Media

Von der Fakultät Bau- und Umweltingenieurwissenschaften der Universität Stuttgart
zur Erlangung der Würde eines Doktors der
Ingenieurwissenschaften (Dr.-Ing.) genehmigte Abhandlung

Vorgelegt von

Andreas Lauser

aus Kirchheim unter Teck

Hauptberichter:	Prof. Dr.-Ing. Rainer Helmig
Mitberichter:	Prof. Dr. rer. nat. Barbara Wohlmuth, apl. Prof. Dr.-Ing. Holger Class
Tag der mündlichen Prüfung:	28. Juni 2013

Institut für Wasser- und Umweltsystemmodellierung der Universität Stuttgart

2014

Heft 228

Theory and Numerical Applications of Compositional Multi-Phase Flow in Porous Media

von
Dr.-Ing.
Andreas Lauser

Eigenverlag des Instituts für Wasser- und Umweltsystemmodellierung
der Universität Stuttgart

D93 Theory and Numerical Applications of Compositional Multi-Phase Flow in Porous Media

Bibliografische Information der Deutschen Nationalbibliothek
Die Deutsche Nationalbibliothek verzeichnet diese Publikation in der Deutschen Nationalbibliografie; detaillierte bibliografische Daten sind im Internet über `http://www.d-nb.de` abrufbar

Lauser, Andreas:
Theory and Numerical Applications of Compositional Multi-Phase Flow in Porous Media /
Institut für Wasser- und Umweltsystemmodellierung, Universität Stuttgart, Stuttgart, 2014

(Mitteilungen / Institut für Wasser- und Umweltsystemmodellierung,
Universität Stuttgart ; Heft 228)
Zugl.: Stuttgart, Univ., Diss., 2014
ISBN 978-3-942036-32-0
NE: Institut für Wasser- und Umweltsystemmodellierung, Stuttgart: Mitteilungen

Herausgegeben 2014 vom Eigenverlag des Instituts für Wasser- und Umweltsystemmodellierung der Universität Stuttgart
Druck: DCC Kästl GmbH & Co. KG, Ostfildern

Thanks

That's a giant leap for a man, one small step for mankind.
—loosely based on a quote by NEIL ARMSTRONG

The thesis you are about to read would not have been possible without the support of many people who I whish to thank for: First of all, I obviously am in debt with my supervisors Rainer Helmig, Barbara Wohlmuth, and Holger Class who inspired many of the ideas presented in this work—all stupidities which you will undoubtedly encounter are purely my own work. I also want to thank Rainer and Holger for allowing me the luxury to work full-time on this thesis at their department whilst still getting a full salary most of the time. In addition, I profited tremendously from the nicely written overview articles of Wikipedia and the discussions I had, amongst others, with Corinna Hager, Ivar Aavatsmark, Atgeirr Rasmussen, Ove Sævareid, Alexandru Tatomir, and Onur Dogan. Further, this thesis would be much worse if I would not have gotten the feedback from its rigorous but always benevolent proof readers Alexander Lauser, Heinz Isengard, and Rainer Helmig.

Also, I would like to thank Kristin Flornes, Ivar Aavatsmark, Ove Sævareid, Holger Class, and Bartek Vik for making my visit at the Center of Integrated Petroleum Engineering in Bergen possible and as pleasant as it was. I would also like to express my gratitude to Alf Birger Rustad for the warm reception in the cool city of Trondheim and for his philosophical inspirations. When I was not hanging around in Norway, my time in Stuttgart was much more enjoyable in the company of my apartment mates Markus Üffinger, Steffen Frey, my fellow sufferer Oliver Kopp, and the faithful friends of "Uncle K." Alexandru Tatomir, Jeffrey Thutan, Onur Dogan, David Werner, Yufei Cao, and Vishal Jambhekar.

Finally, and most importantly, I am deeply grateful for the warm and unconditional support of my girlfriend Meike and my family during all those interesting times.

You guys rock!

Stuttgart, March 2013

Contents

List of Figures IV

List of Tables VI

Notation VII

Abstract IX

Deutschsprachige Kurzfassung XI

1 Introduction 1

2 Continuum-Scale Fluid Flows 5

2.1 Representative Elementary Volumes . . . 5
2.2 Continuum-Scale Conservation Equations . . . 8
2.3 Conserved Quantities . . . 11
  2.3.1 Conservation of Mass . . . 11
  2.3.2 Conservation of Momentum . . . 11
  2.3.3 NEWTONIAN Fluids . . . 13
  2.3.4 Creeping Flows . . . 14
  2.3.5 Conservation of Energy . . . 15
2.4 Porous Media . . . 17
  2.4.1 Volume Averaging . . . 17
  2.4.2 Applicability . . . 23
  2.4.3 Multi-Phase Flows . . . 24
  2.4.4 Multi-Phase, Multi-Component Flows . . . 25
  2.4.5 Experimental Derivation of the Momentum Conservation Equation . . . 25
  2.4.6 Filter Velocity and Seepage Velocity . . . 27
2.5 Chapter Synopsis . . . 28

3 Supplementary and Closure Relations 29

3.1 Saturation Closure Condition . . . 29
3.2 Given Parameters and Empiric Relations . . . 30
3.3 Thermodynamic Relations . . . 30
  3.3.1 Equations of State . . . 30
  3.3.2 Local Thermodynamic Equilibrium . . . 33
3.4 Capillary Pressure and Relative Permeability . . . 36
  3.4.1 Generic Two-Phase Relations for Relative Permeability . . . 37

3.4.2 Relation of BROOKS and COREY . . . 38
3.4.3 Curve of VAN GENUCHTEN . . . 38
3.4.4 Three-Phase Systems . . . 39
3.4.5 Advanced Concepts . . . 40
3.5 Model Constraints . . . 40
3.5.1 Immiscibility . . . 41
3.5.2 Primary Variable Switching . . . 42
3.5.3 Non-Linear Complementarity Functions . . . 43
3.5.4 Black-Oil . . . 43
3.6 Chapter Synopsis . . . 47

4 Numerics 49
4.1 Spatial Discretization . . . 49
4.2 Time Discretization . . . 54
4.3 Method of NEWTON and RAPHSON . . . 55
4.3.1 Calculation of the JACOBIAN Matrix . . . 56
4.3.2 Discretized Partial Differential Equations . . . 57
4.4 Linear Solvers . . . 58
4.4.1 Direct Solution . . . 58
4.4.2 Iterative Solvers . . . 59
4.4.2.1 Steepest Descent . . . 59
4.4.2.2 Conjugate Gradients . . . 60
4.4.2.3 Bi-Conjugate Gradients . . . 61
4.4.2.4 GMRES . . . 62
4.4.3 Preconditioners . . . 62
4.5 Parallelization . . . 63
4.5.1 Domain Decomposition Methods . . . 63
4.5.2 Distributed Linearization . . . 64
4.5.3 Parallel Iterative Linear Solvers . . . 65
4.6 Chapter Synopsis . . . 66

5 Implementation Aspects 69
5.1 DUNE . . . 69
5.2 eWoms . . . 70
5.2.1 General Structure . . . 70
5.2.2 Flow Models . . . 71
5.2.3 Implementational Complexity . . . 74

6 Numerical Applications 77
6.1 The Heat-Pipe Problem . . . 77
6.1.1 Uniform Domain Extrusion . . . 78
6.1.2 Semi-Analytical Solution . . . 78
6.1.3 Results . . . 80
6.2 A Radially Symmetric CO_2 Injection Problem . . . 82
6.2.1 Radial Domain Extrusion . . . 83

6.2.2 Results 85
6.3 The Ninth SPE Benchmark Problem 87
6.4 The Fifth SPE Benchmark Problem 92
6.5 The Ketzin CO_2 Storage Project 94

7 Summary and Conclusion 99

A Reproducibility and Raw Data 105

Bibliography 107

List of Figures

1.1 Applications of Multi-Phase Flow in Porous Media 2

2.1 Concept of Representative Elementary Volumes 6
2.2 Upscaling from Molecular- to Continuum-Scale 7
2.3 EULERIAN and LAGRANGIAN Points of View 9
2.4 COUETTE Flow 13
2.5 Internal Energy and Enthalpy 16
2.6 Porous Medium 17
2.7 DARCY's Experiment 26
2.8 Tortuosity 27

3.1 Shapes of Cubic Equations of State 32
3.2 BROOKS-COREY and VAN GENUCHTEN Functions 37
3.3 Definition of the Black-Oil Parameters 44

4.1 Conforming Grid 49
4.2 Finite Volume Discretization 51
4.3 Concept of Upstreaming 52
4.4 Two-Point Gradient Approximation 53
4.5 Vertex-Centered Finite Volume Discretization 53
4.6 NEWTON-RAPHSON Method 56
4.7 Steepest Descent Algorithm 61
4.8 Domain Decomposition 64

5.1 The DUNE Framework 70

6.1 Initial Configuration of the Heat-Pipe Experiment 78
6.2 Uniform Domain Extrusion 78
6.3 Results of the Heat-Pipe Problem 81
6.4 Spatial Domain of the Synthetic CO_2 Injection Problem 82
6.5 Concept of Radial Domain Extrusion 83
6.6 Results of the Synthetic CO_2 Injection Problem 84
6.7 Scalability of the Synthetic CO_2 Injection Problem 86
6.8 The SPE-9 Problem 88
6.9 Production and Injection Rates of the SPE-9 Problem 89
6.10 Typical Behavior of the PVS Model for the SPE-9 Problem 90
6.11 The SPE-5 Problem 91
6.12 Production and Injection Rates of the SPE-5 Problem 93

6.13 Grid and Intrinsic Permeability of the Ketzin Project 95
6.14 Material Parameters of the Ketzin Simulations 96
6.15 Gas Phase Plume Shapes of the Ketzin Simulations 97
6.16 Predicted Share of Dissolved CO_2 at the Ketzin Project 98

List of Tables

3.1 Parameterizations of Cubic Equations of State for Pure Substances 31

5.1 Implementational Complexity of Numerical Models in eWoms 74

6.1 Computational Performance of the Heat-Pipe Problem 82
6.2 Material Parameters of the Synthetic CO_2 Injection Problem 83
6.3 Computational Performance of the Synthetic CO_2 Injection Problem 87
6.4 Computational Performance of the SPE-9 Problem 90
6.5 PENG-ROBINSON Parameters of the SPE-5 Problem 92
6.6 Computational Performance of the SPE-5 Problem 94

Notation

Symbol	Description
$\boldsymbol{N}$	Set of natural numbers
$\boldsymbol{R}$	Set of real numbers
a	Scalar quantity
f	Scalar function
$\boldsymbol{a}$	Vector
$\mathbf{F}$	Vector-valued function
$\boldsymbol{a}^T$	Transposed vector
$\boldsymbol{A}$	Matrix
$\boldsymbol{A}^T$	Transposed matrix
$\boldsymbol{I}$	Identity matrix
$\boldsymbol{a} \cdot \boldsymbol{b}$	Scalar product of $\boldsymbol{a}$ and $\boldsymbol{b}$
$\boldsymbol{a} \otimes \boldsymbol{b}$	Tensor product of $\boldsymbol{a}$ and $\boldsymbol{b}$
$\mathcal{V}$	Arbitrary, small spatial domain
$\lVert a \rVert$	Absolute value of a
$\lVert \boldsymbol{a} \rVert$	Two-norm of $\boldsymbol{a}$
$\lVert \mathcal{V} \rVert$	Space occupied by $\mathcal{V}$
$\langle \mathrm{f} \rangle$	Spatial average of f
$\langle \mathrm{f} \rangle^{\alpha}$	Intrinsic phase average of f for fluid phase α
$\mathbf{grad}\, \mathrm{f}$	Spatial gradient of f
$\mathrm{div}\, \mathbf{F}$	Divergence of $\mathbf{F}$
$\mathrm{f} * \mathrm{g}$	Convolution of f with g

Subscripts and Superscripts

Subscript/Superscript	Description
$\langle \cdot \rangle_{\mathrm{mass}}$	Mass-based quantity
$\langle \cdot \rangle_{\mathrm{mol}}$	Molar quantity
$\langle \cdot \rangle_{\mathrm{mom}}$	Momentum-related quantity
$\langle \cdot \rangle_{\mathrm{energy}}$	Energy-related quantity
$\langle \cdot \rangle_{\alpha}$	Fluid phase α
$\langle \cdot \rangle^{\kappa}$	Component κ
$\langle \cdot \rangle^{[k]}$	Value at iteration k

Quantities

If not explicitly stated otherwise, all quantities should be assumed to be arbitrary, smooth functions which depend on the spatial position $\boldsymbol{x}$ and time t.

Symbol	SI-Unit	Description
t	[s]	Time
$\boldsymbol{x}$	[m]	Spatial position
Ω	[m]	Complete spatial domain
$\mathcal{V}$	[m]	Small, arbitrary spatial subdomain (averaging volume)
$\boldsymbol{n}$	[m]	Outer unit normal of a spatial domain
$\boldsymbol{v}$	[m/s]	Velocity
b	$[\langle\cdot\rangle]$	Arbitrary conservation quantity
q	$[\langle\cdot\rangle/\mathrm{m^3\,s}]$	Source term of conservation quantity
M	[−]	Number of phases (fluids)
N	[−]	Number of components (chemical compounds)
p_α	[Pa]	Pressure of phase α
$p_{\mathrm{c},\alpha\beta}$	[Pa]	Pressure difference between phases α and β
S_α	[−]	Saturation of phase α
T	[K]	Temperature
M^κ	[kg/mol]	Molar mass of component κ
$\overline{M}_\alpha$	[kg/mol]	Mean molar mass of phase α
x_α^κ	[−]	Mole fraction of component κ in phase α
X_α^κ	[−]	Mass fraction of component κ in phase α
ϕ	[−]	Porosity of the medium
$\boldsymbol{K}$	$[\mathrm{m^2}]$	Intrinsic permeability
$k_{\mathrm{r},\alpha}$	[−]	Relative permeability of phase α
μ_α	[Pa s]	Dynamic viscosity of phase α
ρ_α	$[\mathrm{kg/m^3}]$	Mass density of phase α
$\rho_{\mathrm{mol},\alpha}$	$[\mathrm{mol/m^3}]$	Molar density of phase α
$\boldsymbol{\tau}$	$[\mathrm{N/m^2}]$	Stress tensor
$\boldsymbol{T}$	$[\mathrm{N/m^2}]$	Shear stress tensor
f_α^κ	[Pa]	Fugacity of component κ in phase α
Φ_α^κ	[−]	Fugacity coefficient of component κ in phase α
D_α^κ	$[\mathrm{mol/m\,s}]$	Molecular diffusion coefficient of component κ in phase α
λ_α	$[\mathrm{W/K\,m}]$	Thermal conductivity of phase α
λ_{pm}	$[\mathrm{W/K\,m}]$	Overall thermal conductivity of the porous medium

Abstract

For many multi-phase flow and transport processes in porous media, miscibility of the constituent components (*i.e.*, the chemical compounds of the fluids) is a non-negligible part of the governing physics. This thesis covers several theoretical and numerical aspects of such flows. First, the continuum-scale equations are motivated starting from the molecular scale. Then, techniques to discretize these equations are presented while keeping their parallel implementation by computer programs in mind. After the theoretical, numerical, and implementation-related aspects of such flows are covered, this thesis examines some sample applications to illustrate various computational and physical properties of such flows. Finally, this thesis is concluded and a list of related fields which it does not cover is given.

The main contribution of this thesis to the scientific state of the art is the proposal of non-linear complementarity problem (NCP) based model assumptions to handle phase transitions in compositional simulations of flow in porous media as well as an extensive evaluation of its properties relative to established approaches – such as the primary variable switching (PVS) and the black-oil models.

Kurzfassung

Mischbarkeitseffekte sind für eine Reihe von technisch, wissenschaftlich und wirtschaftlich bedeutsamen Anwendungen von Fluidströmungen in porösen Medien von herausragender Bedeutung. Eine Auswahl dieser Anwendungsgebiete ist in Abbildung 1 wiedergegeben: Sie umfasst Techniken zur Erdöl- und Erdgasförderung, die Speicherung von klimaaktiven Gasen wie CO_2 in geologischen Formationen, Aufgabenstellungen zur Bodendekontamination, sowie Anwendungen aus der chemischen Verfahrenstechnik, welche an dieser Stelle beispielhaft durch Polymer-Elektrolyt-Membran-Brennstoffzellen repräsentiert werden.

Bei derartigen Anwendungen ist die Erstellung geeigneter physischer Modelle zur Auslegung und Optimierung des Systems oft sehr teuer oder im Extremfall unmöglich. Um dieser Tatsache zum Trotz ein Verständnis der relevanten physikalischen Prozesse zu gewinnen, ist die numerische Simulation häufig das Mittel der Wahl. Eine der Hauptschwierigkeiten dieser Simulationen ist die numerische Behandlung von Stoffgemischen und hierbei insbesondere die Präsenz der Fluidphasen innerhalb des betrachteten Raumgebiets.

In der vorliegenden Arbeit werden wir uns in den Kapiteln 2 und 3 näher mit der theoretischen Behandlung von Strömungen in porösen Medien beschäftigen. In diesem Kontext werden wir einen besonderen Schwerpunkt auf die Einbeziehung von Mischbarkeitseffekten legen. Im anschließenden Kapitel 4 werden wir kurz die numerische Behandlung der sich daraus ergebenden Gleichung besprechen, während wir in Kapitel 5 die im Kontext dieser Arbeit verwendete numerische Software näher betrachten und in Kapitel 6 Ergebnisse für ausgewählte numerische Experimente vorstellen und auswerten werden. Abschließend folgt eine Zusammenfassung sowie ein Ausblick auf wichtige weiterführende Themenfelder, die den Umfang dieser Arbeit übersteigen würden.

Erhaltungsgleichungen für Fluidströmungen in porösen Medien

Im ersten Teil von Kapitel 2 beschäftigen wir uns mit Kontinuumsmechanik im Allgemeinen. Hierzu werden wir zunächst die kontinuumsmechanische Betrachtungsweise basierend auf molekularen Größen motivieren. In diesem Kontext werden wir feststellen, dass dies mit dem mathematischen Konzept der Faltung von molekularen Größen erreicht werden kann, wie Abbildung 2 illustriert: Zunächst definieren wir eine *Dichtefunktion*

$$\zeta_b := \sum_i \psi_i b_i \ ,$$

die die mit den individuellen molekularen oder atomaren Partikeln assoziierte Größe b_i räumlich verteilt. Hierbei ist $\psi_i : \boldsymbol{R}^3 \to \boldsymbol{R}$ eine glatte und an der Position des i-ten Moleküls

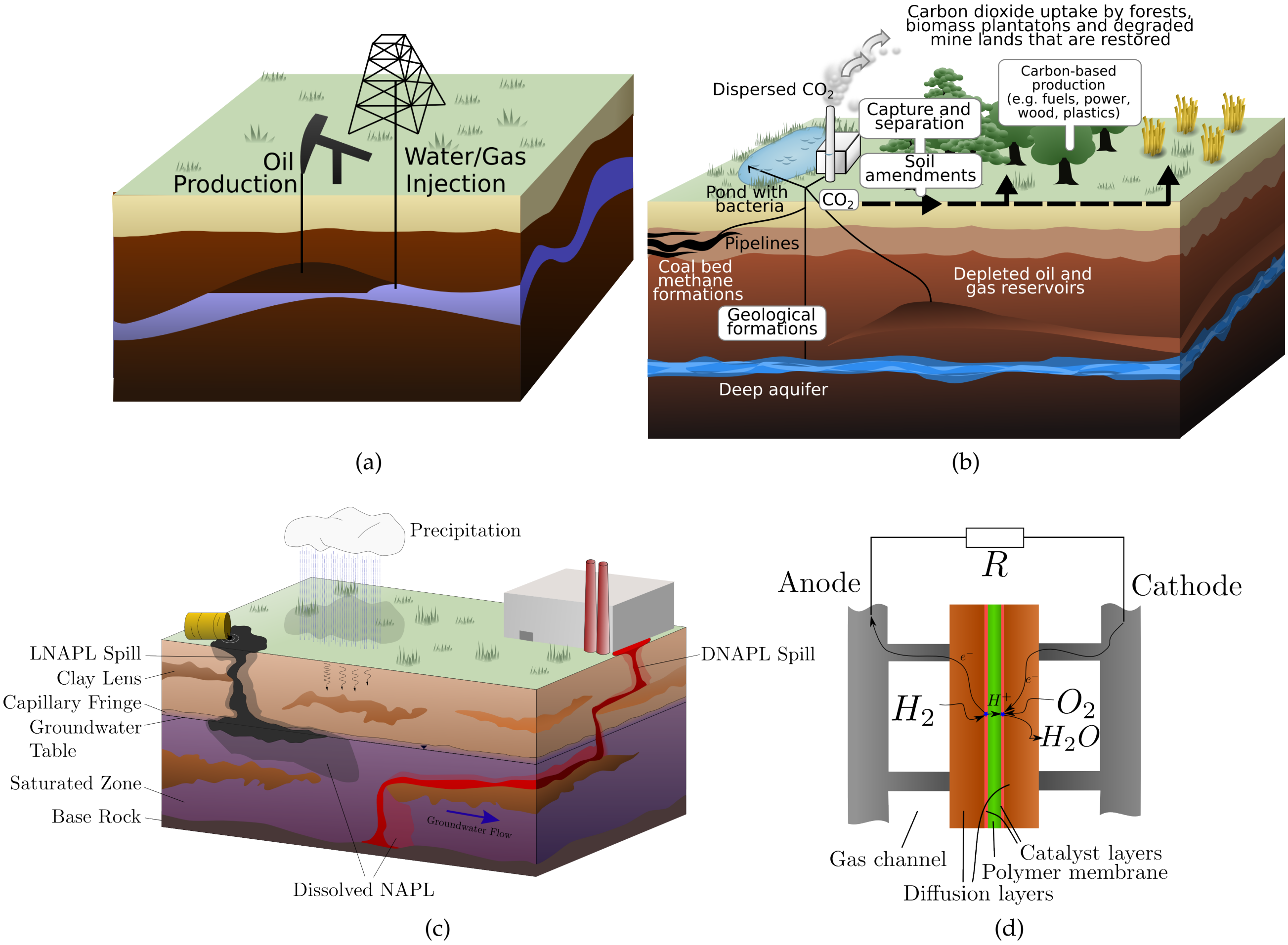

(a) (b)

(c) (d)

Abbildung 1: Anwendungsgebiete von Mehrphasenströmungen in porösen Medien bei denen Mischbarkeitseffekte berücksichtigt werden sollten: **(a)** Erdölproduktion. **(b)** Geologische Speicherung von CO_2. (Bildquelle: [90]) **(c)** Bodendekontamination. (Bildquelle: [39]) **(d)** Polymer-Elektrolyt-Membran-Brennstoffzellen.

zentrierte Funktion, deren Integral über den Definitionsbereich 1 ergibt.

Nachdem wir eine passende Dichtefunktion definiert haben, können wir diese nach Anwenung der Faltungsoperation

$$b(\boldsymbol{x}) = (\zeta_b * \chi)(\boldsymbol{x}) := \int_{\boldsymbol{R}^3} \zeta_b(\boldsymbol{x} - \boldsymbol{y}) \cdot \chi(\boldsymbol{y})\, \mathrm{d}\boldsymbol{y}$$

mit einem *Glättungskern* $\chi : \boldsymbol{R}^3 \to \boldsymbol{R}$ auf Kontinuumsebene behandeln. Der Glättungskern χ können wir dabei als eine um den Koordinatenursprung zentrierte, radial monoton fallende Funktion mit der Eigenschaft annehmen, dass ihr Integral über den Defintionsbereich 1 ergibt. Um Oszillationen in b vernachlässigen zu können, muss der Träger der Glättungsfunktion einerseits groß genug sein, dass die Eigenschaften einzelner Moleküle keinen wesentlichen Einfluss auf das Ergebnis der Faltungsoperation haben. Andererseits muss der Träger jedoch

(a) Partikel (b) Dichtefunktion ζ_b (c) Kontinuumsgröße b

Abbildung 2: Illustration des Übergangs von der Molekular- zur Kontinuumsskala.

klein genug sein, um makroskopische Änderungen der Eigenschaften der Größe b nicht zu sehr zu mitteln. Zur Verdeutlichung dieses Konzepts bietet sich als einfaches Beispiel die Massendichte ρ an: Hierzu verwenden wir die Dichtefunktion

$$\zeta_\rho = \sum_i \psi_i m_i \ ,$$

wobei m_i der Masse des i-ten Partikels entspricht. Nach der anschließenden Anwendung der Faltungsoperation erhalten wir als Kontinuumsgröße die Massendichte ρ.

Nach dieser kurzen Motivation der kontinuumsmechanischen Betrachtungsweise, werden wir im selben Kapitel partielle Differenzialgleichungen herleiten, welche die Erhaltung beliebiger Größen auf Kontinuumsebene beschreiben. Diese Gleichungen wenden wir sodann auf verschiedene Erhaltungsgrößen der klassischen Physik an und betrachten hierbei insbesondere den Spezialfall der NEWTONSCHEN Fluide, bei denen die viskosen Kräfte linear zur Schergeschwindigkeit des Fluids angenommen werden. Wir beschränken unseren Diskurs hierbei auf die Erhaltungsgrößen Masse, Impuls und Energie; andere physikalischen Erhaltungsgrößen – etwa elektrische Ladung – werden wir also nicht berücksichtigen. Als Ergebnis unserer Bemühungen erhalten wir für NEWTONSCHE Fluide die Massenerhaltungsgleichung

$$\frac{\partial x^\kappa \rho_{\text{mol}}}{\partial t} + \operatorname{div}(x^\kappa \rho_{\text{mol}}\, \boldsymbol{v} - D^\kappa \mathbf{grad}\ x^\kappa) = q^\kappa \ ,$$

die Energieerhaltungsgleichung

$$\frac{\partial\ \rho \left(u + {}^1\!/_2 \|\boldsymbol{v}\|^2 + \boldsymbol{z} \cdot \boldsymbol{g}\right)}{\partial t} + \operatorname{div}(h\rho\, \boldsymbol{v} - \lambda\, \mathbf{grad}\ T) = q_{\text{energy}} - \rho \boldsymbol{v} \cdot \boldsymbol{g}$$

und die NAVIER-STOKES-Gleichungen zur Impulserhaltung

$$\rho \frac{\partial \boldsymbol{v}}{\partial t} + \rho \boldsymbol{v} \cdot \mathbf{grad}\ \boldsymbol{v} = -\mathbf{grad}\ p + \mu \operatorname{div} \mathbf{grad}\ \boldsymbol{v} + \rho \boldsymbol{g} + \boldsymbol{q}_{\text{mom}} \ .$$

Die Energieerhaltungsgleichung können wir weiter zu

$$\frac{\partial\, u\rho}{\partial t} + \operatorname{div}(h\rho\boldsymbol{v} - \lambda\,\mathbf{grad}\,T) = q_{\mathrm{energy}}$$

vereinfachen, falls wir annehmen, dass die kinetischen und potentiellen Anteile vernachlässigbar sind gegenüber der spezifischen inneren Energie u.

Bei schleichenden inkompressiblen Strömungen können wir weiterhin die Trägheitsterme der NAVIER-STOKES-Gleichungen als vernachlässigbar gegenüber den viskosen Termen annehmen. Dies führt uns zu den STOKES-Gleichungen

$$-\,\mathbf{grad}\,p + \mu\,\operatorname{div}\mathbf{grad}\,\boldsymbol{v} + \rho\,\boldsymbol{g} + \boldsymbol{q}_{\mathrm{mom}} = 0\;.$$

Nach dieser Herleitung der für uns relevanten Erhaltungsgleichungen, erörtern wir in Abschnitt 2.4 die Verhältnisse in porösen Medien. Hierbei ist zu beachten, dass für die meisten technischen und wissenschaftlichen Anwendungen die genaue Geometrie der Poren unbekannt ist. Dieser Umstand ist analog zur initialen Partikelkonfiguration beim Übergang von der molekularskaligen zur kontinuumsskaligen Betrachtungsweise, da auch diese normalerweise unbekannt ist. Üblicherweise wird bei dieser Herleitung, wie bei der Motivation der kontinuumsmechanischen Betrachtungsweise, ein Mittelungsansatz verwendet; es Medien werden jedoch die Erhaltungsgleichungen der Kontinuumsskala gemittelt. Diese Mittelungsansätze können wir auch als Spezialfälle von Faltungsoperationen auffassen. In der vorliegenden Arbeit verwenden wir die von WHITAKER [89] vorgestellte Vorgehensweise, welche ausgehend von der Massenerhaltungs-, den vereinfachten Energieerhaltungs- und den STOKES-Gleichungen die bestimmenden Gleichungen für die makroskopische Berschreibung von Strömungen von NEWTONSCHEN Fluiden in porösen Medien ergibt. Als Massenerhaltungsgleichung einer Komponente[1] κ in einem porösen Medium erhalten wir

$$\sum_{\alpha} \frac{\partial \phi S_\alpha \langle x_\alpha^\kappa\rangle^\alpha \langle\rho_{\mathrm{mol},\alpha}\rangle^\alpha}{\partial t} + \sum_{\alpha} \operatorname{div}(\langle x_\alpha^\kappa\rangle^\alpha \langle\rho_{\mathrm{mol},\alpha}\rangle^\alpha \langle\boldsymbol{v}_\alpha\rangle - \langle D_\alpha^\kappa\rangle \mathbf{grad}\,\langle x_\alpha^\kappa\rangle) = q_{\mathrm{mol}}^\kappa\;,$$

wobei wir die Quellterme der Komponente zu

$$q_{\mathrm{mol}}^\kappa := \sum_\alpha \left\langle q_{\mathrm{mol},\alpha}^\kappa \right\rangle$$

zuammenfassen und

$$\langle b(\boldsymbol{x})\rangle = \frac{1}{\|\mathcal{V}(\boldsymbol{x})\|} \int_{\mathcal{V}_\alpha(\boldsymbol{x})} b(\boldsymbol{y})\,\mathrm{d}\boldsymbol{y}$$

die Mittelungsoperation der Größe $b(\boldsymbol{x})$ über das Raumgebiet $\mathcal{V}(\boldsymbol{x})$ repräsentiert. Ferner

---

[1] Eine Komponente bezeichnet hier eine chemische Verbindung die in Phasen enthalten sein kann, während eine Phase als Materialgemisch definiert ist, das eine Grenzfläche zu allen anderen Phasen ausbildet. Als Beispiel soll hier das Zweiphasen-, Zweikomponentensystem Wasser-Stickstoff dienen, bei dem die flüssige und gasförmige Phase jeweils Gemische der Verbindungen Wasser (H_2O) und Stickstoff (N_2) sind.

definieren wir das auf die Fluidphase α bezogene Mittel an Position $\boldsymbol{x}$ als

$$\langle b(\boldsymbol{x})\rangle^{\alpha} = \frac{1}{S_{\alpha}\phi}\langle b(\boldsymbol{x})\rangle \ .$$

Analog zur Massenerhaltungsgleichung erhalten wir die Impulserhaltungsgleichungen

$$\langle \boldsymbol{v}_{\alpha}\rangle = -\frac{k_{\mathrm{r},\alpha}\boldsymbol{K}}{\langle \mu_{\alpha}\rangle^{\alpha}}\left(\mathbf{grad}\ \langle p_{\alpha}\rangle^{\alpha} - \langle \rho_{\alpha}\rangle^{\alpha}\boldsymbol{g}\right)$$

und die Energieerhaltungsgleichung

$$\begin{aligned}
&\frac{\partial}{\partial t}\left((1-\phi)\langle u_s\rangle^{s}\ \langle \rho_s\rangle^{s} + \sum_{\alpha} \phi S_{\alpha}\langle u_{\alpha}\rangle^{\alpha}\ \langle \rho_{\alpha}\rangle^{\alpha}\right) \\
&- \mathrm{div}\left(\langle \lambda_s\rangle^{s}\,\mathbf{grad}\ \langle T_s\rangle + \sum_{\alpha}\left(\langle h_{\alpha}\rangle^{\alpha}\langle \rho_{\alpha}\rangle^{\alpha}\langle \boldsymbol{v}_{\alpha}\rangle - \langle \lambda_{\alpha}\rangle^{\alpha}\,\mathbf{grad}\ \langle T_{\alpha}\rangle\right)\right) \\
&= \langle q_{\mathrm{energy}}\rangle \ .
\end{aligned}$$

Hierbei bezeichnet $\langle\cdot\rangle^{s}$ eine für die Feststoffphase definierte Größe. Diese Gleichung können wir unter Annahme des lokalen thermischen Gleichgewichts zu

$$\begin{aligned}
&\frac{\partial}{\partial t}\left((1-\phi)\langle u_s\rangle^{s}\ \langle \rho_s\rangle^{s} + \sum_{\alpha} \phi S_{\alpha}\langle u_{\alpha}\rangle^{\alpha}\ \langle \rho_{\alpha}\rangle^{\alpha}\right) \\
&\quad - \mathrm{div}\left(\sum_{\alpha} \langle h_{\alpha}\rangle^{\alpha}\langle \rho_{\alpha}\rangle^{\alpha}\langle \boldsymbol{v}_{\alpha}\rangle + \lambda_{\mathrm{pm}}\,\mathbf{grad}\ \langle T\rangle\right) = \langle q_{\mathrm{energy}}\rangle
\end{aligned}$$

vereinfachen.

Für die folgenden Betrachtungen werden wir die Mittelungsoperatoren nicht mehr explizit schreiben, so dass wir die Erhaltungsgleichungen wie folgt ausdrücken werden:

$$\sum_{\alpha}\frac{\partial \phi S_{\alpha} x_{\alpha}^{\kappa}\rho_{\mathrm{mol},\alpha}}{\partial t} + \sum_{\alpha}\mathrm{div}\big(x_{\alpha}^{\kappa}\rho_{\mathrm{mol},\alpha}\boldsymbol{v}_{\alpha} - D_{\mathrm{pm},\alpha}^{\kappa}\mathbf{grad}\ x_{\alpha}^{\kappa}\big) = q_{\mathrm{mol}}^{\kappa}$$

$$\boldsymbol{v}_{\alpha} = -\frac{k_{\mathrm{r},\alpha}}{\mu_{\alpha}}\boldsymbol{K}\left(\mathbf{grad}\ p_{\alpha} - \rho_{\alpha}\boldsymbol{g}\right)$$

$$\frac{\partial}{\partial t}\left((1-\phi)u_s\rho_s + \sum_{\alpha}\phi S_{\alpha}u_{\alpha}\ \rho_{\alpha}\right) - \mathrm{div}\left(\sum_{\alpha} h_{\alpha}\rho_{\alpha}\boldsymbol{v}_{\alpha} - \lambda_{\mathrm{pm}}\,\mathbf{grad}\ T\right) = q_{\mathrm{energy}}$$

Schlussbedingungen und ergänzende Gleichungen

Nach dieser Herleitung der Erhaltungsgleichungen beschäftigen wir uns anschließend in Kapitel 3 damit, ein mathematisch geschlossenes Gleichungssystem für die Erhaltungsgleichungen zu erhalten. Das Erreichen dieses Ziels beinhaltet insbesondere die Notwendigkeit, den *per se* unbekannten Größen eine gleiche Anzahl an Gleichungen gegenüberzustellen. Wenn wir die Anzahl der Fluidphasen als M und die Anzahl der Komponenten als N bezeichnen, treten in den Masse- und Impulserhaltungsgleichungen folgende $2N \cdot M + N + 10M + 3$ Größen auf:

- Die gravitative Beschleunigung $\boldsymbol{g}$,
- die Porosität ϕ,
- die intrinsische Permeabilität $\boldsymbol{K}$,
- 3 M Unbekannte zur Definition der Phasengeschwindigkeiten $\boldsymbol{v}_\alpha$,
- M Sättigungen S_α,
- M Drücke p_α,
- M relative Permeabilitäten $k_{\mathrm{r},\alpha}$,
- M dynamische Viskositäten μ_α,
- M Massedichten der Fluidphasen ρ_α,
- M molare Phasendichten $\rho_{\mathrm{mol},\alpha}$,
- M Phasentemperaturen T_α,
- N Quellterme q^κ_{mol},
- $M \cdot N$ Molenbrüche x^κ_α und
- $M \cdot N$ Diffusionskoeffizienten $D^\kappa_{\mathrm{pm},\alpha}$.

Dem stehen bislang nur die N Erhaltungsgleichungen der einzelnen Komponenten, sowie die 3 M Erhaltungsgleichungen des Impulses gegenüber. Allerdings können wir die gravitative Beschleunigung $\boldsymbol{g}$, die Porosität ϕ und die intrinsische Permeabilität $\boldsymbol{K}$ als gegebene Funktionen in Abhängigkeit der räumlichen Position annehmen. Ferner können wir die dynamischen Viskositäten μ_α, die Quellterme q^κ_{mol}, die Massedichten der Fluidphasen ρ_α und die Diffusionskoeffizienten $D^\kappa_{\mathrm{pm},\alpha}$ als gegebene geschlossene Funktionen in Abhängigkeit des Drucks, der Temperatur und der Zusammensetzung der Fluidphase α annehmen [68, 22]. Des Weiteren besteht der Zusammenhang

$$\rho_\alpha = \rho_{\mathrm{mol},\alpha} \sum_\kappa x^\kappa_\alpha M^\kappa$$

zwischen der Massendichte einer Fluidphase ρ_α und der molaren Dichte $\rho_{\mathrm{mol},\alpha}$ dieser Phase.

Weiterhin muss das gesamte zur Verfügung stehende Porenvolumen von den Fluiden eingenommen werden, so dass die Summe aller Fluidsättigungen 1 ergibt. Die relativen Permeabilitäten sind weiterhin gegeben durch geschlossene empirisch ermittelte Funktionen in Abhängigkeit der Phasensättigungen.

Wenn wir nun annehmen, dass zu jedem Zeitpunkt lokal thermodynamisches Gleichgewicht herrscht, erhalten wir weitere $(M-1)$ Relationen, die das mechanische, $(M-1)$ Relationen, die das thermische und $N \cdot (M-1)$ Relationen, die das chemische Gleichgewicht beschreiben. Im Kontext von Fluidströmungen in porösen Medien müssen wir bei der Definition des mechanischen Gleichgewichts das Konzept des *Kapillardrucks* einführen, welches die Differenz der absoluten Drücke der Fluidphasen im stationären Zustands im porösen Medium ausdrückt. Die Kapillardrücke werden für gewöhnlich gemeinsam mit den relativen Permeabilitäten als geschlossene empirisch ermittelte Funktionen in Abhängigkeit der Phasensättigungen behandelt.

Bisher wurden erst die folgenden $2N \cdot M + N + 9M + 3$ Relationen identifiziert:

- $3\,M$ Impulserhaltungsgleichungen,
- N Massenerhaltungsgleichungen,
- drei gegebene räumliche Funktionen für $\boldsymbol{g}$, $\boldsymbol{K}$ und ϕ,
- eine Schlussbedingung für die Phasensättigungen,
- M Gleichungen für die Verknüpfung zwischen der molaren Dichte und der Massendichte der Fluidphasen,
- M geschlossene Funktionen, die für die dynamischen Viskositäten μ_α wiedergeben,
- M empirisch gegebene Funktionen für die relativen Permeabilitäten $k_{\mathrm{r},\alpha}$,
- N Quellterme q^κ,
- $M \cdot N$ geschlossene Funktionen $D^\kappa_{\mathrm{pm},\alpha}$ zur Berechnung der molekularen Diffusionskoeffizienten,
- M Zustandsgleichungen,
- $M-1$ Gleichungen für die aus dem lokale thermischen Gleichgewicht stammen,
- $M-1$ Gleichungen, die das lokale mechanische Gleichgewicht beschreiben sowie
- $(M-1) \cdot N$ Gleichungen für das chemische Gleichgewicht und
- ein extern vorgegebenes, räumlich abhängiges Temperaturfeld T falls wir die Energieerhaltungsgleichung ignorieren, ansonsten die Energieerhaltungsgleichung.

Um ein geschlossenes Gleichungssystem zu erhalten, fehlen also noch M Relationen. Diese M Gleichungen bilden Modellannahmen ab, wobei wir die Annahmen folgender Modelle näher betrachten:

Unmischbarkeit [39]: Bei diesem Modell wird die Anzahl der Fluidphasen mit der Anzahl der Komponenten gleichgesetzt, also $M = N$ angenommen. Ferner wird angenommen, dass jede Fluidphase aus genau einer Komponente besteht. Diesen Umstand können wir mittels

$$x^\kappa_\alpha = \begin{cases} 1 & \text{wenn } \alpha \text{ die Fluidphase der Komponente } \kappa \text{ ist,} \\ 0 & \text{sonst} \end{cases}$$

ausdrücken.

Primärvariablentausch [33, 23]: Falls wir für alle Fluidphasen Mischbarkeit annehmen, können wir für den Fall, dass eine Fluidphase an einem Raumpunkt präsent ist, annehmen, dass die Summe der Komponentenmolenbrüche für diese Fluidphase 1 ergibt, also dass

$$\sum_\kappa x_\alpha^\kappa = 1$$

gilt. Andererseits muss die Sättigung einer Fluidphase die nicht präsent ist Null sein; also muss in diesem Fall

$$S_\alpha = 0$$

gelten. Diese beiden Gleichungen können zusammengefasst werden zu

$$0 = \begin{cases} 1 - \sum_\kappa x_\alpha^\kappa & \text{falls die Fluidphase } \alpha \text{ präsent ist,} \\ S_\alpha & \text{sonst.} \end{cases}$$

Zur Bestimmung der Menge der zu einem gegebenen Zeitpunkt vorhandenen Fluidphasen wird diese initial vorgegeben und bei physikalisch unmöglichen Zuständen – etwa bei negativen Sättigungen – während der Simulation angepasst.

Komplementaritätsprobleme [48, 41]: Die Bedingungen des Primärvariablentauschmodells können wir auch direkt in das Gleichungssystem einbeziehen: Zu diesem Zweck werden wir uns zuerst der Tatsache bewusst, dass die Summe der „Molenbrüche“ für diese Phase nur kleiner 1 werden kann, wenn die Sättigung einer Fluidphase Null ist, wenn also

$$S_\alpha = 0 \implies \sum_\kappa x_\alpha^\kappa \leq 1$$

gilt. Umgekehrt kann die Sättigung einer Fluidphase nur dann größer als 0 werden, wenn diese Phase präsent sein kann, also die Summe der Molenbrüche 1 ist. Es gilt also

$$\sum_\kappa x_\alpha^\kappa = 1 \implies S_\alpha \geq 0\ .$$

Da jede Fluidphase immer entweder präsent oder abwesend ist, muss eine der beiden Gleichungen auf der linken Seite erfüllt sein und wir erhalten das nichtlineare Komplementaritätsproblem

$$S_\alpha \left(1 - \sum_\kappa x_\alpha^\kappa \right) = 0 \quad \wedge \quad 1 - \sum_\kappa x_\alpha^\kappa \geq 0 \quad \wedge \quad S_\alpha \geq 0\ .$$

Dieses können wir mittels einer *nichtlinearen Komplementaritätsfunktion* $\Psi : \boldsymbol{R}^2 \to \boldsymbol{R}$, welche die Eigenschaft

$$\Psi(a,b) = 0 \iff a \geq 0 \wedge b \geq 0 \wedge a \cdot b = 0$$

erfüllt, direkt in das zu lösende Gleichungssystem einbeziehen. In diesem Zusammenhang ist es hilfreich zu erwähnen, dass die oben aufgeführte Eigenschaft die Funktion Ψ nicht eindeutig definiert, also mehrere Funktionsklassen existieren, die diese Eigenschaft aufweisen. Im Kontext dieser Arbeit verwenden wir aufgrund ihrer stückweisen Linearität als nichtlineare Komplementaritätsfunktion jedoch stets die Minimumfunktion

$$\Psi(a,b) := \min(a,b)\ .$$

Black-Oil [19]: Die letzten Modellannahmen die im Kontext dieser Dissertation besprochen werden, sind die des Black-Oil Modells. Diese Annahmen werden häufig im Bereich der Förderung von Erdöl angewandt und beschreiben die Eigenschafen der Fluidphasen Öl, Gas und Wasser mittels der drei gleichnamigen Pseudokomponenten Öl, Gas und Wasser. Sowohl die Wasser- als auch die Gasphase werden hierbei als unmischbar vorausgesetzt, während die Ölphase als Gemisch der Öl- und der Gaspseudokomponente angenommen wird. Die Black-Oil-Parameter definieren nun die Massendichten aller Phasen sowie den maximal möglichen Gasanteil der Ölphase in Abhängigkeit des Drucks. Aus diesen Parametern können wir die benötigten Modellannahmen herleiten.

Diskretisierung

Nachdem wir nun die zu lösenden Gleichungssysteme bestimmt haben, widmen wir Kapitel 4 Methoden zum Finden von Näherungslösungen für jene Gleichungen. Unsere abstrakte Vorgehensweise ist dabei folgende:

- Die partiellen Differenzialgleichungen werden zunächst räumlich diskretisiert. Zu diesem Zweck wird das zu untersuchende räumliche Gebiet in ein *konformes Gitter* partitioniert und die zu lösende Differenzialgleichung für jedes Element dieses Gitters einzeln betrachtet und anschließend addiert. Als Ergebnis erhalten wir ein – im Allgemeinen sehr großes – nichtlineares, gekoppeltes System gewöhnlicher Differenzialgleichungen.

- Auf dieses System gekoppelter gewöhnlicher Differenzialgleichungen wenden wir nun eine Zeitdiskretisierung an. Zur Herleitung dieser verwenden wir den Satz von TAYLOR und erhalten für jeden Zeitschritt ein großes gekoppeltes System nichtlinearer algebraischer Gleichungen. Das Finden einer Näherungslösung des ursprünglichen Gleichungssystems reduziert sich also auf das wiederholte Lösen solcher nichtlinearer algebraischer Gleichungsysteme.

- Jedes der sich ergebenden nichtlinearen algebraischen Gleichungssysteme lösen wir anschließend iterativ mit Hilfe des NEWTON-RAPHSON-Ansatzes. Hierzu müssen wir das zu lösende nichtlineare Gleichungssystem wiederholt linearisieren.

- Die sich aus der NEWTON-RAPHSON-Methode ergebenden linearen Gleichungssysteme werden im finalen Schritt mittels einer direkten oder einer iterativen Methode exakt oder näherungsweise gelöst.

In Kapitel 4 werden wir uns mit jedem dieser Schritte näher beschäftigen.

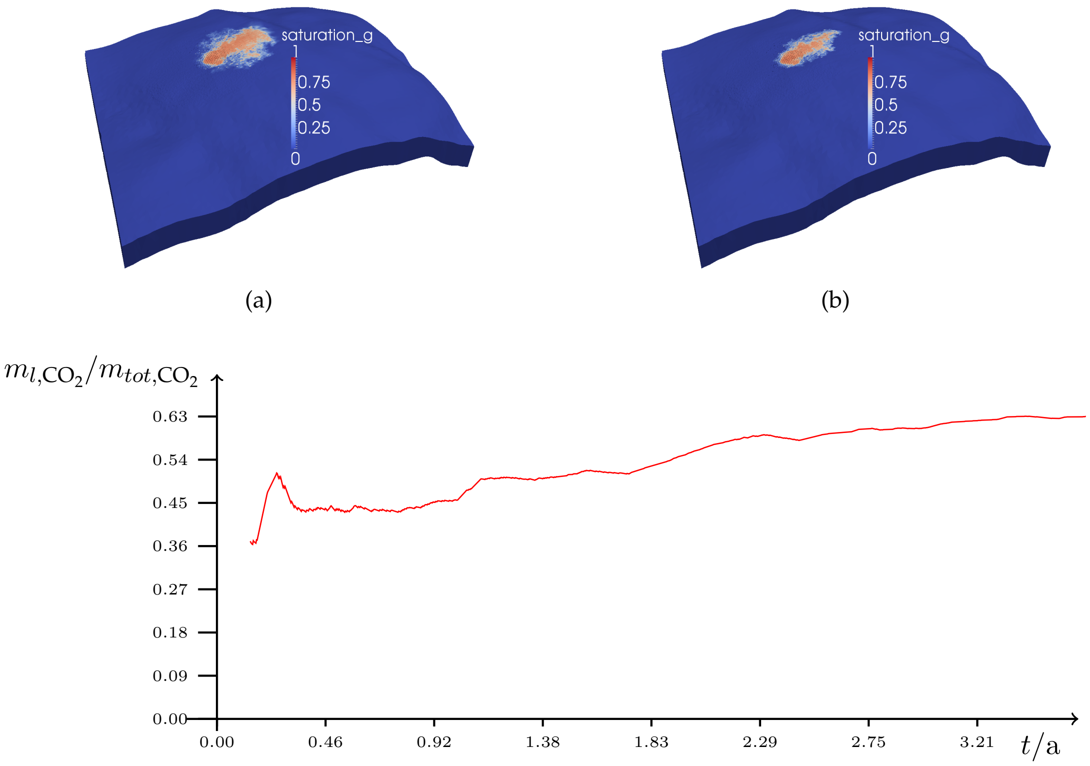

(a) (b)

(c)

Abbildung 3: Ergebnisse der Modellrechnungen für das Experiment zur Untersuchung der geologischen CO_2-Speicherung in Ketzin/Havel [55]. **(a)** Gassättigung nach dreijähriger CO_2-Injektion bei Annahme von Unmischbarkeit von CO_2 und Salzwasser. **(b)** Gassättigung nach dreijähriger CO_2-Injektion unter Berücksichtigung der Mischbarkeit von CO_2 und Salzwasser. **(c)** Anteil des injizierten CO_2 das in der Salzwasserphase gelöst ist.

Numerische Anwendungen

Nachdem wir die theoretischen und numerischen Grundlagen zur numerischen Simulation von Fluidströmungen in porösen Medien abgehandelt haben, werden wir uns in Kapitel 5 kurz mit eWoms beschäftigen, des C++ Softwarepakets in dessen Rahmen die hier vorgestellten Konzepte implementiert wurden. Ein besonderes Augenmerk dieses Kapitels wird der benötigte Aufwand zur Implementierung der oben genannten Modellkonzepte bilden.

Nach diesem kurzen Abstecher zur Softwareimplementierung, werden wir uns in Kapitel 6 den physikalischen und numerischen Eigenschaften der obigen Modelle anhand ausgewählter Beispiele zuwenden und sie untereinander vergleichen. Die numerischen Anwendungen werden hierbei grob in der Reihenfolge ihrer Komplexität abgehandelt:

- Zunächst beschäftigen wir uns mit dem Heatpipeproblem von UDELL [84]. Dieses beschreibt einen eindimensionalen nicht-isothermen Versuchsaufbau, für den die Lösung im stationären Fall semi-analytisch berechnet werden kann. Wir vergleichen dabei das

Konvergenzverhalten der Raumdiskretisierung unter Verwendung des Primärvariablentauschmodells und des Modells, das die nichtlinearen Komplementaritätsprobleme direkt in das zu lösende Gleichungssystem einbettet. Außerdem werden wir in diesem Abschnitt den benötigten Rechenaufwand der beiden betrachteten Modelle miteinander vergleichen.

- Nach dem Heatpipeproblem werden wir die vorgestellten Modelle mit Hilfe der von Darcis [25] vorgestellten synthetischen Problemstellung zur geologischen Speicherung von CO_2 untersuchen. Hierbei widmen wir uns zunächst dem Einfluss der Energieerhaltungsgleichung sowie den Einfluss von Mischbarkeitseffekten. Des Weiteren werden wir anhand dieses Beispiels das Konzept der radialen Gebietsextrusion vorstellen, welches es erlaubt, radialsymmetrische dreidimensionale Raumgebiete mittels eines zweidimensionalen Raumgebiets abzubilden. Ergebnisse, die mit Hilfe dieser Methode erzeugt wurden, werden dann mit denjenigen einer dreidimensionalen Simulation desselben Problems verglichen. Ferner werden wir anhand dieses Beispiels das Verhalten der vorgestellten Methoden für parallele Berechnungen analysieren.
- Anschließend werden wir eine leicht vereinfachte Version des neunten Benchmarkproblems der Society of Petroleum Engineers (SPE-9) [45] näher untersuchen. In diesem Kontext vergleichen wir die Ergebnisse der Modelle welche auf den Ansätzen des Primärvariablentauschs (PVS) und den nicht-linearen Komplementaritätsproblemen (NCP) beruhen mit den Ergebnissen die mit Hilfe des Black-Oil-Modells berechnet wurden. Wir werden dabei feststellen, dass sich das PVS-Modell für dieses Problem sehr instabil verhält und deshalb nicht anwendbar ist. Die Ergebnisse der beiden verbleibenden Modelle, zeigen eine gute Übereinstimmung hinsichtlich der prognostizierten Injektions- und Produktionsraten, der benötigte Rechenaufwand ist jedoch für das Black-Oil-Modell bedeutend geringer.
- Nach dem neunten Benchmarkproblem der Society of Petroleum Engineers werden wir uns näher mit dem fünften Benchmarkproblem (SPE-5) [46] beschäftigen. Die Besonderheit dieser Problemstellung liegt weniger in einer komplexen geologischen Abbildung des Problems, als vielmehr in der außerordentlichen Komplexität der verwendeten thermodynamischen Relationen: Die Problemspezifikation umfasst drei Fluidphasen sowie sieben Komponenten, welche mittels einer nicht-linearen kubischen Zustandsgleichung definiert werden. Das Problem wurde mit Hilfe des NCP- und des PVS-Modells simuliert. Die hierbei erhaltenen Ergebnisse sind sich sehr ähnlich. Der benötigte Berechnungsaufwand war auch in diesem Fall für das PVS-Modell höher als für das NCP-Modell. Im Gegensatz zu den anderen hier beschriebenen Vergleichsproblemen benötigt das PVS-Modell zur Lösung des SPE-5 Problems jedoch nicht nur eine größere Anzahl an Zeitschritten als das NCP-Modell, sondern weist auch einen höheren Rechenaufwand pro Newton-Raphson-Iteration auf. Letzteres liegt wahrscheinlich daran, dass die zu lösenden lokalen Gleichungssysteme für Dreiphasensysteme mit vielen Komponenten relativ groß werden, während die Anzahl der Fluidphasen beim NCP-Modell keine Rolle spielt.
- Zuletzt werden wir Ergebnisse für eine Anwendung besprechen, welche die Verhältnisse des realen CO_2-Speicherungsexperiments nahe der brandenburgischen Stadt

Ketzin/Havel [55] abbilden. Ketzin/Havel wurde als deutscher Pilotstandort zur Untersuchung der Realisierbarkeit geologischer CO_2-Speicherung ausgewählt. Hierbei werden wir zeigen, dass die vorgestellten Methoden auch großskalig einsetzbar sind – im Falle des vorgestellten Beispiels beträgt die planare Ausdehnung des Simulationsgebiets $5\,\mathrm{km}$ mal $5\,\mathrm{km}$ bei einer mittleren Dicke des Speichergesteins von ca. $130\,\mathrm{m}$; dieses Gebiet wurde mittels gut vier Millionen Tetraedern diskretisiert. Anhand dieser Aufgabenstellung zeigen wir außerdem, dass Mischbarkeit von Stoffen bei geologischen Anwendungen eine nicht vernachlässigbare Rolle spielen kann.

Die wichtigsten Ergebnisse dieser Modellrechnungen sind in Abbildung 3 zusammengefasst. Bei der Interpretation dieser Ergebnisse sollten wir uns allerdings der Tatsache bewusst sein, dass die Menge des im Salzwasser gelösten CO_2 aufgrund der hier verwendeten Finite-Volumen-Raumdiskretisierungen systematisch überschätzt wird. Im Falle des Ketziner CO_2-Speicherprojekts wird diese Einschätzung durch seismische Daten gestützt [55].

Abschließend findet sich eine Zusammenfassung dieser Arbeit mit Empfehlungen zur Anwendung der vorgestellten Modelle und ein Ausblick auf wichtige Themenfelder die im Rahmen dieser Arbeit nicht besprochen werden konnten.

1 Introduction

For many multi-phase flow and transport processes in porous media, miscibility of the constituent components is a non-negligible part of the governing physics. Some of these applications are depicted in Figure 1.1, and include the fields of petroleum production [19], geological storage of CO_2 [69], substantial parts of chemical engineering [42] (exemplified here by polymer-electrolyte-membrane (PEM) fuel cells [7]) and advanced *in-situ* ground remediation procedures [64, 61, 22]. Most of these fields are of significant economic, environmental, and scientific interest.

Petroleum Production

Our focus when using numerical simulation of multi-phase flows in porous media for petroleum reservoir engineering applications is to make predictions of the expected oil and gas production rates to maximize the amount of hydrocarbons which can be profitably extracted from a given reservoir. Some of the particular issues which need to be overcome in this field are the enormous physical extends of hydrocarbon reservoirs [91]—commonly, their volume is in the range of cubic kilometers—, complex thermodynamics involving high pressures and temperatures [19] as well as high heterogeneity in the material of the reservoir with a large uncertainty in its parameters [54].

Geological Storage of CO_2

The purpose of geological CO_2 storage applications [69] is to curb the greenhouse effect by preventing the injected CO_2 from entering the atmosphere of the earth. In this context, our main goal is thus to make long-term predictions about the risk of the injected CO_2 escaping from the reservoir formation [69] and to make predictions on the amount of CO_2 which can be safely injected into a given formation [69]. Like for oil production applications, one of the major challenges of numerical simulations for CO_2 injection problems is the enormous size of the spatial domains involved [69, 55]. Moreover, the uncertainties in the parameters for the material of the geological formation are typically even larger than for petroleum production applications. The primary reasons for these issues is the lower economic incentive of the CO_2 storage application compared to petroleum production.

Another similarity of CO_2 injection and reservoir engineering applications is the complex thermodynamics of the fluid systems involved: Due to the high pressures and relatively high temperatures, both applications potentially require to deal with critical as well as subcritical fluids. Having said that, the fact that these applications usually only involve two phases (gas

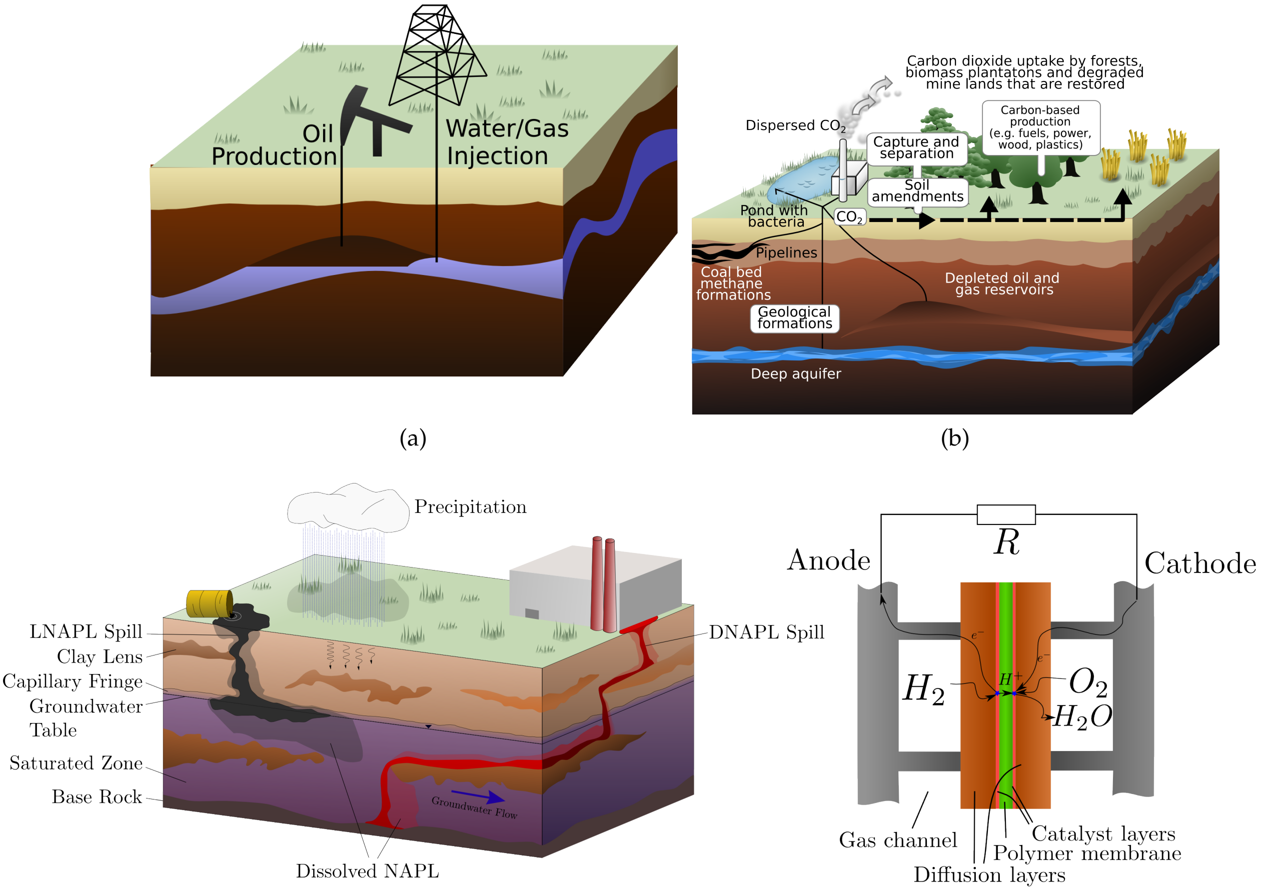

(a) (b)

(c) (d)

Figure 1.1: Important applications for multi-phase flow in porous media for which miscibility is relevant: **(a)** Petroleum production, **(b)** Geological storage of CO_2 (image courtesy of [90]). **(c)** Ground decontamination (image courtesy of [39]), **(d)** Polymer-electrolyte membrane fuel cells.

and brine) instead of the three fluids gas, brine, and oil which are typically considered by reservoir engineering problems simplify matters considerably for CO_2 injection scenarios.

Ground Decontamination

Another topic which exhibits some similarities to oil reservoir engineering are *in-situ* ground remediation methods [64, 61, 22]. Like in petroleum production scenarios, the aim of these applications is to remove hydrocarbons from the subsurface. In the case of ground decontamination methods, the depths at which the contaminants are to be removed are typically much lower compared to the hydrocarbon production applications, which implies much lower pressures and temperatures. Thus, we can often use much simpler thermodynamic relations [61, 22] in the context of such problems. Another difference to reservoir engineering is that the commercial value of the extracted hydrocarbons is usually significantly lower than the monetary costs of the methods to extract them. In fact, the extracted hydrocarbons are typically treated as waste, and thus impose additional costs for their disposal.

Although, in principle, we could apply the methods described in this thesis to ground remediation tasks, such applications are not the focus of this work. Instead, interested readers are referred to the works of OCHS [61] and of CLASS *et al.* [22].

Chemical Engineering

Shifting our attention away from geological applications of compositional multi-phase fluid flows in porous media, a multitude of technical applications for such flows can be found in the field of chemical engineering [42]. One example of such an application that has recently been a focus of research is polymer-electrolyte membrane (PEM) fuel cells [7].

Compared to geological applications, the extend of the spatial domain is usually quite small for chemical engineering applications. In some cases, this property causes issues with the assumption of continuum mechanics which we will use throughout this thesis, and it also implies that, for such applications, molecular diffusion is a much more relevant effect than for geological ones. Other differences include the facts that chemical reactions can obviously not be ignored, and that such applications often involve fast turbulent flows coupled to creeping fluid flows in porous media. This means that besides an adequate description of turbulent flows and flows in porous media, the interaction of these two regimes needs to be described sufficiently well.

Like soil decontamination problems, we will not cover chemical engineering problems in this work, since the focus of this thesis is the description of fluid flows in porous media. Readers interested in chemical engineering applications are referred to JAKOBSEN [42] for the chemical engineering aspects, and to MOSTHAF *et al.* [57] for a coupling approach between the involved flow regimes.

Previous Work

To overcome the problems associates with handling phase transitions in such numerical simulations, several approaches have been proposed to date: The one which we will eventually focus on in this thesis is based on embedding non-linear complementarity functions [48, 41] into the system of equations. We will compare this procedure with two more widely known approaches for handling miscibility effects: One based on locally adapting the set of primary variables depending on which fluids are present at a given location [33, 23], and the black-oil model [19], a model which is tailored for oil reservoir engineering applications. Further, we will also investigate the impact of miscibility effects by ignoring them altogether using the model which is described for example by HELMIG [39].

We note that several other approaches to tackle the issues that occur in compositional multiphase flows in porous media have been proposed. For example, ABADPOUR *et al.* [2] proposed using negative saturation, NOLEN *et al.* [60] described an approach based on flash calculations, and NEUMANN *et al.* [58] use the pressure of each phase to determine the composition of the fluids at phase equilibrium. Like the models which we will investigate here, all of these models exhibit specific challenges, and some of them are restricted in their versatility. For example, a common restriction of many models is to assume only two fluid phases and a fixed number of components.

Structure of this Thesis

Before we can describe compositional multi-phase fluid flows in porous media, we first need to introduce the concept of *continuum mechanics*. Based on this, we derive the fundamental partial differential equations that govern the physical conservation laws for mass, energy, and momentum in the continuum mechanical context in Chapter 2. In the final part of this chapter, we will proceed to adapt these equations for macroscopic porous media flow problems by means of volume averaging.

In Chapter 3, we will look at how the equations derived for macroscopic flow in porous media in Chapter 2 can be made mathematically well-defined in the sense that there exists a unique solution. Besides using thermodynamic constraints, we also have to use semi-empirical closure relations and auxiliary assumptions, so-called *model constraints*.

Proceeding to Chapter 4 we will discuss discretization schemes, *i.e.*, how to transform the resulting system of non-linear partial differential equations into a set of non-linear algebraic equations. Generally, we divide this process into two conceptually independent parts: First we apply a spatial discretization – which we will cover in Section 4.1 – which transforms the partial differential equations into a set of coupled ordinary differential equations. Then a time discretization – discussed in Section 4.2 – transforms this set of ordinary differential equations into a system of coupled non-linear algebraic equations. The solution for these non-linear systems of equations is then calculated using the NEWTON-RAPHSON method. We will see that this method repeatedly linearizes the non-linear systems of equations and solving these linearized systems of equations. Finally, Chapter 4 concludes with a brief overview of linear solvers.

After the discourse on numerics, we will briefly discuss the computer software implementation of these concepts which was used in the context of this thesis in Chapter 5. Chapter 6, then follows with an investigation of the results obtained using this software. The results presented in this chapter are mainly intended to compare the numerical performance and the physical quality of the discretized mathematical models. The discourse on the individual applications is roughly ordered by their complexity: We will first investigate a one-dimensional problem for which a semi-analytical steady-state solution is known; then we will proceed to a synthetic, radially symmetric CO_2 injection problem. Following that, we will compare the NCP fully-compositional model with the black-oil model using the ninth benchmark problem of the society of petroleum engineers (SPE-9) followed by a comparison of the NCP and PVS models using the fifth SPE benchmark problem (SPE-5). Finally, we will conclude the chapter with a discussion of some results of simulations of the Ketzin project, a geological scale, real-world CO_2 storage application.

After this, we will conclude this thesis with a brief summary and some suggestions for possible future work in Chapter 7.

2 Continuum-Scale Fluid Flows

In this chapter, we will discuss the mathematical basis of this work. We first motivate the relevant equations on the continuum scale by introducing the concept of representative elementary volumes (REVs) in Section 2.1, then we will briefly derive the general form of conservation equations in Section 2.2, and finally we will look at the actual conservation equations for mass, momentum, and energy in Section 2.3.

2.1 Representative Elementary Volumes

On a very small scale, all conventional matter composed of atomic particles like molecules, atoms or ions. Thus, one approach we could take to describe the physical world is to directly simulate the interactions between those individual particles. This approach is called *molecular dynamics* [18], and requires to solve an enormously large system of coupled ordinary differential equations—typically one equation per particle.

Using this approach, we are able to approximate the physical world quite well [8], but even when using the largest available supercomputers we need to restrict ourselves to tiny systems because of the enormous number of particles involved. For example, to describe a single droplet of water using this approach, we need to account for approximately 10^{21} molecules (assuming a droplet exhibiting a weight of 0.03 grams). For engineering and geological applications, we thus need to use an alternative approach. Typically, this approach is based on *continuum mechanics*: Instead of defining the physical laws on a molecular scale, we describe the system in terms of average or *bulk* properties of the constituent molecules.

To illustrate this concept, let us look at Figure 2.1: In order to calculate, for example, the *mass density*, *i.e.*, the average mass contained in a given amount of space, one can sum up the weight of the individual molecules and divide it by the size of the considered spatial domain. If we subsequently apply this method to domains of increasing size, we will obtain a graph similar to the one outlined on the right of Figure 2.1. There, the value of the mass density varies considerably for small averaging domains, whilst it becomes nearly constant for large ones. The cause for this is that, for an averaging domain that contains a large number of particles, the addition of an individual molecule does not have a significant effect on the total amount of the mass inside the considered domain. On the large end of the scale, the mass density would start to fluctuate again; this is due to macroscopic effects like variations in pressure. We call spatial averaging domains which domains which are large enough not to change the value of the averaged quantity significantly by the addition or removal of a single particle but small enough to capture macroscopic fluctuations *representative elementary volumes* (REVs).

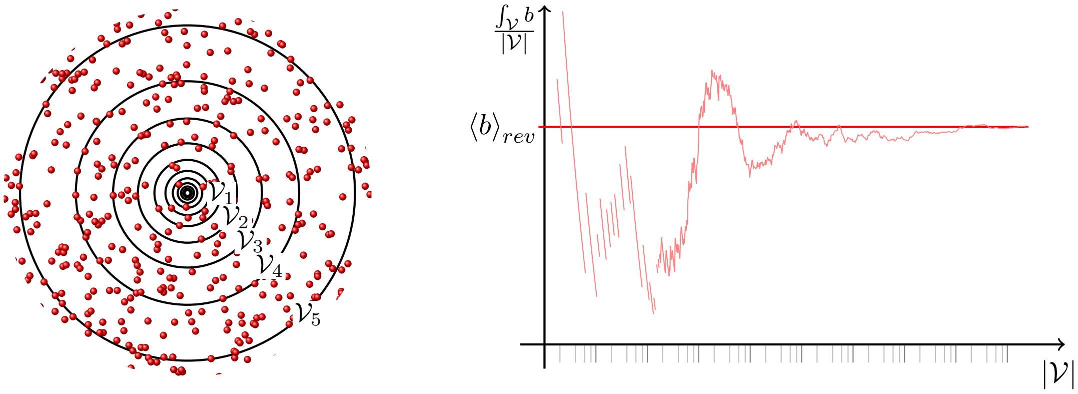

Figure 2.1: Averaging a quantity for successively larger spatial volumes $\mathcal{V}_i$ first yields strongly oscillating values. These oscillations become smaller as the size of the averaging volume gets larger. For very large averaging volumes, oscillations originating from macroscopic variations of the quantity appear (not depicted).

To get a mathematical rigorous definition of the above, we may use the procedure illustrated in Figure 2.2: First we distribute b_i, *i.e.*, the amount of a quantity associated with each particle i in space. This can be achieved using a radial function $\psi_i : \boldsymbol{R}^3 \times \boldsymbol{R} \to \boldsymbol{R}$ which is centered at the position of particle i and which has the property that the integral over $\boldsymbol{R}^3$ is one. We get the following spatial distribution function for the particle i:

$$\bar{b}_i := \psi_i b_i \ .$$

Now, we calculate the sum of these distribution functions, and get

$$\zeta_b := \sum_i \bar{b}_i = \sum_i \psi_i b_i \ ,$$

which represents a density function for the quantity b. If we now apply a convolution using the kernel χ, we get

$$b(\boldsymbol{x}) := \int_{\boldsymbol{R}^3} \zeta_b(\boldsymbol{x} - \boldsymbol{y}) \cdot \chi(\boldsymbol{y}) \, \mathrm{d}\boldsymbol{y} = (\chi * \zeta_b)(\boldsymbol{x}) \ , \tag{2.1}$$

which is a continuum-scale representation of the quantity b as depicted in Figure 2.2c. Note that in order to obtain a smooth result, we need to use a convolution kernel with a sufficiently large spatial support.

Using this abstract framework, we can replicate the procedure depicted in Figure 2.1, by choosing the convolution kernel

$$\chi(\boldsymbol{x}) = \begin{cases} 1/\|\mathcal{V}\| & \text{if } \boldsymbol{x} \in \mathcal{V} \\ 0 & \text{else,} \end{cases}$$

where $\mathcal{V}$ is a sphere with an arbitrary but fixed radius r centered around the origin of the

(a) Particles (b) Density Function ζ_b (c) Continuum-Scale Quantity b

Figure 2.2: Illustration of the conversion from molecular- to continuum-scale: First, the amount of a quantity associated with each particle is distributed around the location of a particle, and we get a density function ζ_b. Then this density function gets averaged at each spatial point by a convolution kernel χ, and we get the continuum-scale quantity b.

coordinate system, *i.e.*,

$$\mathcal{V} := \left\{ \boldsymbol{y} \in \boldsymbol{R}^3 \mid \|\boldsymbol{y}\| < r \right\} .$$

Using Equation 2.1, we can define the following continuum-scale quantities:

Mass Density: We define the mass density ρ as the mass per volume unit:

$$\zeta_\rho := \sum_i \psi_i m_i$$

where m_i is the mass of particle i.

Bulk velocity: The bulk velocity $\boldsymbol{v}$ is defined as the net velocity of the particles, so we use

$$\zeta_{\boldsymbol{v}} := \sum_i \psi_i \boldsymbol{v}_i$$

as the velocity density function.

Pressure: The pressure of an averaging domain $\mathcal{V}$ is given by the linear momentum of the particles inside $\mathcal{V}$. One complication is that pressure is a quantity which is defined via its effect on a surface, but the distribution function which we need is a volumetric quantity. Neglecting external force-fields, we can use the distribution function

$$\zeta_p := \sum_i \psi_i \frac{\|\boldsymbol{v}_i\|^2}{m_i}$$

for pressure according to MARTYNAL, *et al.* [56].

Internal energy: The specific internal energy u is defined as the energy per unit of mass of the particles inside $\mathcal{V}$. On a molecular scale, each particle exhibits kinetic, rotational, and oscillatory energy. For the specific internal energy, this means that we get the density function

$$\zeta_u := \frac{1}{\rho} \sum_i \psi_i \left(\frac{1}{2} m_i \|\boldsymbol{v}_i\|^2 + E_{\mathrm{r},i} + E_{\mathrm{o},i} \right)$$

where $E_{\mathrm{r},i}$ and $E_{\mathrm{o},i}$ are the energies of particle i due to its rotation and its oscillation.

The hypothesis which we now need to make for continuum mechanics is that the properties of interest of the physical system can be described in terms of quantities that result from a convolution of the form given by Equation 2.1. In this context, we should remember that, if the filter kernel χ exhibits a too small or a too large spatial support, this assertion may not be valid.

Scales

For gases, we can define the minimum size of the support of the convolution kernel χ using the KNUDSEN number Kn [20], which is defined as

$$\mathrm{Kn} := \frac{\lambda}{L} \ ,$$

where λ is the mean free path between molecules, and L is the characteristic length of the spatial support of the convolution kernel. For air at standard conditions, the mean free path is approximately $\lambda \approx 60 \cdot 10^{-9}\ \mathrm{m}$. Assuming that the spatial support of a spherical convolution kernel is sufficiently large if it averages about 5000 molecules, we need to use an averaging volume with a diameter of $L \approx 1.3 \cdot 10^{-6}\,\mathrm{m}$ which corresponds to a KNUDSEN number of $\mathrm{Kn} \approx 0.05$. The Knudsen number for the same averaging domain is typically considerably smaller for liquids, as the average distance of the molecules of the substance is much smaller in this case.

The largest valid size of the characteristic length depends on the properties of the considered setup more strongly than the smallest: If the system exhibits largely uniform conditions, the maximum diameter of the support can be in the magnitude of lightyears (for example in galaxy-scale problems), or it might be at the submillimeter scale (for example in many technical applications).

2.2 Continuum-Scale Conservation Equations

Within the context of this work, we will consider the conservation of the three physical quantities mass, momentum, and energy. Since the conservation equations for these are very similar, we will first derive a common form of them in this section. For this derivation, we will assume that the continuum hypothesis of the previous section holds, *i.e.*, that conservation of these quantities can be described on the continuum-scale.

We start our endeavor by assuming an infinitely large spatial domain. Next, we let $\omega \subset \boldsymbol{R}^3$ be an arbitrary, simply connected, bounded, and open subset of the spatial domain. Further,

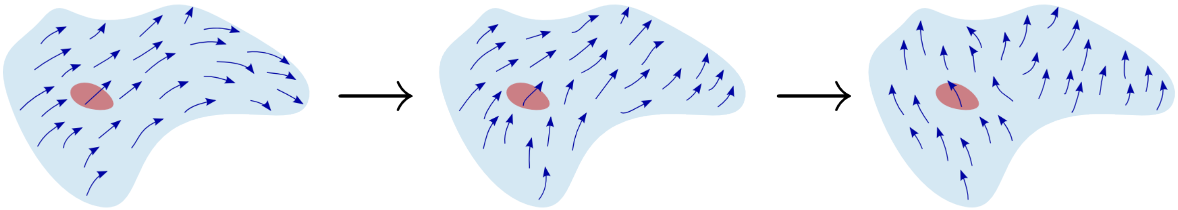

(a) Eulerian

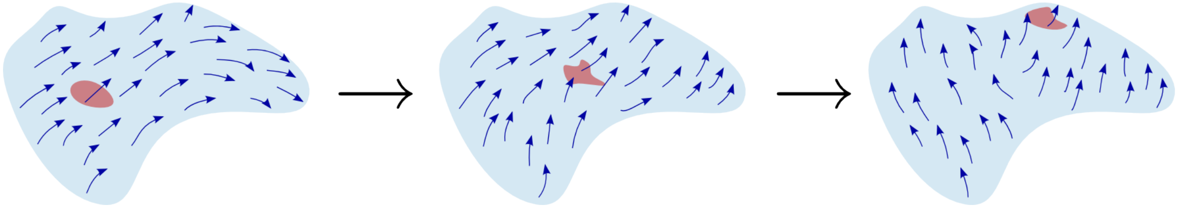

(b) Lagrangian

Figure 2.3: The Eulerian and the Lagrangian points of view: While in the Eulerian point of view, the observed volume stays constant in time, it is transported along with the conserved material in the Lagrangian point of view.

let us now assume that ω "tracks" the quantity b which is to be conserved. In this case, at any given time t, the total amount of the quantity B contained within the volume is given by

$$B(t) = \int_{\omega(t)} b(\boldsymbol{x}, t)\,\mathrm{d}\boldsymbol{x}\ .$$

Since b is conserved, its amount within the tracked volume $\omega(t)$ is constant. This leads us to

$$\frac{\mathrm{d}}{\mathrm{d}t} B(t) = \frac{\mathrm{d}}{\mathrm{d}t} \int_{\omega(t)} b(\boldsymbol{x}, t)\,\mathrm{d}\boldsymbol{x} = 0\ .$$

In a slightly more general setting, we add or remove the conserved quantity at a given rate, which we can describe by a *source term* $\bar{q}$:

$$\frac{\mathrm{d}}{\mathrm{d}t} \int_{\omega(t)} b(\boldsymbol{x}, t)\ \mathrm{d}\boldsymbol{x} = \int_{\omega(t)} \bar{q}(\boldsymbol{x}, t)\ \mathrm{d}\boldsymbol{x}. \tag{2.2}$$

We may interpret Equation 2.2—which was introduced by Joseph-Louis de Lagrange—as the continuum-scale conservation equation for an observer that moves with the conserved quantity b. A different point of view is the one taken by Leonhard Euler: In contrast to Lagrange, Euler always observed the same part of space over time as illustrated in Figure 2.3. We can derive the Eulerian form of any conservation equation from the Lagrangian form (2.2) by taking advantage of the Reynolds transport theorem [72]

$$\frac{\mathrm{d}}{\mathrm{d}t} \int_{\omega(t)} b\,\mathrm{d}\boldsymbol{x} = \int_{\omega(t_0)} \left(\frac{\mathrm{d}}{\mathrm{d}t} b + b \operatorname{div} \boldsymbol{v} \right) \mathrm{d}\boldsymbol{x}$$

which enables us to transpose the ordering of the time derivative and the spatial integration.

Here, t_0 represents an arbitrary but fixed reference time, and $\boldsymbol{v} = \partial \boldsymbol{x}/\partial t$ is the *velocity*[1] of the transported quantity at a given location $\boldsymbol{x}$ at time t. Using this relation, we can transform Equation 2.2 into

$$\int_{\omega(t_0)} \left(\frac{\mathrm{d}}{\mathrm{d}t} b + b \operatorname{div} \boldsymbol{v} \right) \mathrm{d}\boldsymbol{x} = \int_{\omega(t_0)} \left(\frac{\mathrm{d}}{\mathrm{d}t} \bar{q} + \bar{q} \operatorname{div} \boldsymbol{v} \right) \mathrm{d}\boldsymbol{x} \ .$$

In this equation, instead of specifying a source term $\bar{q}$ which tracks the volume occupied by the conserved quantity, we can also use a source term q which is fixed in space, so that we get

$$\int_{\omega(t_0)} \left(\frac{\mathrm{d}}{\mathrm{d}t} b + b \operatorname{div} \boldsymbol{v} \right) \mathrm{d}\boldsymbol{x} = \int_{\omega(t_0)} q \, \mathrm{d}\boldsymbol{x} \ . \tag{2.3}$$

In order to keep the observed volume constant over time, we also have to transform the total time derivative of b in Equation 2.3. For this, we can take advantage of the convective derivative

$$\frac{\mathrm{d}b}{\mathrm{d}t} = \frac{\partial b}{\partial t} + \boldsymbol{v} \cdot \mathbf{grad}\ b$$

and transform Equation 2.3 to

$$\int_{\omega(t_0)} \left(\frac{\partial}{\partial t} b + \boldsymbol{v} \cdot \mathbf{grad}\ b + b \operatorname{div} \boldsymbol{v} \right) \mathrm{d}\boldsymbol{x} = \int_{\omega(t_0)} q \, \mathrm{d}\boldsymbol{x} \ . \tag{2.4}$$

Finally, taking advantage of the vectorial product rule

$$\operatorname{div}(b\boldsymbol{v}) = \boldsymbol{v} \cdot \mathbf{grad}\ b + b \operatorname{div} \boldsymbol{v} \ ,$$

we get

$$\int_{\omega(t_0)} \left(\frac{\partial}{\partial t} b + \operatorname{div}(b\boldsymbol{v}) \right) \mathrm{d}\boldsymbol{x} = \int_{\omega(t_0)} q \, \mathrm{d}\boldsymbol{x} \ , \tag{2.5}$$

the *integral* EULERIAN form of the conservation equation of any quantity b which is to be conserved. To express this in *differential* form, we remember that $\omega(t_0)$ is an *arbitrary* simply connected, bounded, and open subset of the domain. This means that Equation 2.5 is valid pointwise, provided that b is a $\mathcal{C}^1$-continuous function. In other words, we can drop the integrals on both sides of Equation 2.5, and get

$$\frac{\partial b}{\partial t} + \operatorname{div}(b\boldsymbol{v}) = q \ . \tag{2.6}$$

If not explicitly stated otherwise, we will use this form for conservation equations during the rest of this thesis.

---

[1] In the molecular sense, $\boldsymbol{v}$ is the bulk velocity.

2.3 Conserved Quantities

In this section, we will adapt the generic EULERIAN conservation equation (2.6) to specifically express conservation of the three quantities mass, momentum, and energy. In this context, we will not consider any other physical conservation quantity like, for example, electric charge. We will also strictly stay within the bounds of classical mechanics, so advanced concepts like the equivalence of mass and energy will not be considered here.

2.3.1 Conservation of Mass

To obtain an equation for the conservation of mass, we need to insert the mass density ρ into Equation 2.5. This yields

$$\frac{\partial \rho}{\partial t} + \mathrm{div}(\rho \boldsymbol{v}) = q_{\mathrm{mass}} \ . \tag{2.7}$$

Alternatively, we may formulate Equation 2.7 in terms of conservation of molecules instead of mass, which leads to

$$\frac{\partial \rho_{\mathrm{mol}}}{\partial t} + \mathrm{div}(\rho_{\mathrm{mol}} \boldsymbol{v}) = q_{\mathrm{mol}} \ , \tag{2.8}$$

for the conservation the total mass and to

$$\frac{\partial x^{\kappa} \rho_{\mathrm{mol}}}{\partial t} + \mathrm{div}(x^{\kappa} \rho_{\mathrm{mol}} \boldsymbol{v}) = q^{\kappa}_{\mathrm{mol}} \tag{2.9}$$

for the conservation of the mass of an individual component κ.

Molecular Diffusion

Since we derived Equation 2.9 using bulk velocities, it does not account for the mixing of molecular particles due to their random BROWNIAN motion. On the continuum-scale, we can express this mixing by an additional flux term of the form

$$\mathcal{F}^{\kappa}_{\mathrm{D}} := -D^{\kappa} \mathbf{grad}\ x^{\kappa}$$

where D^{κ} describes the *molecular diffusion coefficient* of component κ [68]. This means that we get the mass conservation equation

$$\frac{\partial x^{\kappa} \rho_{\mathrm{mol}}}{\partial t} + \mathrm{div}(x^{\kappa} \rho_{\mathrm{mol}} \boldsymbol{v} - D^{\kappa} \mathbf{grad}\ x^{\kappa}\ ) = q^{\kappa}_{\mathrm{mol}} \tag{2.10}$$

for each individual component κ.

2.3.2 Conservation of Momentum

Analogous to the mass balance, using the volumetric momentum $\rho \boldsymbol{v}$ in Equation 2.6 leads us to the conservation equations for momentum. Since the velocity $\boldsymbol{v}$ is a vectorial quantity, the result is a bit more complicated than Equation 2.7:

$$\frac{\partial \rho \boldsymbol{v}}{\partial t} + \operatorname{div}(\rho \boldsymbol{v} \otimes \boldsymbol{v}) = \boldsymbol{e} + \boldsymbol{q}_{\mathrm{mom}} \ . \tag{2.11}$$

For this equation, we also used a term $\boldsymbol{e}$ capturing forces and a term $\boldsymbol{q}_{\mathrm{mom}}$ for the remaining sources and sinks of momentum in the system.

We can reformulate Equation 2.11 by taking advantage of the product rule for the time derivative

$$\frac{\partial \rho \boldsymbol{v}}{\partial t} = \boldsymbol{v}\frac{\partial \rho}{\partial t} + \rho \frac{\partial \boldsymbol{v}}{\partial t}$$

and for the divergence term

$$\operatorname{div}(\rho \boldsymbol{v} \otimes \boldsymbol{v}) = \rho \boldsymbol{v} \cdot \mathbf{grad}\ \boldsymbol{v} + \boldsymbol{v} \operatorname{div}(\rho \boldsymbol{v}) \ ,$$

and get

$$\boldsymbol{v}\ \frac{\partial \rho}{\partial t} + \rho \frac{\partial \boldsymbol{v}}{\partial t} + \rho \boldsymbol{v} \cdot \mathbf{grad}\ \boldsymbol{v} + \boldsymbol{v}\ \operatorname{div}(\rho \boldsymbol{v}) = \boldsymbol{e} + \boldsymbol{q}_{\mathrm{mom}} \ .$$

Reordering the left-hand side yields

$$\rho \frac{\partial \boldsymbol{v}}{\partial t} + \rho \boldsymbol{v} \cdot \mathbf{grad}\ \boldsymbol{v} + \boldsymbol{v} \left(\frac{\partial \rho}{\partial t} + \operatorname{div}(\rho \boldsymbol{v}) \right) = \boldsymbol{e} + \boldsymbol{q}_{\mathrm{mom}} \ . \tag{2.12}$$

In Equation 2.12, we now notice that the third additive term corresponds to the left-hand side of the mass conservation Equation 2.7, but multiplied with the velocity. Assuming that the source term for mass q_{mass} is zero leads us to

$$\rho \frac{\partial \boldsymbol{v}}{\partial t} + \rho \boldsymbol{v} \cdot \mathbf{grad}\ \boldsymbol{v} = \boldsymbol{e} + \boldsymbol{q}_{\mathrm{mom}} \ . \tag{2.13}$$

Otherwise – *i.e.*, if we do not assume the source term of the mass balance equation to be zero – the third term of Equation 2.12 can be brought to the right-hand side and integrated into the momentum source term $\boldsymbol{q}_{\mathrm{mom}}$. This means that the general form of the equation for the conservation of momentum is given by Equation 2.13.

Let us now have a closer look at the force term $\boldsymbol{e}$ of the right-hand side of Equation 2.13. It should be clear that we can split $\boldsymbol{e}$ into a term $\boldsymbol{f}$ capturing the forces which are exercised upon the surface of a considered domain, and a term $\boldsymbol{h}$, representing forces which attack in the interior:

$$\boldsymbol{e} = \boldsymbol{f} + \boldsymbol{h}$$

The former are called *surface forces* and are exerted on the material by its environment, the latter are called *body forces* and are caused by force fields like gravity or electromagnetism.

It can be shown [72] that the surface forces $\boldsymbol{f}$ can be expressed as

$$\boldsymbol{f} = \operatorname{div} \boldsymbol{\tau} \tag{2.14}$$

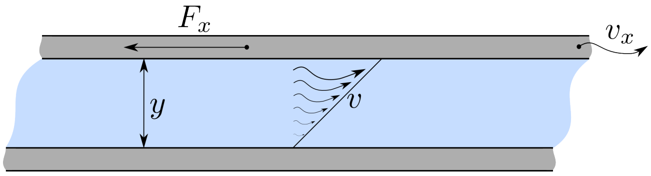

Figure 2.4: The COUETTE thought experiment comprises two infinitely large parallel planar plates with the space between them occupied by a fluid; in the experiment, the upper plate moves with a velocity of v_x relative to the lower one. At each plate, the observed force per area F_x is proportional to the relative velocity of the plates v_x and anti-proportional to the distance y between the plates. The proportionality coefficient μ is determined by the fluid between the two plates, and is called the *dynamic viscosity*.

where $\boldsymbol{\tau} \in \boldsymbol{R}^{3\times 3}$ is called *stress tensor*. Taking advantage of Equation 2.14 and neglecting all body forces except gravity, we get

$$\rho\frac{\partial \boldsymbol{v}}{\partial t} + \rho\boldsymbol{v} \cdot \mathbf{grad}\ \boldsymbol{v} = \operatorname{div} \boldsymbol{\tau} + \rho\,\boldsymbol{g} + \boldsymbol{q}_{\mathrm{mom}} \tag{2.15}$$

as the momentum balance equation where $\boldsymbol{g}$ is the gravitational acceleration.

2.3.3 NEWTONIAN Fluids

For NEWTONIAN fluids, we can substantiate the momentum conservation Equation 2.15 as follows: First, we assume that the stress tensor $\boldsymbol{\tau}$ can be split into

$$\boldsymbol{\tau} = -p\boldsymbol{I} + \boldsymbol{T} \tag{2.16}$$

where the term $p\boldsymbol{I}$ represents pressure, and the term $\boldsymbol{T}$ represents the shear stresses [9]. The reason why the term $p\boldsymbol{I}$ is negative is that the tensor $\boldsymbol{\tau}$ represents the stresses which act upon the material within the observed domain, and not the stresses which this material exercises upon its environment.

Inserting Equation 2.16 into the momentum balance equation (2.15), we get

$$\rho\frac{\partial \boldsymbol{v}}{\partial t} + \rho\boldsymbol{v} \cdot \mathbf{grad}\ \boldsymbol{v} = -\mathbf{grad}\ p + \operatorname{div} \boldsymbol{T} + \rho\boldsymbol{g} + \boldsymbol{q}_{\mathrm{mom}}\ . \tag{2.17}$$

We now consider the fact that the shear stress tensor $\boldsymbol{T}$ of NEWTONIAN fluids does not depend on the absolute deformation of the material relative to its initial position, but only on the rate at which the fluid gets displaced relative to its environment as illustrated in Figure 2.4. Since $\boldsymbol{T}$ needs to be symmetric [9], we get a shear stress tensor $\boldsymbol{T}$ of the form

$$\boldsymbol{T}_{ij} = \mu\left(\frac{\partial \boldsymbol{v}_j}{\partial \boldsymbol{x}_i} + \frac{\partial \boldsymbol{v}_i}{\partial \boldsymbol{x}_j}\right) + \delta_{ij}\lambda \operatorname{div} \boldsymbol{v}\ , \tag{2.18}$$

using the proportionality coefficients $\mu \in \boldsymbol{R}^{+}$ and $\lambda \in \boldsymbol{R}$, with δ_{ij} being the KRONECKER delta. The factor λ captures the stress due to expansion or contraction of the volume of the fluid. Since there are many difficulties for determining λ, it is usually either assumed [9] to be zero as in the following, or $-3\mu/2$.

If we take advantage of Equation 2.18 in the momentum balance equation (2.17), we get

$$\rho\frac{\partial \boldsymbol{v}}{\partial t} + \rho\boldsymbol{v}\cdot\mathbf{grad}\,\boldsymbol{v} = -\mathbf{grad}\,p + \mathrm{div}\big(\mu\left(\mathbf{grad}\,\boldsymbol{v} + (\mathbf{grad}\,\boldsymbol{v})^T\right)\big) \qquad (2.19)$$

$$+\,\rho\,\boldsymbol{g} + \boldsymbol{q}_{\mathrm{mom}}\ ,$$

the NAVIER-STOKES equations for compressible NEWTONIAN fluids.

For incompressible fluids with constant dynamic viscosity we can simplify Equation 2.19 further: First, we use the relation

$$\mathrm{div}\,(\mathbf{grad}\,\boldsymbol{v})^T = \mathbf{grad}\;\mathrm{div}\,\boldsymbol{v}$$

and then consider the fact that $\mathrm{div}\,\boldsymbol{v}$ is identical to zero if the density ρ is constant. We thus get

$$\rho\frac{\partial \boldsymbol{v}}{\partial t} + \rho\boldsymbol{v}\cdot\mathbf{grad}\,\boldsymbol{v} = -\mathbf{grad}\,p + \mu\,\mathrm{div}\,\mathbf{grad}\,\boldsymbol{v} + \rho\,\boldsymbol{g} + \boldsymbol{q}_{\mathrm{mom}} \qquad (2.20)$$

as the conservation equation for momentum.

2.3.4 Creeping Flows

For creeping incompressible flows, we can also neglect the inertia term of the NAVIER-STOKES Equation 2.20, and get the STOKES equation

$$-\,\mathbf{grad}\,p + \mu\;\mathrm{div}\,\mathbf{grad}\,\boldsymbol{v} + \rho\,\boldsymbol{g} + \boldsymbol{q}_{\mathrm{mom}} = 0\ . \qquad (2.21)$$

In order for this assumption to be applicable, we need to be able to define what "creeping" means. Usually, this property is defined using the REYNOLDS number

$$\mathrm{Re} := \frac{v_{\mathrm{c}}\,L_{\mathrm{c}}}{\nu_{\mathrm{c}}}$$

where v_{c} is the *characteristic velocity* of the considered physical system (for example, the absolute value of the maximum velocity of the fluid), L_{c} represents the *characteristic length* of the system (for example, the diameter of the pipe for pipe-flow problems), and $\nu_{\mathrm{c}} = \mu_{\mathrm{c}}/\rho_{\mathrm{c}}$ is the *characteristic kinematic viscosity* of the fluid. We now define a flow as "creeping" if it exhibits a REYNOLDS number smaller than 1.

Since the characteristic length and the characteristic velocity can be chosen arbitrarily, we cannot assign too much meaning to the absolute value of the REYNOLDS number. Having said that, for many important classes of flow problems there are standard conventions of how to determine L_{c} and v_{c}. This means that we can compare the absolute value of the REYNOLDS number only *within a given class of flow problems*. Such classes include, for example, pipe-flows or flows around airfoils.

2.3.5 Conservation of Energy

The last conservation quantity which we will consider in this work is energy. We may think of energy as a scalar quantity that has kinetic, potential, and thermal contributions. Assuming that the gravitational acceleration is constant and that gravity is the only body force, we can express conservation of energy [9] as

$$\frac{\partial}{\partial t}\rho\left(u+\frac{1}{2}\|\boldsymbol{v}\|^2+\boldsymbol{z}\cdot\boldsymbol{g}\right)+\operatorname{div}(h\rho\boldsymbol{v}+\boldsymbol{\tau}\boldsymbol{v}-\lambda\,\mathbf{grad}\;T)=q_{\text{energy}}-\rho\boldsymbol{v}\cdot\boldsymbol{g} \tag{2.22}$$

where u is the specific internal energy of the substance as described in Section 2.1, $\boldsymbol{z}=\boldsymbol{x}-\boldsymbol{x}_{\text{ref}}$ is the distance of a spatial position relative to an arbitrary but fixed reference point in space, λ is the heat conduction coefficient, $h=u+p/\rho$ is the *specific enthalpy* of the substance, and q_{energy} is the source or sink term for energy.

If we neglect the kinetic energy and friction, we get

$$\frac{\partial}{\partial t}\rho\left(u+\boldsymbol{z}\cdot\boldsymbol{g}\right)+\operatorname{div}(h\rho\boldsymbol{v}-\lambda\,\mathbf{grad}\;T)=q_{\text{energy}}-\rho\boldsymbol{v}\cdot\boldsymbol{g}$$

as the equation for the conservation of energy. Amongst others, these assumptions are valid for creeping fluid flows. If we also assume that the considered system only exhibits small variations of its height $\boldsymbol{z}$, we get

$$\frac{\partial\,\rho u}{\partial t}+\operatorname{div}(h\rho\boldsymbol{v}-\lambda\,\mathbf{grad}\;T)=q_{\text{energy}}\;. \tag{2.23}$$

The fact that we need to consider the specific internal energy u in the accumulation term but the specific enthalpy h in the flux term is due to the fact that transported material needs to displace other material before it can occupy a given volume. As illustrated in Figure 2.5, the energy required to displace the other material is equivalent to the volume occupied by the transported material times the force with which the displaced material pushes back. In fluids this "push-back force" is the pressure that the displaced material exercises upon the surface of the transported material.

Dissipation

The third law of thermodynamics states that, in a closed system, all spontaneously occuring processes increase the entropy of the system as a whole[2]. In the context of the conservation of energy, this means that some energy is always converted into heat, *i.e.*, internal energy. In Equation 2.23, we account for this effect by transporting enthalpy, while accumulating only the internal energy. To illustrate the point, let us consider Figure 2.5: There, some material gets transported from the left to the right of a cylinder. The energy which is on the right side at the end is the internal energy which the material originally possessed when it was on

---

[2] There might be parts of the system where entropy is reduced, but this is always compensated by additional entropy elsewhere.

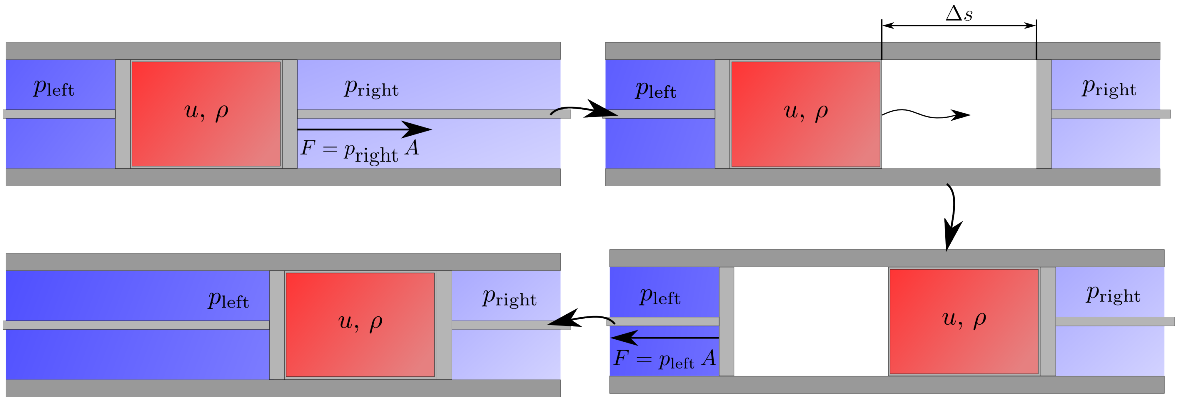

Figure 2.5: To move the substance with the specific internal energy u from the left to the right, one has to displace the material on the right of the cylinder. This can be imagined as a four-step process: First, the right piston creates a vacuum, then the vessel with the substance moves to the right. The work required by the piston to create the vacuum is called the volume changing work $W_{\text{v}} = \int_{s_0}^{s_0+\Delta s} F \ \text{d}s$. Assuming a constant cross-section A of the cylinder and constant pressure p_{right} of the environment of the right side, this is equivalent to $W_{\text{v,right}} = \Delta s A \, p_{\text{right}}$. After the substance has been transferred to the right, the left piston can occupy the void space and "recovers" the volume changing work $W_{\text{v,left}} = \Delta s A \, p_{\text{left}}$.

the left side. But in addition, a piston had to displace the material originally occupying the space on the right side, which requires a physical work of $\Delta s \, A \, p_{\text{right}}$ to be done. Assuming the pressure to be constant at a fixed spatial location, *i.e.*, the moved substance reduces its pressure from p_{left} to p_{right}, requires work of $(p_{\text{left}} - p_{\text{right}}) \, A \, \Delta s$. Since energy is conserved, this work gets converted into internal energy if the transport of material does not happen in a closed vessel that cannot expand.

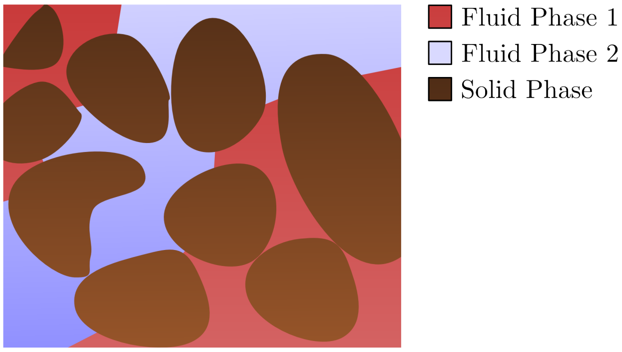

Figure 2.6: An example of a porous medium where two fluid phases are co-located with a solid.

2.4 Porous Media

In this section, we will adapt the conservation equations for fluids, *i.e.*, Equations 2.7, 2.20 and 2.23 to multi-phase flows in porous media. The situation which we face is depicted in Figure 2.6: A solid shares the available space with multiple fluids. In the following, we aim at making macroscopic statements on the behavior of the fluids, assuming that the solid phase is rigid.

To allow such quantitative statements, we will first look at volume averaging. Volume averaging is an upscaling technique which allows us to consider the flow and transport processes without having to know the geometry of the solid-fluid interface. Thus, the resulting equations require much less information, and solving them is much less elaborate than solving the micro-scale equations. After introducing the volume averaging technique, we will sketch how to derive the volume averaged conservation equations for the three considered conservation quantities mass, momentum, and energy. After this, we will give a brief historical overview and discuss how the resulting relation which governs the conservation of momentum was discovered experimentally.

2.4.1 Volume Averaging

To directly solve Equations 2.7, 2.21, and 2.23 we need to provide the geometry of the solid phase of the porous medium. Generally, this is infeasible, but it turns out that in order to get meaningful macroscopic statements about the fluid behavior in such a medium, we usually can avoid having to obtain this information. Equations which do not require the topology of the solid are generally called to be on the *laboratory-scale*, the *macro-scale*, or on the DARCY-*scale*.

Before we can derive these macro-scale equations, we first need to introduce a few concepts based on the definitions of WHITAKER [89]:

- The *characteristic set* $\Omega_\alpha \subseteq \Omega$ of a phase α is the set of points of the spatial domain $\Omega \subseteq \boldsymbol{R}^3$

for which phase α is present, *i.e.,*

$$\Omega_\alpha := \{\boldsymbol{x} \in \Omega \mid \text{Position } \boldsymbol{x} \text{ is occupied by the phase } \alpha\} \ .$$

- We define the *characteristic function* χ_α of a phase α as the function that is one for the part of the domain where the fluid phase α is present, and zero elsewhere, *i.e.,*

$$\chi_\alpha(\boldsymbol{x}) := \begin{cases} 1 & \text{if } \boldsymbol{x} \in \Omega_\alpha \\ 0 & \text{else.} \end{cases}$$

- The *averaging volume* $\mathcal{V}$ for any point $\boldsymbol{x} \in \Omega$ is the sphere of points which are closer to $\boldsymbol{x}$ than an arbitrary but fixed radius r, *i.e.,*

$$\mathcal{V}(\boldsymbol{x}) := \{\boldsymbol{y} \in \Omega \mid \|\boldsymbol{x} - \boldsymbol{y}\| < r\} \ .$$

- The *intrinsic averaging volume* $\mathcal{V}_\alpha$ of a phase α for any point $\boldsymbol{x} \in \Omega$ is the set of points which are in $\mathcal{V}(\boldsymbol{x})$ and in the characteristic set of α, *i.e.,*

$$\mathcal{V}_\alpha(\boldsymbol{x}) := \mathcal{V}(\boldsymbol{x}) \cap \Omega_\alpha \ .$$

- The *interior boundary* $\partial\mathcal{V}_{s\alpha}$ of the averaging volume $\mathcal{V}_\alpha$ of a fluid phase α is the set of points that is on the boundary of $\mathcal{V}_\alpha$ but not on the boundary of $\mathcal{V}$, *i.e.,*

$$\partial\mathcal{V}_{s\alpha} := \partial\mathcal{V}_\alpha \setminus \partial\mathcal{V} \ ,$$

  where the lower index $\langle\cdot\rangle_s$ indicates the solid phase.

- The *porosity* ϕ of the porous medium is defined as

$$\phi := 1 - \frac{\|\mathcal{V}_s\|}{\|\mathcal{V}\|} \ ,$$

  and represents volume fraction of the pores, *i.e.,* the fraction of space which can be occupied by fluids.

- The *saturation* S_α of a fluid phase α is the fraction of the pore space occupied by the fluid phase, *i.e.,*

$$S_\alpha := \frac{\|\mathcal{V}_\alpha\|}{\phi\,\|\mathcal{V}\|} \ .$$

- The *phase average* $\langle b_\alpha\rangle$ of a quantity b_α which is associated with the phase α is defined as

$$\langle b_\alpha\rangle(\boldsymbol{x}) := \frac{1}{\|\mathcal{V}(\boldsymbol{x})\|} \int_{\mathcal{V}_\alpha(\boldsymbol{x})} b_\alpha(\boldsymbol{y})\,\mathrm{d}\boldsymbol{y} \ . \tag{2.24}$$

Note, that we can consider Equation 2.24 as a convolution of $b \cdot \chi_\alpha$ with the kernel

$$m(\boldsymbol{y}) = \begin{cases} \frac{1}{\|\mathcal{V}\|} & \text{if } \|\boldsymbol{y}\| < r \\ 0 & \text{else.} \end{cases}$$

This means that we can think of the procedures discussed in this section as analogous to the upscaling procedure from molecular to continuum-scale which we sketched in Section 2.1.

- The *intrinsic phase average* $\langle b_\alpha \rangle^\alpha$ of the quantity b_α is the average of b_α considering only the points where the phase α is present, *i.e.*,

$$\langle b_\alpha \rangle^\alpha(\boldsymbol{x}) := \frac{1}{\|\mathcal{V}_\alpha(\boldsymbol{x})\|} \int_{\mathcal{V}_\alpha(\boldsymbol{x})} b_\alpha(\boldsymbol{y}) \, \mathrm{d}\boldsymbol{y} \, . \tag{2.25}$$

The phase average and the intrinsic phase average are thus connected by the relation

$$\langle b_\alpha \rangle^\alpha = \frac{\|\mathcal{V}\|}{\|\mathcal{V}_\alpha\|} \langle b_\alpha \rangle = \frac{\langle b_\alpha \rangle}{\phi S_\alpha} \, .$$

The Spatial Averaging Theorem

Using these tools, we can now average the micro-scale conservation Equations 2.7, 2.21, and 2.23. One problem which occurs during this procedure is that we will get averages of gradients in the results but that we would rather like to express the equations in terms of gradients of averages.

We can overcome this issue using the *Spatial Averaging Theorem* [89, 67]

$$\langle \mathbf{grad} \, b_\alpha \rangle = \mathbf{grad} \, \langle b_\alpha \rangle + \frac{1}{\|\mathcal{V}\|} \int_{\partial \mathcal{V}_{s\alpha}} b_\alpha \, \boldsymbol{n} \, \mathrm{d}\boldsymbol{y} \, , \tag{2.26}$$

where $\boldsymbol{n}$ is the outer unit normal vector of $\mathcal{V}_\alpha$ at position $\boldsymbol{y}$.

We will also get an average of the divergence instead of the divergence of averaged quantities. In this case, we can substitute the gradients in Equation 2.26 by divergences [89, 67], and get

$$\langle \operatorname{div} \boldsymbol{b}_\alpha \rangle = \operatorname{div} \langle \boldsymbol{b}_\alpha \rangle + \frac{1}{\|\mathcal{V}\|} \int_{\partial \mathcal{V}_{s\alpha}} \boldsymbol{b}_\alpha \cdot \boldsymbol{n} \, \mathrm{d}\boldsymbol{y} \, . \tag{2.27}$$

Conservation of Mass

Now, let us have a closer look at the mass conservation Equation 2.7. Applying Equations 2.26 and 2.24 to it, we get

$$\begin{aligned}\left\langle \frac{\partial \rho_\alpha}{\partial t} + \operatorname{div}(\rho_\alpha \boldsymbol{v}_\alpha) \right\rangle &= \frac{\partial \langle \rho_\alpha \rangle}{\partial t} + \operatorname{div}(\langle \rho_\alpha \boldsymbol{v}_\alpha \rangle) \\ &\quad + \frac{1}{\|\mathcal{V}\|} \int_{\partial \mathcal{V}_{s\alpha}} \boldsymbol{n} \cdot \rho_\alpha \boldsymbol{v}_\alpha \mathrm{d}\boldsymbol{y} \\ &= \langle q_{\text{mass},\alpha} \rangle \ .\end{aligned}$$

If we now assume a no-slip condition for the internal boundaries of the averaging volume, *i.e.*, $\boldsymbol{v}_\alpha = 0$ on $\partial \mathcal{V}_{s\alpha}$, we get

$$\frac{\partial \langle \rho_\alpha \rangle}{\partial t} + \operatorname{div}(\langle \rho_\alpha \boldsymbol{v}_\alpha \rangle) = \langle q_{\text{mass},\alpha} \rangle$$

as the macro-scale equation for the conservation of mass.

Still, the term inside the divergence is the average of density times velocity, but we would like to formulate the mass conservation equation in terms of the product of the two averages. To achieve this, we use the GRAY decomposition [35] which expresses any quantity b_α as the sum of its intrinsic phase average $\langle b_\alpha \rangle^\alpha$, and of its deviation $\tilde{b}_\alpha$:

$$b_\alpha = \langle b_\alpha \rangle^\alpha + \tilde{b}_\alpha \ .$$

We now observe that the average of the deviation term $\tilde{b}_\alpha$ is zero, and we can thus write the mass conservation equation as

$$\frac{\partial \phi S_\alpha \langle \rho_\alpha \rangle^\alpha}{\partial t} + \operatorname{div}(\langle \rho_\alpha \rangle^\alpha \langle \boldsymbol{v}_\alpha \rangle) = \langle q_{\text{mass},\alpha} \rangle \ .$$

If we repeat this procedure for Equation 2.10, the compositional form of mass conservation, we get

$$\frac{\partial \phi S_\alpha \langle x_\alpha^\kappa \rangle^\alpha \langle \rho_{\text{mol},\alpha} \rangle^\alpha}{\partial t} + \operatorname{div}\big(\langle x_\alpha^\kappa \rangle^\alpha \langle \rho_{\text{mol},\alpha} \rangle^\alpha \langle \boldsymbol{v}_\alpha \rangle - D_{\text{pm},\alpha}^\kappa \mathbf{grad}\ \langle x_\alpha^\kappa \rangle^\alpha\big) = \langle q_\alpha^\kappa \rangle$$

for the conservation of each component in fluid phase α. In this case, we need to adapt the molecular diffusion coefficients D_α^κ to account for the presence of the solid phase.

If there is more than a single component, we have to preserve each in the whole porous medium. This implies that we need to sum up the component conservation equations over all phases in order to get an equation that describes the conservation of the component for the whole multi-phase system. This leads to

$$\sum_\alpha \frac{\partial \phi S_\alpha \langle x^\kappa_\alpha \rangle^\alpha \langle \rho_{\mathrm{mol},\alpha} \rangle^\alpha}{\partial t} + \sum_\alpha \operatorname{div}\left(\langle x^\kappa_\alpha \rangle^\alpha \langle \rho_{\mathrm{mol},\alpha} \rangle^\alpha \langle \boldsymbol{v}_\alpha \rangle - D^\kappa_{\mathrm{pm},\alpha} \mathbf{grad}\, \langle x^\kappa_\alpha \rangle^\alpha\right) = \sum_\alpha \langle q^\kappa_\alpha \rangle \; . \tag{2.28}$$

Conservation of Momentum

The procedure for conservation of momentum is much more elaborate than the one for the conservation of mass. Thus, we will only sketch it here and refer the interested reader to WHITAKER [89] for further details.

First, we neglect compressibility and the inertia terms of the NAVIER-STOKES equations, and start with the STOKES Equations 2.21. Averaging those leads us to

$$0 = -\langle \mathbf{grad}\, p_\alpha \rangle + \langle \mu_\alpha \operatorname{div} \mathbf{grad}\, \boldsymbol{v}_\alpha \rangle + \langle \rho_\alpha \boldsymbol{g} \rangle + \left\langle \boldsymbol{q}_{\mathrm{mom},\alpha} \right\rangle \; .$$

We now use the GRAY decomposition for the viscosity μ_α and the mass density ρ_α, and assume a sufficiently small averaging volume, so that we may neglect the deviation terms. Further assuming that the gravitational acceleration $\boldsymbol{g}$ is constant within the averaging volume, and that the momentum source term $\boldsymbol{q}_{\mathrm{mom},\alpha}$ is zero, we get

$$0 = -\langle \mathbf{grad}\, p_\alpha \rangle + \langle \mu_\alpha \rangle^\alpha \langle \operatorname{div} \mathbf{grad}\, \boldsymbol{v}_\alpha \rangle + \langle \rho_\alpha \rangle^\alpha \boldsymbol{g} \; . \tag{2.29}$$

Taking advantage of the Spatial Averaging Theorem 2.26, we may write the pressure term as

$$\langle \mathbf{grad}\, p_\alpha \rangle = \mathbf{grad}\, \langle p_\alpha \rangle + \frac{1}{\|\mathcal{V}\|} \int_{\partial \mathcal{V}_{s\alpha}} p_\alpha \boldsymbol{n} \, \mathrm{d}\boldsymbol{y} \; .$$

Now, we apply the GRAY decomposition on p_α, and rewrite p_α as the sum of its intrinsic phase average and the deviation, and get

$$\begin{aligned} \langle \mathbf{grad}\, p_\alpha \rangle = {} & \langle p_\alpha \rangle^\alpha \, \mathbf{grad}(\phi S_\alpha) + \phi S_\alpha \, \mathbf{grad}\, \langle p_\alpha \rangle^\alpha \\ & + \frac{1}{\|\mathcal{V}\|} \int_{\partial \mathcal{V}_{s\alpha}} \boldsymbol{n} \, \langle p_\alpha \rangle^\alpha \, \mathrm{d}\boldsymbol{y} + \frac{1}{\|\mathcal{V}\|} \int_{\partial \mathcal{V}_{s\alpha}} \boldsymbol{n} \, \tilde{p}_\alpha \, \mathrm{d}\boldsymbol{y} \end{aligned} \tag{2.30}$$

after applying the product rule to the first term. Since $\langle p_\alpha \rangle^\alpha$ is constant within an averaging volume,

$$\frac{1}{\|\mathcal{V}\|} \int_{\partial \mathcal{V}_{s\alpha}} \boldsymbol{n} \, \langle p_\alpha \rangle^\alpha \, \mathrm{d}\boldsymbol{y} = \frac{\langle p_\alpha \rangle^\alpha}{\|\mathcal{V}\|} \int_{\partial \mathcal{V}_{s\alpha}} \boldsymbol{n} \, \mathrm{d}\boldsymbol{y}$$

holds. Now we use the spatial averaging theorem with $b_\alpha \equiv 1$ to obtain

$$\frac{1}{\|\mathcal{V}\|} \int_{\partial \mathcal{V}_{s\alpha}} \boldsymbol{n} \, \mathrm{d}\boldsymbol{y} = -\mathbf{grad}(\phi S_\alpha) \; . \tag{2.31}$$

Taking advantage of Equations 2.31 and 2.30 in Equation 2.29, and using the same procedure to the phase velocities, we get

$$0 = -\phi S_\alpha \mathbf{grad}\,\langle p_\alpha\rangle^\alpha - \frac{1}{\|\mathcal{V}\|}\int_{\partial\mathcal{V}_{s\alpha}} \boldsymbol{n}\,\tilde{p}_\alpha\,\mathrm{d}\boldsymbol{y} + \frac{\langle\mu_\alpha\rangle^\alpha}{\|\mathcal{V}\|}\int_{\partial\mathcal{V}_{s\alpha}} \boldsymbol{n}\cdot\mathbf{grad}\,\tilde{\boldsymbol{v}}_\alpha\,\mathrm{d}\boldsymbol{y} + \langle\rho_\alpha\rangle^\alpha\boldsymbol{g}\;. \tag{2.32}$$

The problem we now face is that we need to define $\tilde{p}_\alpha$ and $\tilde{\boldsymbol{v}}_\alpha$. WHITAKER [89] argues that

$$\tilde{\boldsymbol{v}}_\alpha = \boldsymbol{B}_\alpha\langle\boldsymbol{v}_\alpha\rangle^\alpha \quad \text{and} \tag{2.33}$$

$$\tilde{p}_\alpha = \boldsymbol{b}_\alpha\cdot\langle\mu_\alpha\rangle^\alpha\langle\boldsymbol{v}_\alpha\rangle^\alpha \tag{2.34}$$

hold, where $\boldsymbol{B}_\alpha$ and $\boldsymbol{b}_\alpha$ are the solutions of the following boundary value problem:

$$\begin{aligned}
-\mathbf{grad}\,\boldsymbol{b}_\alpha + \operatorname{div}\mathbf{grad}\,\boldsymbol{B}_\alpha &= \frac{1}{\|\mathcal{V}_\alpha\|}\int_{\mathcal{V}_\alpha} -\mathbf{grad}\,\boldsymbol{b}_\alpha + \operatorname{div}\mathbf{grad}\,\boldsymbol{B}_\alpha\,\mathrm{d}V\\
\boldsymbol{B}_\alpha &= -\boldsymbol{I} \quad \text{on } \mathcal{V}_\alpha\\
\boldsymbol{B}_\alpha &= \boldsymbol{G}_{\boldsymbol{\alpha}} \quad \text{on } \partial\mathcal{V}_\alpha \setminus \partial\mathcal{V}_s\\
\langle\boldsymbol{B}_\alpha\rangle^\alpha &= \langle\boldsymbol{b}_\alpha\rangle^\alpha = 0\;.
\end{aligned}$$

Inserting Equations 2.33 and 2.34 into Equation 2.32, we get

$$0 = -\mathbf{grad}\,\langle p_\alpha\rangle^\alpha + \left\{\frac{\langle\mu_\alpha\rangle^\alpha}{\|\mathcal{V}\|}\int_{\partial\mathcal{V}_{s\alpha}} \boldsymbol{n}\cdot\mathbf{grad}\,\boldsymbol{B}_\alpha - \boldsymbol{n}\otimes\boldsymbol{b}_\alpha\,\mathrm{d}\boldsymbol{y}\right\}\langle\boldsymbol{v}_\alpha\rangle^\alpha + \langle\rho_\alpha\rangle^\alpha\boldsymbol{g}\;. \tag{2.35}$$

Using the abbreviation

$$\boldsymbol{C}_\alpha = -\frac{1}{\|\mathcal{V}\|}\int_{\partial\mathcal{V}_{s\alpha}} \boldsymbol{n}\cdot\mathbf{grad}\,\boldsymbol{B} - \boldsymbol{n}\otimes\boldsymbol{b}_\alpha\,\mathrm{d}\boldsymbol{y}$$

we get a relation for the intrinsic phase velocity of fluid phase α:

$$\langle\boldsymbol{v}_\alpha\rangle^\alpha = -\frac{\boldsymbol{C}_\alpha^{-1}}{\langle\mu_\alpha\rangle^\alpha}\left(\mathbf{grad}\,\langle p_\alpha\rangle^\alpha - \langle\rho_\alpha\rangle^\alpha\boldsymbol{g}\right)\;. \tag{2.36}$$

We can convert Equation 2.36 from the intrinsic phase velocity to the more common phase velocity by introducing

$$\boldsymbol{K}_\alpha = \phi S_\alpha\boldsymbol{C}_\alpha^{-1}$$

which yields

$$\langle\boldsymbol{v}_\alpha\rangle = -\frac{\boldsymbol{K}_\alpha}{\langle\mu_\alpha\rangle^\alpha}\left(\mathbf{grad}\,\langle p_\alpha\rangle^\alpha - \langle\rho_\alpha\rangle^\alpha\boldsymbol{g}\right)\;. \tag{2.37}$$

Conservation of Energy

To obtain an equation for the conservation of energy in a fluid phase, we neglect potential and kinetic energy, and start with Equation 2.23. After applying the phase average (2.24) and

GRAY's decomposition, we get

$$\frac{\partial\ \phi S_\alpha \langle u_\alpha\rangle^\alpha\ \langle\rho_\alpha\rangle^\alpha}{\partial t} + \operatorname{div}(\langle h_\alpha\rangle^\alpha \langle\rho_\alpha\rangle^\alpha\ \langle \boldsymbol{v}_\alpha\rangle - \langle\lambda_\alpha\rangle^\alpha\, \mathbf{grad}\ \langle T_\alpha\rangle) = \langle q_{\text{energy}}\rangle\ .$$

Unlike mass and momentum, energy can be transported by the solid. Since we assumed a rigid solid phase, the advective part of the divergence term is zero for the solid, and we get

$$\frac{\partial\ (1-\phi)\langle u_s\rangle^s\ \langle\rho_s\rangle^s}{\partial t} - \operatorname{div}(\langle\lambda_s\rangle^s\, \mathbf{grad}\ \langle T_s\rangle) = \langle q_{\text{energy}}\rangle\ .$$

In this context we usually assume the internal energy u_s of the solid to be proportional to temperature, *i.e.*,

$$u_s = c_{\mathrm{p},s} T_s$$

holds with a constant *heat capacity* $c_{\mathrm{p},s}$.

2.4.2 Applicability

To derive the macro-scale conservation equations, and especially the momentum conservation equation (2.37), we had to make several assumptions:

- These equations are only valid for creeping flows, and we required an incompressible fluid with constant dynamic viscosity when simplifying the NAVIER-STOKES equations (2.20) to the STOKES equations (2.21). At this point, we note that we do not need to consider these simplifications in practice, since in order to derive Equation 2.37, we only used the STOKES equations within the averaging volumes where compressibility and variations in viscosity can usually be neglected.
- The averaging volume must be large enough for the continuum assumption to be applicable for the macro-scale system. This means that slightly increasing or decreasing the size of the averaging volume only leads to small changes of the averaged quantities [89].
- The averaging volume must be small enough so that we may neglect the deviation of all physical quantities from their average within an averaging volume. This assumption is potentially problematic for systems featuring low absolute pressures in conjunction with highly compressible fluids.

Of these assumptions, we usually have to pay most attention to the constraint of the flow velocity. To get a feeling about this, we first need to specify a REYNOLDS number, *i.e.*, we define a characteristic length L_c and a characteristic kinematic viscosity $\nu_\mathrm{c} = {}^{\mu_\mathrm{c}}/_{\rho_\mathrm{c}}$. In this case, we choose the diameter of a typical pore of the porous medium as the characteristic length; for the characteristic kinematic viscosity ν_c we choose the value of the fluid at a representative temperature and pressure. Allowing REYNOLDS numbers smaller than 1, Equation 2.37 is valid up to relatively high velocities[3]: For example, if the typical pore diameter of a porous medium is the one of a typical sand with $100 \cdot 10^{-6}$ m, and the characteristic kinematic

---

[3] At least "high" velocities in the context of fluid flows in porous media.

viscosity is $20 \cdot 10^{-5}$ $^{\mathrm{m}^2}/_{\mathrm{s}}$ (roughly the value of air at $20\,°\mathrm{C}$), the velocity constraints implied by Equation 2.37 are met for intrinsic phase velocities smaller than about 2 $^{\mathrm{m}}/_{\mathrm{s}}$.

Simplification of Notation

In order to simplify notation, we will not write the averaging operator henceforth, so we will use the conservation equations

$$\frac{\partial \rho_\alpha \phi S_\alpha}{\partial t} + \mathrm{div}(\rho_\alpha \boldsymbol{v}_\alpha) = q_{\mathrm{mass},\alpha} \quad \text{for mass,} \tag{2.38}$$

$$\boldsymbol{v}_\alpha = -\frac{\boldsymbol{K}_\alpha}{\mu_\alpha}\left(\mathbf{grad}\, p_\alpha - \rho_\alpha \boldsymbol{g}\right) \quad \text{for momentum,} \tag{2.39}$$

$$\frac{\partial u_\alpha \rho_\alpha \phi S_\alpha}{\partial t} + \mathrm{div}(h_\alpha \rho_\alpha \boldsymbol{v}_\alpha - \lambda_\alpha\, \mathbf{grad}\, T_\alpha) = q_{\mathrm{energy},\alpha} \quad \text{for energy within a fluid, and} \tag{2.40}$$

$$\frac{\partial (1-\phi)\rho_s\, c_{\mathrm{p},s} T_s}{\partial t} - \mathrm{div}(\lambda_s\, \mathbf{grad}\, T_s) = q_{\mathrm{energy},s} \quad \text{for energy within the solid.} \tag{2.41}$$

Also, since the momentum conservation equation (2.39) determines the phase velocities explicitly, we can also insert it into the mass and energy conservation equations. In this case momentum is conserved implicitly, and we get

$$\frac{\partial \rho_\alpha \phi S_\alpha}{\partial t} - \mathrm{div}\left(\rho_\alpha \frac{\boldsymbol{K}_\alpha}{\mu_\alpha}\left(\mathbf{grad}\, p_\alpha - \rho_\alpha \boldsymbol{g}\right)\right) = q_{\mathrm{mass},\alpha} \tag{2.42}$$

for mass conservation as well as

$$\frac{\partial \rho_\alpha u_\alpha \phi S_\alpha}{\partial t} - \mathrm{div}\left(h_\alpha \rho_\alpha \frac{\boldsymbol{K}_\alpha}{\mu_\alpha}\left(\mathbf{grad}\, p_\alpha - \rho_\alpha \boldsymbol{g}\right) + \lambda_\alpha\, \mathbf{grad}\, T_\alpha\right) = q_{\mathrm{energy},\alpha} \tag{2.43}$$

for energy conservation within a fluid.

2.4.3 Multi-Phase Flows

When considering flow of more than a single fluid in a porous medium, it is convenient to decompose the permeability matrix of the fluids $\boldsymbol{K}_\alpha$ into a part which only depends on the properties of the porous medium, a part which only depends on the fluid characteristics, and a part which describes the interactions between the fluids. We call the first of these factors the *intrinsic permeability tensor* $\boldsymbol{K}$. It describes the permeability tensor of a medium if the pore space were completely filled with a fluid that exhibits a dynamic viscosity of $1\ \mathrm{Pa\,s}$. The fluid-dependent part is $^1/_{\mu_\alpha}$, the inverse of the dynamic viscosity of the fluid; and the interactions between the fluids are usually expressed by *relative permeabilities* $0 \leq k_{\mathrm{r},\alpha} \leq 1$. This leads to [14]

$$\boldsymbol{K}_\alpha = \frac{k_{\mathrm{r},\alpha}}{\mu_\alpha}\boldsymbol{K}\ . \tag{2.44}$$

We note that Equation 2.44 assumes that blocking flow paths is the only mutual interaction of fluid phases, and that this happens isotropically, *i.e.*, only the magnitude of the fluid velocity gets reduced by blocked pores but its direction remains unaltered.

If we consider the energy equation for multiple fluid phases, we must conserve the *total* energy within the system, so we get the energy conservation equation

$$\begin{aligned}\frac{\partial}{\partial t}\left(\sum_\alpha \phi\, u_\alpha\, \rho_\alpha\, S_\alpha + (1-\phi) c_{\mathrm{p},s}\, T_s\, \rho_s\right) \\ + \sum_\alpha \operatorname{div}(h_\alpha\, \rho_\alpha\, \boldsymbol{v}_\alpha - \lambda_{\mathrm{pm},\alpha}\, \mathbf{grad}\, T_\alpha) \\ - \operatorname{div}(\lambda_{\mathrm{pm},s}\, \mathbf{grad}\, T_s) = q_{\mathrm{energy}}\ .\end{aligned} \tag{2.45}$$

Since the temperature usually equilibrates quickly within an averaging volume, we may assume local thermal equilibrium. This implies that at any point the temperature is equal for all fluid phases as well as for the solid phase, and allows us to merge the heat conduction terms, so we get

$$\frac{\partial}{\partial t}\left(\sum_\alpha \phi u_\alpha\, \rho_\alpha\, S_\alpha + (1-\phi) c_{\mathrm{p},s}\, T\, \rho_s\right) + \operatorname{div}\left(\sum_\alpha h_\alpha \rho_\alpha \boldsymbol{v}_\alpha - \lambda_{\mathrm{pm}}\, \mathbf{grad}\, T\right) = q_{\mathrm{energy}}\ .$$

2.4.4 Multi-Phase, Multi-Component Flows

For multi-phase problems which involve more than a single component, we need to start our considerations at the compositional mass conservation equation (2.8) which conserves each component individually. Since a component can potentially be present in all fluid phases, we get

$$\sum_\alpha \frac{\partial}{\partial t}(\phi S_\alpha \rho_{\mathrm{mol},\alpha}\, x_\alpha^\kappa) + \sum_\alpha \operatorname{div}(\rho_{\mathrm{mol},\alpha}\, x_\alpha^\kappa \boldsymbol{v}_\alpha - D_\alpha^\kappa \mathbf{grad}\, x_\alpha^\kappa) = \sum_\alpha q_\alpha^\kappa \tag{2.46}$$

to conserve the mass of component κ in the fluids.

After taking advantage of the equation for the conservation of momentum (2.39) and merging the right-hand side into a single source term q^κ, we get

$$\sum_\alpha \frac{\partial}{\partial t}(\phi S_\alpha \rho_{\mathrm{mol},\alpha}\, x_\alpha^\kappa) - \sum_\alpha \operatorname{div}\left(\rho_{\mathrm{mol},\alpha}\, x_\alpha^\kappa \frac{k_{\mathrm{r},\alpha}}{\mu_\alpha} \boldsymbol{K}\, (\mathbf{grad}\, p_\alpha - \rho_\alpha \boldsymbol{g}) + D_\alpha^\kappa \mathbf{grad}\, x_\alpha^\kappa\right) = q^\kappa\ , \tag{2.47}$$

which we will use as the mass conservation equation of compositional fluid flows in porous media for the remainder of this work.

2.4.5 Experimental Derivation of the Momentum Conservation Equation

Instead of the theoretical derivation outlined in the previous section, we can also obtain Equation 2.39 experimentally. In fact, this is how it was historically discovered by the French

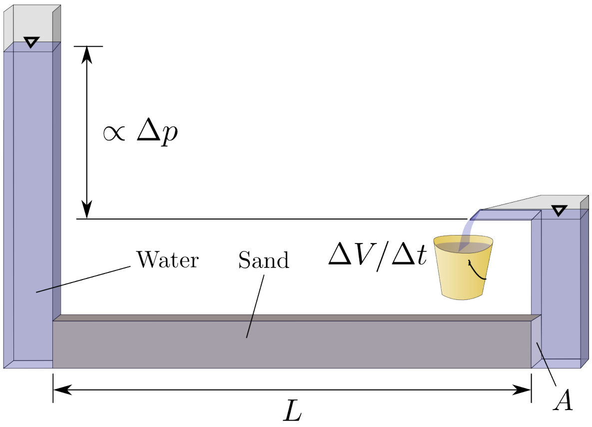

Figure 2.7: Experimental derivation of Equation 2.39, the momentum conservation equation for flows in porous media: A fluid is forced through a sand filter by applying a pressure gradient Δp. The sand filter has a cross-sectional area of A and a length of L. After waiting for a certain time Δt, we measure ΔV as the volume of the fluid in the outlet bucket.

hydraulic engineer HENRY DARCY [11]. While designing the water supply system of the city of Dijon in 1856, DARCY measured how fast water seeps through a filter of sand, such as the one illustrated in Figure 2.7. This filter has a cross-sectional area of A and a length of L. DARCY observed, that the volume ΔV of water which trickles out of the sand filter during a given period of time Δt is proportional to Δp, the difference in pressure at the inlet of the filter and its outlet, and the cross-sectional area A of the filter. Further, he observed that it is inversely proportional to the length L of the filter and to the viscosity of the fluid which seeps through the sand. We can combine these observations, and get

$$\frac{\Delta V}{\Delta t} \propto -\Delta p \frac{A}{\mu L} \, .$$

After introducing a proportionality constant K we get

$$\frac{\Delta V}{\Delta t} = -\frac{K}{\mu} \Delta p \frac{A}{L} \, , \tag{2.48}$$

the equation discovered by DARCY.

If we now take the limit of A, Δt and L to zero, and divide both sides with the cross-sectional area, we get

$$v = -\frac{K}{\mu} \frac{\partial p}{\partial x} \, . \tag{2.49}$$

Additionally including gravity by subtracting its contribution to hydrostatic pressure, we end up with the DARCY equation for one-dimensional single-phase flow

$$v = -\frac{K}{\mu} \left(\frac{\partial p}{\partial x} - \rho g \right) \, . \tag{2.50}$$

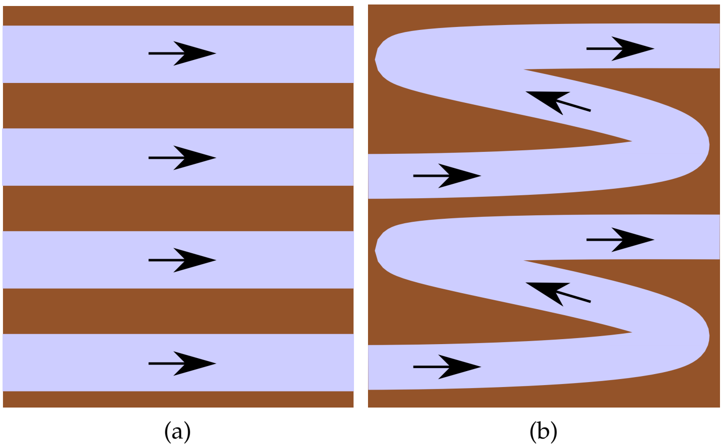
(a) (b)

Figure 2.8: Flow through a porous medium with **(a)** no tortuosity, and **(b)** high tortuosity.

Generalizing Equation 2.50 to multiple dimensions, we get

$$\boldsymbol{v} = -\frac{\boldsymbol{K}}{\mu} \left(\mathbf{grad}\, p - \rho \boldsymbol{g} \right) \ . \tag{2.51}$$

In the case of multiple fluid phases, the simplest approach we can take for the filter velocity of fluid phase α is to assume that pores occupied by fluids other than α are blocked, and the proportionality coefficient $\boldsymbol{K}$ gets reduced by a factor $k_{\mathrm{r},\alpha}$ depending on the ratio of pores being blocked by other fluids. In this case we can use

$$\boldsymbol{v}_\alpha = -\frac{k_{\mathrm{r},\alpha}}{\mu_\alpha} \boldsymbol{K} \left(\mathbf{grad}\, p_\alpha - \rho_\alpha \boldsymbol{g} \right) \tag{2.52}$$

to determine the *filter velocity*.

2.4.6 Filter Velocity and Seepage Velocity

We can consider DARCY's Equation 2.52 as a relation between the average phase velocities $\langle \boldsymbol{v}_\alpha \rangle$ and the potential gradient of its driving force, *i.e.*, the pressure gradient corrected by gravity. If the filter contained no solid, $\boldsymbol{v}_\alpha$ would be the velocity that the fluid exhibits as it moves through the filter. Thus, we call $\boldsymbol{v}_\alpha$ the filter velocity. In contrast, the velocity which is actually experienced by the fluids is higher, and we call it the *seepage velocity* $v_{\mathrm{sp},\alpha}$. We can estimate the seepage velocity using the relation

$$v_{\mathrm{sp},\alpha} \geq \frac{\|\boldsymbol{v}_\alpha\|}{\phi} \ . \tag{2.53}$$

In some cases, such as illustrated in Figure 2.8b, Relation 2.53 *cannot* be assumed to be an equality. This is due to an effect called *tortuosity*. In the context of this work we will neglect this effect.

2.5 Chapter Synopsis

In this chapter we have sketched a procedure to transform a molecular-scale description of a physical system to a continuum-scale description in Section 2.1. Mathematically, this procedure can be considered to be a convolution with an adequate kernel. Then, starting at the continuum-scale, we derived the equations for the conservation of mass, momentum, and energy in Section 2.3 and adapted them to the special case of NEWTONIAN fluids in Section 2.3.3. This lead us to the conservation equations

$$\frac{\partial x^{\kappa}\rho_{\mathrm{mol}}}{\partial t} + \operatorname{div}(x^{\kappa}\rho_{\mathrm{mol}}\boldsymbol{v} - D^{\kappa}\mathbf{grad}\; x^{\kappa}\;) = q^{\kappa}_{\mathrm{mol}}\;,$$

$$\rho\frac{\partial \boldsymbol{v}}{\partial t} + \rho\boldsymbol{v}\cdot\mathbf{grad}\;\boldsymbol{v} = -\mathbf{grad}\;p + \mu\,\operatorname{div}\mathbf{grad}\;\boldsymbol{v} + \rho\,\boldsymbol{g} + \boldsymbol{q}_{\mathrm{mom}}\;\text{and}$$

$$\frac{\partial\,u\,\rho}{\partial t} + \operatorname{div}(h\rho\boldsymbol{v} - \lambda\,\mathbf{grad}\;T) = q_{\mathrm{energy}}$$

for mass, momentum, and energy, respectively.

In Section 2.4 we then applied the volume averaging approach by WHITAKER [89] to these equations, and obtained a macro-scale description of NEWTONIAN fluid flows in porous media. To see the link to the upscaling procedure from the molecular to the continuum-scale, we noted that the volume averaging approach can be comprehended as a special case of a convolution. Using volume averaging, we then derived the macro-scale conservation equations for fluid flows in porous media, and got

$$\frac{\partial\sum_{\alpha}\phi S_{\alpha}x^{\kappa}_{\alpha}\rho_{\mathrm{mol},\alpha}}{\partial t} + \sum_{\alpha}\operatorname{div}\big(x^{\kappa}_{\kappa}\rho_{\mathrm{mol},\alpha}\;\boldsymbol{v}_{\alpha} - D^{\kappa}_{\mathrm{pm}.\alpha}\,\mathbf{grad}\;x^{\kappa}_{\alpha}\;\big) = q^{\kappa}\;,$$

$$\boldsymbol{v}_{\alpha} = -\frac{k_{\mathrm{r},\alpha}}{\mu_{\alpha}}\boldsymbol{K}\;(\mathbf{grad}\;p_{\alpha} - \rho_{\alpha}\boldsymbol{g})\;\text{and}$$

$$\frac{\partial}{\partial t}\big(\sum_{\alpha}\phi\,S_{\alpha}\,\rho_{\alpha}\,u_{\alpha} + (1-\phi)\rho_{s}\,c_{\mathrm{p},s}\,T\big) + \operatorname{div}\left(\sum_{\alpha}h_{\alpha}\rho_{\alpha}\;\boldsymbol{v}_{\alpha} - \lambda_{\mathrm{pm}}\,\mathbf{grad}\;T\right) = q_{\mathrm{energy}}$$

for mass, momentum, and energy, respectively.

Analogous to the upscaling procedure from molecular to continuum-scale where we lost the information about individual particles, we lost the information of the microscopic fluid configuration within the porous medium when going to the macro-scale. This has the practical advantage that we only need to specify macroscopic properties—which are relatively easy to determine using physical experiments—and that we do not need to specify the exact geometry of the solid phase of the porous medium.

3 Supplementary and Closure Relations

To solve any system of equations, we have to make sure that it is mathematically *well-defined*. This means that the equations are independent, *i.e.*, that no equation can be expressed in terms of the others, that a unique solution exists and that the number of unknowns equals the number of equations. We assert that the first two properties hold for the compositional mass conservation equation (2.47). When counting the unknowns in these equations, we get $2N \cdot M + N + 6M + 3$ where M is the number of fluid phases, and N is the number of components:

- One gravitational acceleration function $\boldsymbol{g}$,
- One porosity distribution function ϕ,
- One absolute permeability distribution $\boldsymbol{K}$,
- M saturations S_α,
- M pressures p_α,
- M relative permeabilities $k_{\mathrm{r},\alpha}$,
- M dynamic viscosities μ_α,
- M mass densities ρ_α,
- M molar densities $\rho_{\mathrm{mol},\alpha}$,
- N source terms q^κ,
- $M \cdot N$ mole fractions x_α^κ, and
- $M \cdot N$ diffusion coefficients $D_{\mathrm{pm},\alpha}^\kappa$.

On the side of the equations, we currently have only N mass conservation equations of the components (2.47). In the following sections, we will examine the remaining relations required to get a well-defined system of equations.

3.1 Saturation Closure Condition

One additional equation is implied by the simple fact that all pore space must be occupied by fluids[1]. We express this by the relation

$$\sum_\alpha S_\alpha = 1 \; . \tag{3.1}$$

---

[1] In this context, we consider vacuum as gas.

3.2 Given Parameters and Empiric Relations

Further, we assume the following quantities to be known *a priori*:

- Gravitational acceleration $\boldsymbol{g}$,
- intrinsic permeability of the porous medium $\boldsymbol{K}$,
- porosity of the medium ϕ, and
- the source terms q^κ of all components.

Also, we can assume that the dynamic viscosities of the fluids μ_α and the molecular diffusion coefficients $D^\kappa_{\mathrm{pm},\alpha}$ are given closed functions depending on the fluid composition, temperature, and on pressure. Moreover, we know that the mass and molar densities are connected by

$$\rho_\alpha = \rho_{\mathrm{mol},\alpha} \sum_\kappa x^\kappa_\alpha M^\kappa \ .$$

In general, we need to consider the relative permeabilities $k_{\mathrm{r},\alpha}$ as spatially parameterized functions which depend on *all* phase compositions $\{x^\kappa_\beta\}$, *all* temperatures $\{T_\beta\}$, *all* pressures $\{p_\beta\}$, and *all* saturations $\{S_\beta\}$. Having said that, we note that most of the commonly used empiric relations for relative permeability, like the ones discussed in Section 3.4, only depend on the phase saturations $\{S_\alpha\}$.

3.3 Thermodynamic Relations

At this point, we count $M \cdot N + 2N + 3M + 4$ equations, which means that we still need $(M-1) \cdot N + 3M - 1$ additional relations to get a mathematically closed system. Most of these can be obtained by considering the thermodynamics which governs the system.

3.3.1 Equations of State

First, we get M additional equations by defining the equations of state for all fluid phases. An equation of state of a phase is the link between temperature T_α, pressure p_α, composition $\{x^\kappa_\alpha\}$, and density ρ_α or—more commonly—the molar volume $V_{\mathrm{mol},\alpha} := {}^1\!/\rho_{\mathrm{mol},\alpha}$ of a phase, *i.e.*,

$$p_\alpha = p_\alpha(V_{\mathrm{mol},\alpha}, T_\alpha, \{x^\kappa_\alpha\}) \ . \tag{3.2}$$

The most simple equation of state,

$$p_g = \frac{RT_g}{V_{\mathrm{mol},g}} \ ,$$

with $R = 8.314462\ {}^{\mathrm{J}}\!/_{\mathrm{K\ mol}}$ describes ideal gases. This equation is a good approximation for real gases at low temperature and low pressure, *i.e.*, for situations where the values of the temperature and pressure are much lower than the critical values of the substance. On the

Name	u_α	w_α	b^κ_α	a^κ_α
VAN DER WAALS	0	0	$\frac{1}{8}\frac{RT^\kappa_\mathrm{crit}}{p^\kappa_\mathrm{crit}}$	$\frac{27}{64}\frac{(RT^\kappa_\mathrm{crit})^2}{p^\kappa_\mathrm{crit}}$
REDLICH-KWONG	1	0	$\frac{0.08664RT^\kappa_\mathrm{crit}}{p^\kappa_\mathrm{crit}}$	$\frac{0.42748(RT^\kappa_\mathrm{crit})^2}{p^\kappa_\mathrm{crit}\sqrt{T_\mathrm{r}}}$ with $T_\mathrm{r} = {}^{T_\alpha}/_{T^\kappa_\mathrm{crit}}$
SOAVE	1	0	$\frac{0.08664RT^\kappa_\mathrm{crit}}{p^\kappa_\mathrm{crit}}$	$\frac{0.42748(RT^\kappa_\mathrm{crit})^2}{p^\kappa_\mathrm{crit}}\left(1 + (1 - \sqrt{T_\mathrm{r}})\, f_{\omega^\kappa}\right)^2$ with $f_{\omega^\kappa} = 0.48 + \omega^\kappa(1.574 - 0.176\omega^\kappa)$
PENG-ROBINSON	2	-1	$\frac{0.07780RT^\kappa_\mathrm{crit}}{p^\kappa_\mathrm{crit}}$	$\frac{0.45724(RT^\kappa_\mathrm{crit})^2}{p^\kappa_\mathrm{crit}}\left(1 + (1 - \sqrt{T_\mathrm{r}})\, f_{\omega^\kappa}\right)^2$ where $f_{\omega^\kappa} = 0.37464 + \omega^\kappa(1.54226 - 0.26992\omega^\kappa)$

Table 3.1: Parameters for common cubic equations of state as outlined by REID*et al.* [68]. T^κ_crit and p^κ_crit correspond to the critical temperature and critical pressure of a pure component κ, and ω^κ is the acentric factor of the component. All these quantities can either be taken from the literature or they can be estimated [68].

molecular scale, this relation implies that the interactions between particles of the gas are well approximated by elastic collisions.

Since for real gases, molecular particles also interact by means of their electric force fields, a more complex EOS is needed. Such a class of equations of state are *cubic equations of state*. These equations can be expressed in the form [68]

$$p_\alpha = \frac{RT_\alpha}{V_{\mathrm{mol},\alpha} - b_\alpha} - \frac{a_\alpha}{V^2_{\mathrm{mol},\alpha} + u_\alpha\, b_\alpha\, V_{\mathrm{mol},\alpha} + w_\alpha\, b^2_\alpha}\ . \tag{3.3}$$

Here we call the quantity b_α the *covolume* of the fluid phase α since it resembles the volume occupied by the particles of the substance directly, and we call a_α the *attractive factor* of fluid phase α since it describes how strongly the particles attract each other. Finally, u_α and w_α are constants given by the chosen equation of state.

Table 3.1 outlines some common parameterizations for pure substances. Of those relations, the VAN DER WAALS and REDLICH-KWONG parameterizations are primarily of historical interest [68]. For the SOAVE and PENG-ROBINSON approaches, we cannot specify the most accurate one *a priori* as the error of a parameterization strongly depends on the molecular properties of the considered substance [68].

For mixtures of multiple substances, we may also use Equation 3.3 as the equation of state, but we need to calculate the parameters a_α and b_α for the mixture from the parameters of the pure constituting components using a *mixing rule*. The most common mixing rule [68] is

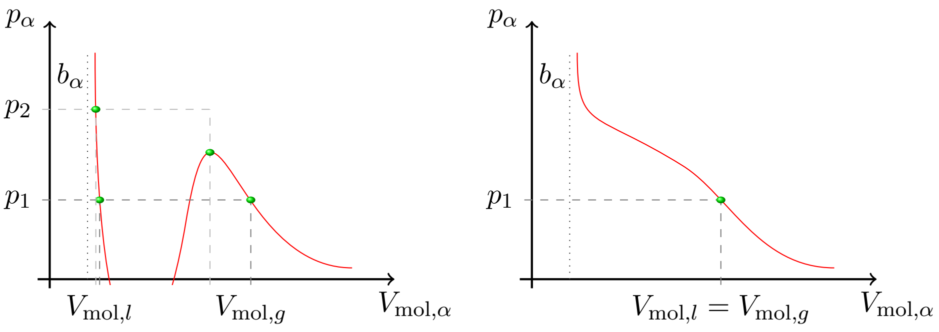

(a) Under-Critical Fluid

(b) Critical Fluid

Figure 3.1: Possible shapes of cubic equations of state. For these, the pressure of a fluid phase p_α is defined in terms of the molar volume $V_{\text{mol},\alpha} = {}^1\!/\rho_{\text{mol},\alpha}$ of the fluid.

given by

$$\begin{aligned} a_\alpha &= \sum_\kappa \sum_\lambda x_\alpha^\kappa x_\alpha^\lambda \sqrt{a_\alpha^\kappa a_\alpha^\lambda}(1 - \bar{k}_\alpha^{\kappa\lambda}) \quad \text{and} \\ b_\alpha &= \sum_\kappa x_\alpha^\kappa b_\alpha^\kappa \,, \end{aligned} \tag{3.4}$$

where $\bar{k}_\alpha^{\kappa\lambda}$ is the *interaction coefficient* of the components κ and λ in the fluid phase α.

Multiple Phases

We can use the same cubic equations of state for multiple phases: In the most simple case, outlined in Figure 3.1a, an isotherm of the equation of state has three intersections with the isobar p_1 that are larger than the covolume b_α. In this case, we can choose the molar volume for the liquid $V_{\text{mol},l}$ as the value of the smallest intersection, and the molar volume of the gas $V_{\text{mol},g}$ as the value of the largest intersection.

Another case is also illustrated in Figure 3.1a: If we increase the pressure to p_2, the isotherm of the equation of state has only one intersection with the isobar. Given the fact that we have to choose the molar volume of each phase in a way that is continuous with regard to pressure, the molar volume of the physically impossible phase becomes undefined. This issue can be mended if the equation of state features two extrema at physically meaningful molar volumes. In this case, we can use the molar volume of the largest extremum for gas and the molar volume of the smallest extremum for the liquid. Also, we can decide which phase is unphysical by considering the intersection of the isotherm with the isobar p_2: If the molar volume of the intersection is higher than the value of both extrema, the value of the intersection is the molar volume of the gas phase, else it corresponds to the value of the liquid phase.

If we increase the temperature—or alternatively change the composition of the fluid—the fluid becomes *critical*, and the isotherms of the equation of state resemble the curve depicted in Figure 3.1b. Given the fact that such curves only exhibit a single intersection with any pressure, and they also do not feature physically meaningful extrema, we need a different approach to achieve continuity of the molar volume regarding temperature, pressure, and composition. In this case, we can calculate the critical point for a substance with the parameters a_α and b_α, and use its molar volume as the molar volume for the unphysical phase.

3.3.2 Local Thermodynamic Equilibrium

Besides the M equations of state which essentially yield the mass density of all phases at a given temperature, pressure, and composition, we obtain further thermodynamic relations by assuming *local thermodynamic equilibrium*.

The term "local thermodynamic equilibrium" means that we can always consider the fluids at each point of the spatial domain to be at steady-state if we would isolate this location from the rest of the system. This statement is equivalent to saying that, after isolating any infinitesimally small subdomain $\mathcal{V}$ from the rest of the system at any time, the fluids contained in the extracted domain $\mathcal{V}$ would be thermodynamic equilibrium. Thermodynamic equilibrium itself is defined as the superposition of the following three subequilibria:

Thermal equilibrium, which is defined as the temperature of all phases in any infinitesimally small and isolated sub-domain $\mathcal{V}$ being constant in time,

Mechanical equilibrium, meaning that the pressure of all phases is constant in time within such an isolated sub-domain $\mathcal{V}$, and

Chemical equilibrium, which represents the fact that the composition of any fluid phase does not change with time within an isolated sub-domain $\mathcal{V}$.

In the following, we will discuss these three equilibria independently.

Thermal Equilibrium

Thermal equilibrium is defined as the temperature of all phases of a thermodynamic system being constant in time, *i.e.*,

$$\frac{\partial T_\alpha}{\partial t} = 0 \tag{3.5}$$

holds. By the "zeroth" law of thermodynamics, this implies that the temperature equal within the system, *i.e.*,

$$T_\alpha = T_\beta =: T \tag{3.6}$$

holds for arbitrary phases α and β.

If we consider conservation of energy, the energy balance equation (2.46) determines the additional unknown T. In this case, we can assume the specific enthalpies h_α to be closed functions which depend on the fluid composition, pressure, and temperature [68]. Further, we can consider the thermal conductivity coefficient λ_{pm} to be a given function depending on the saturations, temperature, fluid compositions, and pressures. We also know that the relation between specific internal energy u_α and enthalpy h_α of phase α is given by

$$u_\alpha = h_\alpha - \frac{p_\alpha}{\rho_\alpha} \; .$$

In contrast, if we do *not* conserve energy, we must impress the temperature T externally on the system, *i.e.*, we need to consider temperature as a spatially and time dependent parameter like, for example, the intrinsic permeability $\boldsymbol{K}$.

Mechanical Equilibrium

Mechanical equilibrium is defined as the pressure of all fluids being stationary, *i.e.*,

$$\frac{\partial p_\alpha}{\partial t} = 0 \tag{3.7}$$

holds for all phases α.

In the context of fluid flows in porous media, this does *not* imply that the pressures of all fluid phases are equal. Instead, it implies that the differences between the pressures of all fluid phases are static. We can express this fact using

$$p_\alpha = p_\beta + p_{\mathrm{c},\alpha\beta} \; , \tag{3.8}$$

where we call the quantity $p_{\mathrm{c},\alpha\beta}$ *capillary pressure*[2] between fluid phases α and β. In the most general case, the quantity $p_{\mathrm{c},\alpha\beta}$ potentially depends on all fluid pressures, all phase saturations, all temperatures and the composition of all fluid phases like the relative permeability functions $k_{\mathrm{r},\alpha}$. Having said that, the most common approaches— which we will discuss in Section 3.4—only depend on the phase saturations.

Chemical Equilibrium

For chemical equilibrium, the fluid compositions must be time-invariate, *i.e.*,

$$\frac{\partial x_\alpha^\kappa}{\partial t} = 0 \tag{3.9}$$

is true for all phases α and all components κ. This means that the *chemical potentials* ζ_α^κ of each component are identical for all phases, *i.e.*,

$$\zeta_\alpha^\kappa = \zeta_\beta^\kappa =: \zeta^\kappa \tag{3.10}$$

---

[2] Note that the term *capillary pressure* is a bit of a misnomer because the capillary effect is not the only microscopic effect which determines macroscopic pressure differences [38].

holds for any two fluid phases α, β, and any component κ. The chemical potential of a component in a fluid is defined as

$$\zeta_\alpha^\kappa = \frac{\partial g_\alpha}{\partial n_\alpha^\kappa}$$

where $g_\alpha = h_\alpha - T_\alpha s_\alpha$ is the GIBBS free energy of phase α, and $n_\alpha^\kappa = N_\mathrm{A}\, x_\alpha^\kappa \rho_{\mathrm{mol},\alpha}$ is the total number of molecular particles of component κ per unit of volume. Here, the specific entropy of the fluid is represented by s_α, and $N_\mathrm{A} = {}^{6.022 \cdot 10^{23}}/_{\mathrm{mol}}$ is AVOGADRO's constant.

Since chemical potentials become infinite for non-present components, it is advisable to use *fugacities* instead. The fugacity f_α^κ of a component in a phase is connected to the chemical potential of the component by the equation

$$f_\alpha^\kappa = f_\alpha^{\kappa,\circ} \exp\left(\frac{\zeta_\alpha^\kappa - \zeta_\alpha^{\kappa,\circ}}{RT_\alpha}\right) , \tag{3.11}$$

where $f_\alpha^{\kappa,\circ}$ is the fugacity of component κ in phase α at an arbitrary but fixed reference state of the pure component, and $\zeta_\alpha^{\kappa,\circ}$ is the chemical potential at the same reference state. We note that the fugacity is a smooth, monotonous function mapping $\boldsymbol{R}$ to $\boldsymbol{R}^+$.

If we assume thermal equilibrium, the condition for equality of all chemical potentials in all fluids (3.10) can thus be reformulated as equivalence of component fugacities, *i.e.*,

$$f_\alpha^\kappa = f_\beta^\kappa \tag{3.12}$$

holds for any component κ and arbitrary phases α and β.

To calculate the fugacity f_α^κ of a component in a phase, we usually use the relation

$$f_\alpha^\kappa := p_\alpha x_\alpha^\kappa \Phi_\alpha^\kappa \ . \tag{3.13}$$

Further, we can determine the *fugacity coefficient* Φ_α^κ of component κ using the equation of state. According to REID *et al.* [68], the relation for this is

$$RT_\alpha \ln f_\alpha^\kappa = -\int_\infty^{V_{\mathrm{mol},\alpha}} \frac{\partial p_\alpha}{\partial n_\alpha^\kappa} - \frac{RT_\alpha}{\hat{V}_{\mathrm{mol},\alpha}} \,\mathrm{d}\hat{V}_{\mathrm{mol},\alpha} + RT_\alpha \ln Z_\alpha \ , \tag{3.14}$$

where $Z_\alpha = {}^{p_\alpha V_{\mathrm{mol},\alpha}}/_{RT_\alpha}$ is the *compressibility factor* of the phase, and $n_\alpha^\kappa = {}^{N_\mathrm{A}\, x_\alpha^\kappa}/_{\hat{V}_{\mathrm{mol},\alpha}}$ is the total number of molecules of component κ per volume.

Cubic Equations of State

For cubic equations of state, Equation 3.14 can be evaluated analytically if we use Equation 3.4 as mixing rule. We get [68]

$$\begin{aligned}\ln \Phi_\alpha^\kappa = {} & \frac{b_\alpha^\kappa}{b_\alpha}(Z_\alpha - 1) - \ln(Z_\alpha - B_\alpha^\star) \\ & + \frac{A_\alpha^\star}{B^\star \sqrt{u_\alpha^2 - 4w_\alpha}} \left(\frac{b_\alpha^\kappa}{b_\alpha} - \delta_\alpha^\kappa \right) \ln \frac{2Z_\alpha + B_\alpha^\star (u_\alpha + \sqrt{u_\alpha^2 - 4w_\alpha})}{2Z_\alpha + B_\alpha^\star (u_\alpha - \sqrt{u_\alpha^2 - 4w_\alpha})} \,,\end{aligned} \tag{3.15}$$

with the abbreviations

$$A_\alpha^\star = \frac{a_\alpha p_\alpha}{(RT_\alpha)^2} \,,$$

$$B_\alpha^\star = \frac{b_\alpha p_\alpha}{RT_\alpha} \,, \quad \text{and}$$

$$\delta_\alpha^\kappa = \frac{\sqrt{a_\alpha^\kappa}}{2\, a_\alpha} \sum_\lambda x_\alpha^\lambda (1 - \bar{k}_\alpha^{\kappa\lambda}) \sqrt{a_\alpha^\lambda} \,.$$

Ideal Mixtures

Often, we assume a fluid phase to be an ideal mixture of its constituent components. In this case, all fugacity coefficients are independent of the composition of the phases, and we get the relation

$$f^\kappa = p_\alpha x_\alpha^\kappa \, \Phi_\alpha^\kappa (T_\alpha, p_\alpha) \,.$$

For ideal gases, Φ_α^κ is equal to 1; for liquid phases, the fugacity coefficient and the fluid pressure are usually combined into a single coefficient

$$P_\alpha^\kappa (T_\alpha, p_\alpha) := p_\alpha \, \Phi_\alpha^\kappa (T_\alpha, p_\alpha^\kappa) \,.$$

For components that exhibit a low miscibility with the liquid, this coefficient is called HENRY coefficient; otherwise, the component is the dominant constituent of the liquid, and P_α^κ is either called RAOULT *coefficient*, *vapor pressure* or *saturation pressure*.

3.4 Capillary Pressure and Relative Permeability

After our detailed discussion of thermodynamic equilibrium in the previous section, we will now cover the most widely used heuristic capillary pressure curves in greater detail.

In the case of two fluid phases with the capillary pressure only depending on the phase saturations, we can apply one of the two most commonly used capillary pressure and relative permeability functions —the one proposed by to BROOKS and COREY or the function of VAN

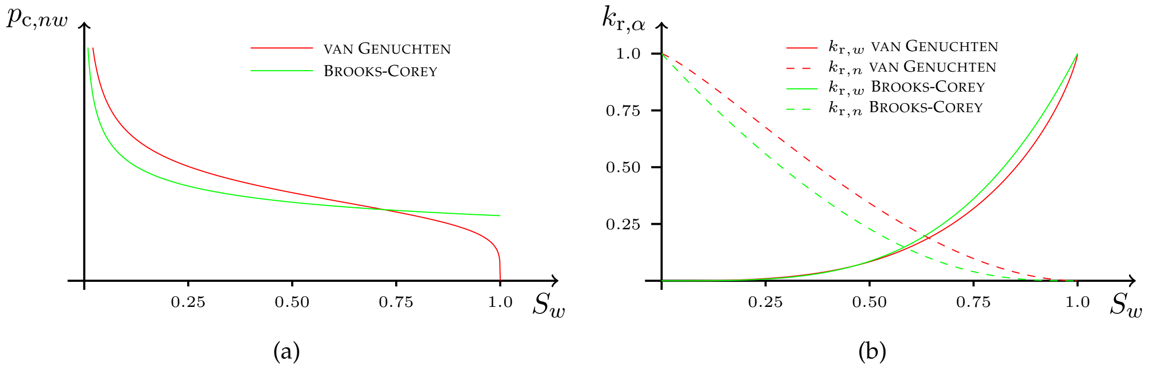

(a) (b)

Figure 3.2: Principle shapes of the BROOKS-COREY and VAN GENUCHTEN functions for two-phase flow in porous media. The parameters of the functions have been converted using the approach proposed by LENHARD, PARKER, and MISHRA [50]. **(a)** Capillary pressure. **(b)** Relative Permeability.

GENUCHTEN. These functions will also be the subject of the following subsections and are illustrated in Figure 3.2.

3.4.1 Generic Two-Phase Relations for Relative Permeability

Before we deal with the saturation-dependent two-phase capillary pressure curves, we need to discuss the connection between the capillary pressure and the relative permeability for them. As it turns out that, although in general we can regard the relative permeabilities $k_{r,\alpha}$ and the capillary pressures $p_{c,\alpha}$ as independent quantities, they have been shown to be related in the most common cases [39]. If only two fluid phases are involved, and the capillary pressure between those only depends on the fluid saturations, the relative permeabilities are given by the equations [39]

$$k_{r,w} = {S_w}^A \left(\frac{\int_0^{S_w} \left(p_{c,nw}(\hat{S}_w)\right)^{-B} \, d\hat{S}_w}{\int_0^1 \left(p_{c,nw}(\hat{S}_w)\right)^{-B} \, d\hat{S}_w} \right)^C \quad \text{and} \tag{3.16}$$

$$k_{r,n} = (1 - S_w)^A \left(\frac{\int_{S_w}^1 \left(p_{c,nw}(\hat{S}_w)\right)^{-B} \, d\hat{S}_w}{\int_0^1 \left(p_{c,nw}(\hat{S}_w)\right)^{-B} \, d\hat{S}_w} \right)^C \tag{3.17}$$

with some constants A, B, and C. We note that it is not possible to directly apply these equations to capillary pressure functions without choosing concrete values for A, B, and C.

3.4.2 Relation of BROOKS and COREY

The most widely applied approach for capillary pressure in two-phase flows is the one proposed by BROOKS and COREY [13, 39]. This approach considers two fluid phases, the wetting and the non-wetting phases. There, the fluid for which the contact angle of the fluid-fluid interface with the surface of the solid is smaller than $90°$ is defined as the *wetting* fluid, the other fluid is called *non-wetting*. The capillary pressure relation proposed by BROOKS and COREY now assumes that the only quantity on which the difference in pressure between the wetting and the non-wetting phase depends, is the saturation of the wetting phase. Under these preconditions, BROOKS and COREY proposed [13] the relation

$$p_{\mathrm{c},nw} = p_n - p_w = p_{\mathrm{e}} S_w^{-\frac{1}{\lambda_{\mathrm{bc}}}} , \tag{3.18}$$

where p_{e} is the *entry pressure* and λ_{bc} is a *shape parameter*. Both of these parameters are highly specific to the properties of the porous medium as well as to the properties of the considered fluids [39]. For this reason, these two parameters are usually obtained experimentally [39].

In conjunction with the BROOKS-COREY capillary pressure curve, the BURDINE parameterization $A = B = 2$, and $C = 1$ is normally used [39] for relations of the relative permeabilities which are implied by Equations 3.16 and 3.17. This yields

$$k_{\mathrm{r},w} = S_w^{\frac{2+3\,\lambda_{\mathrm{bc}}}{\lambda_{\mathrm{bc}}}} \quad \text{and} \tag{3.19}$$

$$k_{\mathrm{r},n} = (1 - S_w)^2 \left(1 - S_w^{\frac{2+\lambda_{\mathrm{bc}}}{\lambda_{\mathrm{bc}}}}\right) . \tag{3.20}$$

3.4.3 Curve of VAN GENUCHTEN

As an alternative to the curves proposed by BROOKS and COREY, we can also use the relation proposed by VAN GENUCHTEN [87, 39]. Like the BROOKS-COREY curves, the VAN GENUCHTEN approach presumes that the value of capillary pressure depends solely on the saturation of the wetting phase, but in contrast to the BROOKS-COREY relation, it does not use the concept of entry pressure. Instead, the VAN GENUCHTEN approach assumes that the capillary pressure is zero in a medium which is fully saturated by the wetting phase. Also clearly visible in Figure 3.2 is the fact that for VAN GENUCHTEN curves, the slope is infinite if the porous medium is fully saturated by the wetting phase. This property is thus similar to the entry pressure concept in the BROOKS-COREY approach.

The concrete function proposed by VAN GENUCHTEN [87] is given by

$$p_{\mathrm{c},nw} = p_n - p_w = \frac{1}{\alpha_{\mathrm{vg}}} \left(S_w^{-\frac{1}{m_{\mathrm{vg}}}} - 1 \right)^{\frac{1}{n_{\mathrm{vg}}}} ,$$

where α_{vg}, m_{vg}, and n_{vg} are shape parameters. Like for the BROOKS-COREY relation, at least two of those parameters must be obtained by fitting experimental data. For the third, it is often possible to use the relation

$$m_{\mathrm{vg}} = 1 - {}^{1}\!/_{n_{\mathrm{vg}}}$$

as proposed by VAN GENUCHTEN [87]. We note that instead of using this equation, we also may take advantage of others which better fit experimentally obtained capillary pressure curves [47].

Like for the BROOKS-COREY capillary pressure curves, we can evaluate Equations 3.16 and 3.17 to gain closed relative permeability functions. In contrast to the BROOKS-COREY approach, the parameterization proposed by MUALEM is usually used [39], *i.e.*, $A = 0.5$, $B = 1$, and $C = 2$. With these values, we get

$$k_{\mathrm{r},w} = {S_w}^{\epsilon_{\mathrm{vg}}} \left(1 - \left(1 - {S_w}^{\frac{1}{m_{\mathrm{vg}}}}\right)^{m_{\mathrm{vg}}}\right)^{2} \quad \text{and} \tag{3.21}$$

$$k_{\mathrm{r},n} = (1 - S_w)^{\gamma_{\mathrm{vg}}} \left(1 - \left(1 - {S_w}^{\frac{1}{m_{\mathrm{vg}}}}\right)^{m_{\mathrm{vg}}}\right)^{2\,m_{\mathrm{vg}}} \tag{3.22}$$

where ϵ_{vg} and γ_{vg} are parameters that depend on the microscopic properties of the porous medium. Often [39] we can assume their values to be $\epsilon_{\mathrm{vg}} = {}^{1}\!/_{2}$ and $\gamma_{\mathrm{vg}} = {}^{1}\!/_{3}$.

3.4.4 Three-Phase Systems

The final capillary pressure relations which we will cover in detail were proposed by STONE [79, 39], and are concerned with three-phase flow in porous media.

For such systems, we assume three potentially present phases called "wetting liquid", "non-wetting liquid", and "gas", indicated by $\langle\cdot\rangle_w$, $\langle\cdot\rangle_n$, and $\langle\cdot\rangle_g$ in the following. For such systems, it has been observed [52], that in many situations the relative permeability of the wetting liquid phase $k_{\mathrm{r},w}$ and the relative permeability of the gas phase $k_{\mathrm{r},g}$ primarily depend on the saturations of the wetting liquid and the gas, respectively. Also, the capillary pressures between the wetting liquid and the non-wetting liquid $p_{\mathrm{c},nw}$ has been shown to depend mainly on the saturation of the wetting liquid and we can assume that the only non-negligible dependency of the capillary pressure between the gas and the non-wetting liquid phases $p_{\mathrm{c},gn}$ is the saturation of the gas phase [39].

The main idea of the two approaches proposed by STONE [79, 80] is to take advantage of the capillary pressure relations for the two-phase cases with the wetting and the non-wetting liquids—which we will indicate by $\langle\cdot\rangle_{\mathrm{wn}}$ in the following—as well as the capillary pressure curves for the two-phase system featuring the non-wetting liquid and the gas—indicated by $\langle\cdot\rangle_{\mathrm{ng}}$. Under these assumptions, we can use the appropriate two-phase relations to define the three-phase capillary pressure relations, *i.e.*,

$$p_{\mathrm{c},nw}(S_w, S_n, S_g) = p_{\mathrm{cwn},nw}(S_w) \quad \text{and} \tag{3.23}$$

$$p_{\mathrm{c},gn}(S_w, S_n, S_g) = p_{\mathrm{cnw},gn}(1 - S_g)\ . \tag{3.24}$$

Similarly, we define the wetting liquid and the gas relative permeabilities of the corresponding two-phase systems, *i.e.*,

$$k_{\mathrm{r},w}(S_w, S_n, S_g) = k_{\mathrm{rwn},w}(S_w) \quad \text{and} \tag{3.25}$$

$$k_{\mathrm{r},g}(S_w, S_n, S_g) = k_{\mathrm{rng},g}(1 - S_g)\ . \tag{3.26}$$

For the relative permeability of the non-wetting liquid $k_{\mathrm{r},n}$, STONE proposed two approaches: The first [79] uses the relation

$$k_{\mathrm{r},n}(S_w, S_n, S_g) = S_n \frac{k_{\mathrm{rwn},n}(S_w)}{1 - S_w} \frac{k_{\mathrm{rng},n}(1 - S_g)}{1 - S_g}\ , \tag{3.27}$$

whilst the second [80] defines $k_{\mathrm{r},n}$ as

$$\begin{aligned} k_{\mathrm{r},n}(S_w, S_n, S_g) =& (k_{\mathrm{rng},n}(1 - S_g) + k_{\mathrm{rng},g}(1 - S_g)) \cdot (k_{\mathrm{rwn},n}(S_w) + k_{\mathrm{rwn},w}(S_w)) \\ & - (k_{\mathrm{rwn},w}(S_w) + k_{\mathrm{rng},g}(1 - S_g))\ . \end{aligned}$$

3.4.5 Advanced Concepts

We note that, the approaches which we covered so far do not take residual saturations [39] into account in order to simplify the discussion. We can imagine the residual saturation of a phase as the saturation of the fluid that cannot be transported by advection – an effect that is caused by various mechanisms that trap fluids within a porous medium [39]. Having said that, this material can be dissolved by the other fluids and be transported this way.

Also, there are quite a few advanced concepts when it comes to capillary pressure: Amongst these are temperature [73] and fluid composition [27] dependence, approaches which discard the assumption of mechanical equilibrium [38], and methods to take hysteresis into account [65, 59, 10].

3.5 Model Constraints

At this point, if we count the number of independent equations which we have defined for our M-phase, N-component system, we get $2N \cdot M + N + 6M + 3$:

- The three externally impressed functions gravitational acceleration $\boldsymbol{g}$, intrinsic permeability $\boldsymbol{K}$, and porosity ϕ,
- a closure condition for saturations (3.1),
- M relations connecting the molar density $\rho_{\mathrm{mol},\alpha}$ with the mass density ρ_α,
- M functions for the dynamic viscosities μ_α,
- M relations capturing the relative permeabilities $k_{\mathrm{r},\alpha}$,

- N source terms q^κ,
- $M \cdot N$ closed functions for the molecular diffusion coefficients in the porous medium $D^\kappa_{\mathrm{pm},\alpha}$,
- M equations of state (3.2),
- $M - 1$ constraints from the thermal equilibrium (3.5),
- $M - 1$ equations for the mechanical equilibrium (3.7),
- N mass balance equations (2.47),
- an impressed temperature function if we neglect conservation of energy, or an energy conservation equation in the other case, and
- $(M - 1) \cdot N$ conditions stemming from the chemical equilibrium (3.9).

On the side of the unknowns, we additionally need M phase temperatures T_α, so we now have $2N \cdot M + N + 7M + 3$ unknowns. This means that, at this point, we are still missing M equations to make the system of equations well-defined. In the context of this thesis, we will call these M relations *model constraints*, and in the next few sections we will discuss several approaches which define these model constraints.

3.5.1 Immiscibility

The first set of model constraints we will cover here is the one which ignores miscibility altogether. It is a reasonable approximation of a real system if all fluid phases exhibit a highly preferred component. Immiscibility [39] thus means that each phase α is composed of only a single component κ_α, *i.e.*,

$$x^\kappa_\alpha = \begin{cases} 1 & \text{for } \kappa = \kappa_\alpha \text{ and} \\ 0 & \text{else.} \end{cases} \tag{3.28}$$

Using the thermodynamical framework outlined before, we can achieve this by letting the fugacity coefficient of the "non-preferred" components be infinite whilst keeping it finite for the constituent component, for example

$$\Phi^\kappa_\alpha = \begin{cases} 1 & \text{for } \kappa = \kappa_\alpha \text{ and} \\ \infty & \text{else.} \end{cases} \tag{3.29}$$

In this context, we should be aware of the fact that Equation 3.29 cannot be used directly in numerical software because of the occurrence of infinite values in the fugacity coefficients. Instead, we need to implicitly set the mole fractions of all "non-preferred" components of a phase to zero and the mole fraction of the "preferred" component to one.

The M model constraints are then given by the requirement that all phases are always potentially present, *i.e.*,

$$\sum_\kappa x^\kappa_\alpha = x^{\kappa_\alpha}_\alpha = 1 \tag{3.30}$$

holds for any phase α.

3.5.2 Primary Variable Switching

We can obtain a second set of model constraints if the set of fluids which are present at a given location in space at a given time are known: In the case that phase α is present, the sum of the mole fractions which fulfill the condition of chemical equilibrium (3.12) sum up to one, *i.e.*,

$$\sum_\kappa x_\alpha^\kappa = 1$$

holds. In the other case, phase α is not present at the location, so that its saturation must be zero, *i.e.*,

$$S_\alpha = 0$$

This leads to the following set of model constraints [23]

$$0 = \begin{cases} 1 - \sum_\kappa x_\alpha^\kappa & \text{if phase } \alpha \text{ is present, and} \\ S_\alpha & \text{if it is not present.} \end{cases} \tag{3.31}$$

In flow simulations, a phase can appear or disappear, and thus we need to adapt the set of phases which are present at a given location during the process of finding a solution. This can be accomplished by continuing the solution procedure with a given set of present phases, and changing this set if an intermediate state is physically impossible. In such an event, we need to update the set of present phases, and choose physically meaningful quantities as primary variables.

In the following, we use the following switching conditions:

- A present phase vanishes if the saturation of the phase becomes negative, *i.e.*, if

  $$S_\alpha < 0$$

  holds. In this case we remove the saturation S_α of the vanished phase from the set of primary variables, and replace it by a mole fraction of a component for a fluid that is present.

- A non-present phase α appears if the quantities x_α^κ that meet the condition for chemical equilibrium (3.12) are interpretable as mole fractions. This is the case if the sum of x_α^κ in the phase is equal to 1. In numerical simulations we also have to be prepared that sum of x_α^κ can become larger than 1, *i.e.*, we use the condition

  $$\sum_\kappa x_\alpha^\kappa \geq 1$$

  as switching condition.

  If we detect such a state, we remove the mole fraction of a component from the set of primary variables, and replace it by the saturation S_α of the newly appeared phase.

In Section 5.2.2 we will discuss in greater detail how these primary variable switching (PVS) model assumptions can be implemented in numerical software.

3.5.3 Non-Linear Complementarity Functions

An alternative to the procedure above is to directly include the conditions outlined in the previous section into the set of equations to be solved [48]: For this we observe that, as long as phase α is not present, the sum of the mole fractions which meet the chemical equilibrium condition (3.12) are allowed to be smaller than 1, *i.e.*,

$$S_\alpha = 0 \implies \sum_\kappa x_\alpha^\kappa \leq 1 \; .$$

Next, we observe that a necessary precondition for phase α to be present is that its constituent mole fractions sum up to one, *i.e.*,

$$\sum_\kappa x_\alpha^\kappa = 1 \implies S_\alpha \geq 0$$

holds.

Since each phase is either present or non-present, at least one of the above cases must apply, we get the following *non-linear complementarity problem* (NCP) for each fluid phase α:

$$S_\alpha \left(1 - \sum_\kappa x_\alpha^\kappa\right) = 0 \quad \wedge \quad 1 - \sum_\kappa x_\alpha^\kappa \geq 0 \quad \wedge \quad S_\alpha \geq 0 \; . \tag{3.32}$$

Such a problem can be directly included into the system of equations to be solved using a *non-linear complementarity function* $\Psi : \boldsymbol{R}^2 \to \boldsymbol{R}$ which is exhibits the property

$$\Psi(a,b) = 0 \iff a \geq 0 \wedge b \geq 0 \wedge a \cdot b = 0 \; .$$

There are multiple possible choices for Ψ; for example, the FISCHER-BURMEISTER non-linear complementarity function [32] Ψ_{FB} is defined as

$$\Psi_{\mathrm{FB}}(a,b) = a + b - \sqrt{a^2 + b^2} \; .$$

For the remainder of this work, we will use the minimum function $\Psi(a,b) = \min(a,b)$ because of its piecewise linearity. This means that we will use the model constraints

$$\Psi_\alpha\,(S_\alpha,\; 1 - \sum_\kappa x_\alpha^\kappa) = \min\,(S_\alpha,\; 1 - \sum_\kappa x_\alpha^\kappa) = 0 \tag{3.33}$$

when discussing the NCP model.

3.5.4 Black-Oil

The black-oil model is a set of model assumptions widely used in the oil industry [83, 19, 46, 45]. It presumes three potentially present fluids oil, gas, and water—in the following indicated by $\langle\cdot\rangle_o$, $\langle\cdot\rangle_g$, and $\langle\cdot\rangle_w$—as well as three pseudo-components to which we also refer

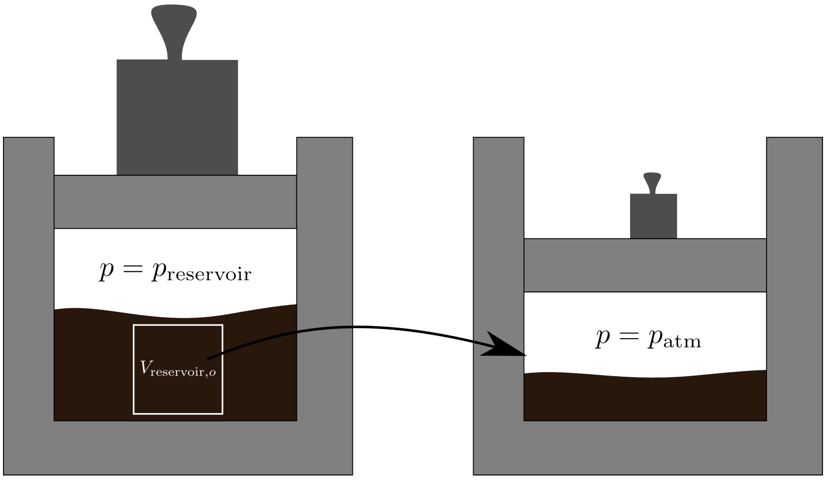

Figure 3.3: Definition of the gas solubility factor R_S in the black-oil model: A given volume of saturated oil $V_{\text{reservoir},o}$ is brought from reservoir pressure $p_{\text{reservoir}}$ to the relatively low atmospheric pressure p_{atm}. Then, the gas solubility factor is defined as the ratio between volume of gas which emerges at the surface and the original volume of the reservoir oil. Typically, the reservoir pressure exceeds 200 bar while p_{atm} is roughly 1 bar.

to as oil, gas, and water, and which will be indicated by $\langle\cdot\rangle^O$, $\langle\cdot\rangle^G$, and $\langle\cdot\rangle^W$. In the terms of the thermodynamic framework of this chapter, the black-oil model presumes $M = N = 3$.

The first assumption of the black-oil model is that the water, and gas phases are immiscible, and that they are solely constituted by the components with the same names. In contrast, the oil phase is assumed to be a mixture of the pseudo-components gas and oil with the composition given by the *gas solubility factor* R_S.

This factor is defined as the volume of the gas phase that emerges from a given amount of gas-saturated oil phase if the of oil is brought from the reservoir to the surface, *i.e.*, that the pressure of the material is reduced from reservoir pressure to atmospheric pressure, as illustrated in Figure 3.3. We thus define R_S as

$$R_\text{S} := \frac{V_{\text{atm},g}}{V_{\text{reservoir},o}} = \frac{S_{\text{atm},g} V_{\text{total,atm}}}{V_{\text{reservoir},o}} \; .$$

Given the gas solubility factor at a certain pressure, the composition of gas saturated oil at reservoir pressure can thus be determined in terms of mass fractions using

$$X^G_{\text{sat},o} = \frac{\rho_g(p_{\text{atm}}) R_\text{S}(p_o)}{\rho_{\text{sat},o}(p_o)} \quad \text{and} \quad X^O_{\text{sat},o} = 1 - X^G_{\text{sat},o}$$

if we assume that the amount of the gas in oil is negligible at atmospheric pressure.

We also need to specify the mass densities of all phases at a given pressure. While we assume the water phase to be incompressible, the density of the gas saturated oil phase ρ_o and the one of the gas phase ρ_g is determined by the *oil and the gas formation volume factors* B_o and B_g.

These two factors express the ratio between the mass density at reservoir pressure and the density at atmospheric pressure, *i.e.*,

$$B_\alpha(p_\alpha) = \frac{\rho_{\mathrm{sat},\alpha}(p_\alpha)}{\rho_{\mathrm{sat},\alpha}(p_{\mathrm{atm}})}, \quad \alpha \in \{o, g\} ,$$

where the atmospheric densities $\rho_{\mathrm{sat},\alpha}(p_{\mathrm{atm}})$ are given constants.

Fugacity Coefficients

In order to fit the set of black-oil parameters into our thermodynamic framework, we need to define fugacity coefficients Φ_α^κ for all components κ and all fluid phases α as well as the mass densities of all fluid phases. In the following, we will outline how we can achieve this goal.

The black-oil parameters assume the gas and the water phases to be immiscible, *i.e.*, the only constituent of the gas phase is the gas component, and that of the water phase is the water component. For this reason, we can use the same approach to the fugacity coefficients as for the immiscible model constraints, *i.e.*,

$$\Phi_\alpha^\kappa = \begin{cases} 1 & \text{if } \kappa = \kappa_\alpha, \\ \infty & \text{else} \end{cases}$$

for $\alpha \in \{w, g\}$, $\kappa \in \{O, W, G\}$, and with $\kappa_w = W$, $\kappa_g = G$.

Since the oil phase is a mixture of the gas and the oil components, we first need to ensure that the oil phase does not contain any water by setting the fugacity coefficient for the water component in the oil phase to infinity. For the fugacity coefficient of the oil component in the oil phase, we can use any finite positive value; usually we use

$$\Phi_o^O = \frac{p_{\mathrm{vap}}^O}{p_o}$$

where p_{vap}^O denotes a typical *vapor* or *saturation pressure* of the oil component.

The most elaborate fugacity coefficient is the one for the gas component in the oil phase. This is due to the facts that the gas component is the only component which is assumed to be potentially present in two fluid phases, *i.e.*, the gas and the oil phase, and that we must choose the fugacity coefficient such that it is consistent with the black-oil parameters. We can achieve this by first calculating the mass fractions $X_{\mathrm{sat},o}^O$ and $X_{\mathrm{sat},o}^G$ for gas saturated oil as outlined in the previous section. Next, we need to convert these mass fractions into mole fractions by solving the system of equations

$$\begin{aligned} X_{\mathrm{sat},o}^G &= \frac{M^G}{\overline{M}_o} x_{\mathrm{sat},o}^G, \\ \overline{M}_o &= x_{\mathrm{sat},o}^O M^O + x_{\mathrm{sat},o}^G M^G \text{ , and} \\ x_{\mathrm{sat},o}^G + x_{\mathrm{sat},o}^O &= 1 \end{aligned}$$

in regard to $x^G_{\mathrm{sat},o}$. This yields

$$x^G_{\mathrm{sat},o} = \frac{M^O X^G_{\mathrm{sat},o}}{M^G + X^G_{\mathrm{sat},o}(M^O - M^G)} \quad \text{and} \quad x^O_{\mathrm{sat},o} = 1 - x^G_{\mathrm{sat},o} \; .$$

For gas saturated oil, we can now define the fugacity coefficient of the gas component in the oil phase using the definition of the fugacity coefficients (3.13), and inserting it into the condition for chemical equilibrium (3.12). Assuming that the capillary pressure is negligible, we get

$$\Phi^G_o = \frac{\Phi^G_g}{x^G_{\mathrm{sat},o}} \; .$$

Mass Density of the Oil Phase

The presented black-oil parameters directly provide densities $\rho_{\mathrm{sat},\alpha}$ for all three saturated phases, but—somewhat surprisingly—we must take quite complex measures to define ρ_o, the mass density of potentially undersaturated oil. The reason for this is that—in contrast to the water and gas phases—the oil phase may dissolve less gas than the maximum physically possible amount but the black-oil parameters only specify oil phase densities for gas saturated oil. To define ρ_o, we take a closer look at the total derivative of the mass density of the saturated oil phase with respect to pressure. Applying the chain rule, we get

$$\frac{\mathrm{d}\rho_{\mathrm{sat},o}}{\mathrm{d}p_o} = \frac{\mathrm{d}}{\mathrm{d}p_o}\rho_o(p_o, X^O_{\mathrm{sat},o}(p_o), X^G_{\mathrm{sat},o}(p_o)) = \frac{\partial \rho_o}{\partial X^G_o}\frac{\partial X^G_{\mathrm{sat},o}}{\partial p_o} + \frac{\partial \rho_o}{\partial X^O_o}\frac{\partial X^O_{\mathrm{sat},o}}{\partial p_o} + \frac{\partial \rho_o}{\partial p_o} \; ,$$

where $X^G_{\mathrm{sat},o}(p_o)$ and $X^O_{\mathrm{sat},o}(p_o)$ are the mass fractions of the gas and oil components of gas saturated oil at pressure p_o as specified by the black-oil parameters. Taking advantage of the fact that the mass fractions of all components sum up to one for oil, we get

$$\frac{\mathrm{d}\rho_{\mathrm{sat},o}}{\mathrm{d}p_o} = \frac{\partial X^G_{\mathrm{sat},o}}{\partial p_o}\left(\frac{\partial \rho_o}{\partial X^G_o} - \frac{\partial \rho_o}{\partial X^O_o}\right) + \frac{\partial \rho_o}{\partial p_o} \; . \tag{3.34}$$

Further, we now suppose that the compressibility of the oil phase is a given constant, *i.e.*,

$$\frac{\partial \rho_o}{\partial p_o} := \mathrm{const}$$

holds, and we already assumed the mass fraction of gas in saturated oil at atmospheric pressure to be negligible. Under these preconditions, we may use the density of the oil at the surface together with the compressibility to define the partial derivative of the mass density of the oil phase regarding the mass fraction of the oil component, *i.e.*,

$$\frac{\partial \rho_o}{\partial X^O_o} := \rho_{\mathrm{sat},o}(p_{\mathrm{atm}})\left(1 + \frac{\partial \rho_o}{\partial p_o}(p_o - p_{\mathrm{atm}})\right) \; .$$

We now observe that Equation 3.34 determines the partial derivative of the gas mass fraction in saturated oil using the black-oil parameters. Resolving, we get

$$\frac{\partial \rho_o}{\partial X_o^G} = \left(\frac{\partial X_{\mathrm{sat},o}^G}{\partial p_o} \right)^{-1} \left(\frac{\mathrm{d}\rho_{\mathrm{sat},o}}{\mathrm{d}p_o} - \frac{\partial \rho_o}{\partial p_o} \right) + \frac{\partial \rho_o}{\partial X_o^O} \; .$$

Assuming that these derivatives stay constant for undersaturated oil, we can finally define the generic mass density of oil as:

$$\rho_o = \rho_{\mathrm{sat},o}(p_o) + \left(X_o^G - X_{\mathrm{sat},o}^G \right) \frac{\partial \rho_o}{\partial X_o^G} + \left(X_o^O - X_{\mathrm{sat},o}^O \right) \frac{\partial \rho_o}{\partial X_o^O} \; .$$

Black-Oil Model Constraints

Now that we defined all relevant quantities using only the black-oil parameters as input, we need to specify the appropriate model constraints in order to use the abstract thermodynamic framework presented in this chapter. First, we observe that we can use the immiscibility model constraints for the water and for the gas phases, *i.e.*,

$$\sum_\kappa x_\alpha^\kappa = x_\alpha^{\kappa_\alpha} = 1$$

for $\alpha \in \{w, g\}$. For the oil phase, we assume that it is always potentially present, which leads to the constraint

$$\sum_\kappa x_o^\kappa = x_o^O + x_o^G = 1 \; .$$

Like for the immiscibility model assumptions, we cannot use some of the presented definitions directly in software implementations since some of the fugacity coefficients exhibit infinite values. Thus, we may either approximate the black-oil model by using very large fugacity coefficients, or we can implement it by directly incorporating them into the software.

3.6 Chapter Synopsis

In this chapter, we made the mathematical description of multi-phase, multi-component flows in a porous medium well-defined. In particular, this implied the need to specify the same number of independent equations as quantities. We obtained some of these relations by assuming a few quantities to be closed functions, a few others were obtained by assuming them to be given parameters depending on the time and the spatial location within the domain. Examples of the former are the dynamic viscosities μ_α and mass densities ρ_α of the fluids, while examples of the latter are the gravitational acceleration vector $\boldsymbol{g}$ and the intrinsic permeability $\boldsymbol{K}$.

We then accounted for the additional relations implied by thermodynamics. At this occasion, we discussed some widely used equations of state, and outlined the conditions implied by assuming local thermodynamic equilibrium.

Finally, we noted that one equation per fluid phase was still missing. We identified these missing relations as model specific constraints, and we discussed three established sets of constraints, *i.e.*, the immiscibility, primary variable switching (PVS), and black-oil models. We also presented a new set of model constraints which are based on solving non-linear complementarity problems (NCP).

4 Numerics

In this chapter we will look at methods to approximately solve the equations outlined in Chapters 2 and 3. First, we will discuss ways of transforming a system of partial differential equations into a system of ordinary differential equations in Section 4.1. In Section 4.2 we then transform these ordinary differential equations into a series of systems of non-linear algebraic equations. Next, we will discuss the NEWTON-RAPHSON scheme, a method to solve such systems of non-linear algebraic equations in Section 4.3. This method repeatedly linearizes the non-linear system of equations, and uses the solution of each of those to calculate the starting point for the next iteration. Then, we will discuss methods for efficiently solving these linear systems of equations in Section 4.4. The final section presented in this chapter, Section 4.5, covers approaches to adapt the resulting numerical methods to loosely coupled parallel computers.

4.1 Spatial Discretization

Conceptually, we first need to transform partial differential equations for mass conservation (2.47) and energy conservation (2.46) into a series of systems of algebraic equations. To achieve this, we utilize a two-stage approach: We first transform them into a system of ordinary differential equations using a spatial discretization, then we apply a time discretization scheme to transform it into a system of coupled algebraic equations. This section is devoted to the conversion of the conservation equations into systems of ordinary differential equations, while the next section covers time discretization methods.

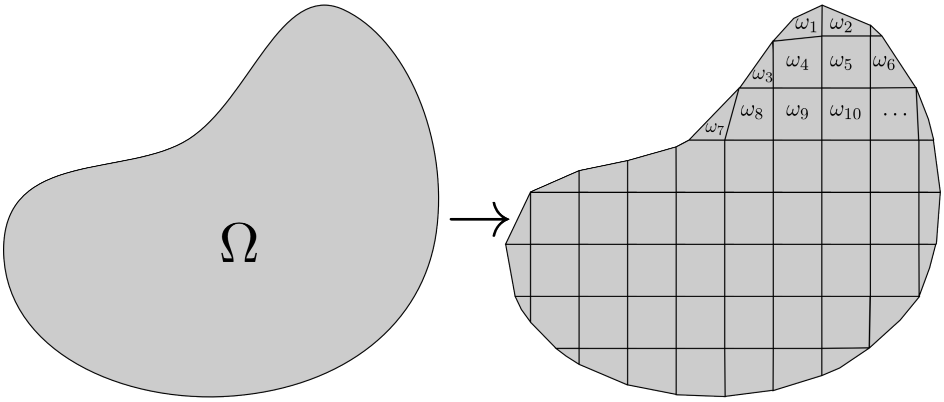

Figure 4.1: A discretization of the spatial domain Ω into a set of conforming convex polygons $\{\omega_1, \dots, \omega_n\}$.

Quite a few spatial discretization schemes have been proposed to date. The ones which are most widely used are based on the ideas of the finite volume [31], finite element [29, 81], and discontinuous GALERKIN approaches [5]. All of these methods share the property that the spatial domain Ω is partitioned into n smaller subdomains $\{\omega_1, \omega_2, \ldots, \omega_n\}$. The individual subdomains are called *elements* or *cells*, whilst the partition itself is called *grid* or *mesh*. In the context of this work, we assume that all elements of a grid are convex polygons, and that the grid is conforming, *i.e.*, that no vertex is located at any non-corner position of any element. Such a grid is depicted in Figure 4.1.

The fundamental idea for partitioning the domain Ω is the fact, that the solution for Ω may be described as the superposition of the solutions of an arbitrary but fixed number subsets of Ω, provided that these subsets do not overlap, and that Ω is fully covered by their union. We thus take advantage of the observation that the partial differential equations are valid for all elements individually. Taking this argument further, if we find *approximate* solutions for all individual subsets, we have found an approximate solution for the whole domain if we combine them. Moreover, if we can make the difference between the approximate and the exact solution arbitrarily small, the approximate solution can be made to be equivalent to the exact one and the discretization scheme is said to be *convergent*. Usually, reducing the accuracy of the approximation requires to increase the number of elements of the partitioning of Ω [29].

To derive the spatial discretization scheme which we will use in the remainder of this work, we use the GAUSS theorem on the integral form of Equation 2.6 for all elements. This yields

$$\begin{aligned} &\int_{\omega_i} \frac{\partial}{\partial t} b \,\mathrm{d}\boldsymbol{x} + \int_{\omega_i} \operatorname{div}(b\boldsymbol{v}) \;\mathrm{d}\boldsymbol{x} - \int_{\omega_i} q \,\mathrm{d}\boldsymbol{x} = \\ &\int_{\omega_i} \frac{\partial}{\partial t} b \,\mathrm{d}\boldsymbol{x} + \int_{\partial\omega_i} \boldsymbol{n}_i \cdot b\boldsymbol{v} \,\mathrm{d}\boldsymbol{y} - \int_{\omega_i} q \,\mathrm{d}\boldsymbol{x} = 0 \end{aligned}$$

for each element ω_i.

Since the EULERIAN approach uses an observation volume which is fixed in time, the time derivative and the spatial integral commute. Thus we get

$$\frac{\partial}{\partial t} \int_{\omega_i} b \,\mathrm{d}\boldsymbol{x} + \int_{\partial\omega_i} \boldsymbol{n}_i \cdot b\boldsymbol{v} \,\mathrm{d}\boldsymbol{y} - \int_{\omega_i} q \,\mathrm{d}\boldsymbol{x} = 0 \; .$$

Taking advantage of the assumption that all elements are polyhedra which exhibit planar surfaces, we may split the integral of the flux term into a sum of fluxes, one for each of the faces $\{\partial\omega_{i,1}, \partial\omega_{i,2}, \ldots, \partial\omega_{i,m_i}\}$ of the element:

$$\frac{\partial}{\partial t} \int_{\omega_i} b \,\mathrm{d}\boldsymbol{x} + \sum_{j=1}^{m_i} \left(\|\partial\omega_{i,j}\| \boldsymbol{n}_{i,j} \cdot \int_{\partial\omega_{i,j}} b\boldsymbol{v} \,\mathrm{d}\boldsymbol{y} \right) - \int_{\omega_i} q \,\mathrm{d}\boldsymbol{x} = 0 \; .$$

From this, we get the standard finite volume scheme by assuming that all quantities are

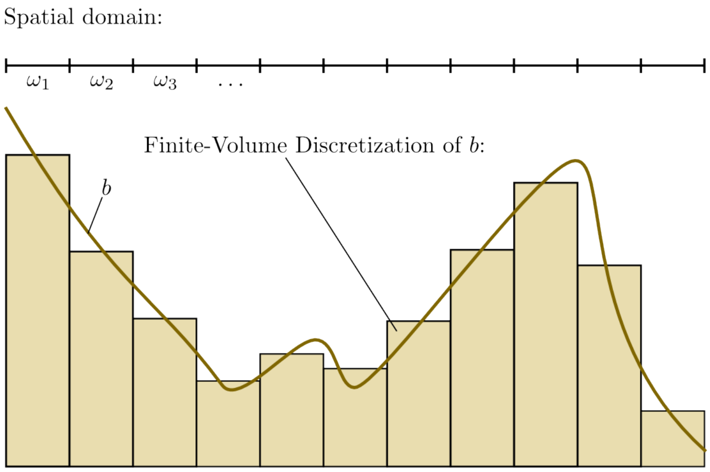

Figure 4.2: Illustration of the finite volume discretization of a function b defined on a one-dimensional spatial domain: After discretizing the continuous spatial domain Ω into multiple line segments $\{\omega_1, \omega_2, \dots, \omega_n\}$, the quantity b is assumed to be constant within each subvolume ω_i, and thus we get discontinuities at the boundaries of the subdomains. For two and three-dimensional domains, the method works in an analogous way.

constant within an element, *i.e.*,

$$\|\omega_i\| \frac{\partial b_i}{\partial t} + \sum_{j=1}^{m_i} \|\partial\omega_{i,j}\| \, b_{i,j} \boldsymbol{n}_{i,j} \cdot \boldsymbol{v}_{i,j} - \|\omega_i\| q_i = 0$$

holds, as illustrated in Figure 4.2 for the one dimensional case.

A problem specific to this scheme is the calculation of the quantities which are required on the boundaries of the finite volumes since the quantities are discontinuous there. We deal with these discontinuities using two approaches:

Averaging: Parameters that do not depend on the solution— like ones impressed externally— can be averaged. In the context of flows in porous media, this is the case for intrinsic permeability $\boldsymbol{K}$ which needs to be averaged using the harmonic mean [40].

Upstreaming: Quantities fully determined by the solution must be *upstreamed* [40]. Upstreaming is the numerical equivalent of the fact that the flux of conservation quantities only depends on the location where these quantities originate. An example are air flows: Whether a smell reaches an observer only depends on whether the air passes the cause of the smell before or after it reaches the observer—*i.e.*, whether the observer is in *downstream* or in *upstream* direction. This correlation is illustrated in Figure 4.3.

In the context of flows in porous media, quantities that need to be upstreamed are the relative permeabilities $k_{\mathrm{r},\alpha}$, molar densities $\rho_{\mathrm{mol},\alpha}$ and mole fractions x_α^κ.

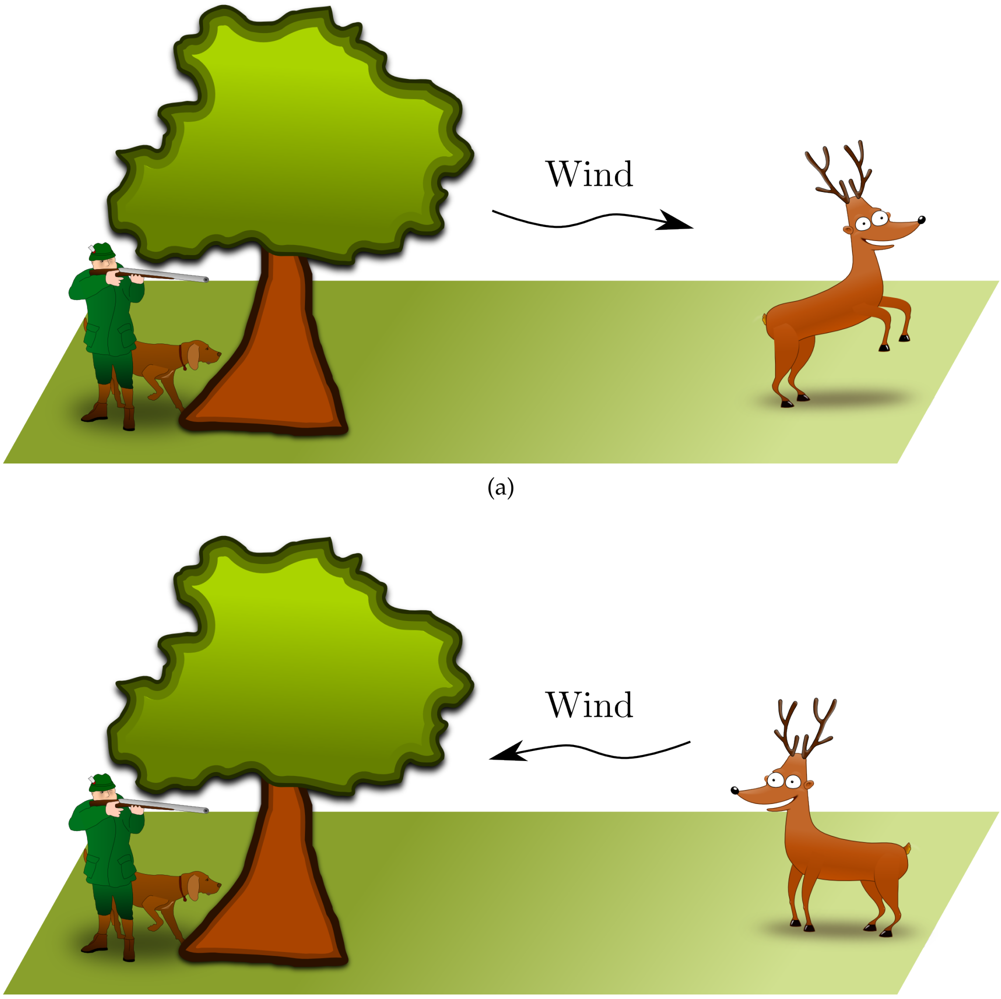

(a)

(b)

Figure 4.3: Illustration of the upstreaming concept: **(a)** The hunter is in the upstream wind direction relative to his prey, *i.e.*, the air passes the hunter before it reaches the deer, and the deer can thus percept the smell of the hunting party. **(b)** The deer is unsuspecting because the hunting party is in the direction of the wind, and the deer thus cannot smell it. (Images are based on works from `http://openclipart.org`.)

Flux Approximation

The final problem which needs to be solved if we use a finite volume method as spatial discretization is that we need a way to calculate spatial gradients at the boundaries of finite volumes to obtain the filter velocities of the fluid phases. Again, this is only a problem because the discretized solutions are discontinuous at the boundaries of the finite volumes. This means that, strictly speaking, spatial gradients within finite volumes are zero, whilst they are undefined at their boundaries.

The most simple method to define these gradients is to apply the *two-point gradient approx-*

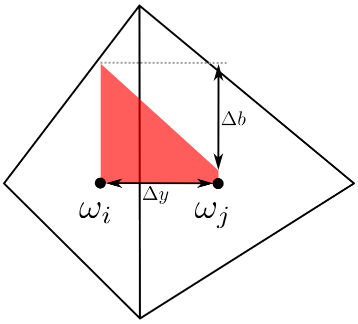

Figure 4.4: Illustration of the two point gradient approximation: The centers of the two finite volumes i and j are $\Delta x := \|\boldsymbol{x}_j - \boldsymbol{x}_i\|$ apart, while the difference of the quantity b for which we seek the gradient at the interface is $b_j - b_i$.

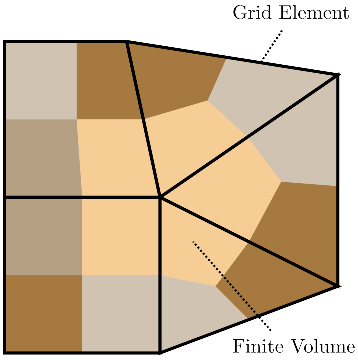

Figure 4.5: The vertex-centered finite volume spatial discretization used for the numerical examples of this thesis: The black lines correspond to the primary grid as described in Section 4.1, areas of identical color are associated with a finite volume on which the conservation equations are considered. The finite volumes are constructed by associating each point of the domain to the closest vertex of the primary grid.

imation scheme as illustrated in Figure 4.4. For this method we assume that the values for all quantities are given at the centers of the two finite volumes adjacent to the boundary for which the gradient needs to be calculated. If we further assume a linear gradient of these quantities, we can approximate the gradient of b by

$$\mathbf{grad}\; b_{i,j} \approx \frac{b_j - b_i}{\|\boldsymbol{x}_j - \boldsymbol{x}_i\|} \;,$$

where b_i and b_j are the values for the quantities of the finite volumes i and j, and $\boldsymbol{x}_i$ and $\boldsymbol{x}_j$ are the positions of their centers.

Another method is to construct a *dual grid*. As illustrated in Figure 4.5, we define an element of the dual grid to be the set of points for which a given vertex of the primary grid is the nearest one. The conservation equations are then solved for the volumes centered at the vertices of the original grid, and the gradients on the faces of the dual grid elements of the quantities we are interested in may be calculated using the gradients of the set of the linear finite element shape functions defined on the primary grid. Since the finite volumes for which the conservation equations are solved can be uniquely identified by the vertex of the primary grid, we call these discretizations *vertex-centered finite volume* methods [39].

In this context, we note that more elaborate gradient approximation schemes have been proposed [1]. These have not been implemented for this work, though.

4.2 Time Discretization

Using the methods presented in the previous section, we can transform partial differential equations of the form

$$\frac{\partial b}{\partial t} + \operatorname{div}(b\boldsymbol{v}) = q$$

into a large coupled system of ordinary differential equations of the form

$$\frac{\partial \boldsymbol{B}}{\partial t} = \boldsymbol{Q}\,. \tag{4.1}$$

We now need to transform it into a system of algebraic equations. This can be achieved by taking advantage of TAYLOR's theorem: Any smooth function f which depends on the variable t can be expressed by

$$\mathrm{f}(t) = \sum_{i=0}^{\infty} \frac{1}{i!}\frac{\partial^i \mathrm{f}(t_\mathrm{e})}{\partial t^i}(t - t_\mathrm{e})^i\,,$$

where t_e is called the *expansion point*. This theorem also applies to vectorial functions like Equation 4.1:

$$\boldsymbol{B}(t) = \sum_{i=0}^{\infty} \frac{1}{i!}\frac{\partial^i \boldsymbol{B}(t_\mathrm{e})}{\partial t^i}(t - t_\mathrm{e})^i\,. \tag{4.2}$$

Truncating the right-hand side of Equation 4.2 after the second term we get

$$\boldsymbol{B}(t) = \boldsymbol{B}(t_\mathrm{e}) + \frac{\partial \boldsymbol{B}(t_\mathrm{e})}{\partial t}(t - t_\mathrm{e}) + O((t - t_\mathrm{e})^2)\,.$$

Reordering and neglecting the $O((t - t_\mathrm{e})^2)$ error term—which is acceptable for small values of $t - t_\mathrm{e}$—we get

$$\frac{\partial \boldsymbol{B}(t_\mathrm{e})}{\partial t} \approx \frac{\boldsymbol{B}(t) - \boldsymbol{B}(t_\mathrm{e})}{t - t_\mathrm{e}}\,.$$

For time discretization we now have two options: To advance one step from $t^{[k]}$ to $t^{[k+1]} := t^{[k]} + \Delta t^{[k]}$, we can either discretize *explicitly, i.e.,* exclusively using quantities for the already calculated time $t^{[k]}$; or we can discretize *implicitly, i.e.,* also using quantities defined for time $t^{[k+1]}$. For the explicit approach we set the expansion point to $t_\mathrm{e} = t^{[k]}$, and evaluate at $t = t^{[k+1]}$; for the implicit approach, we use $t_\mathrm{e} = t^{[k+1]}$ as expansion point and evaluate at $t = t^{[k]}$. This yields

$$\boldsymbol{B}(t^{[k+1]}) = \boldsymbol{B}(t^{[k]}) + \frac{\partial \boldsymbol{B}(t^{[k]})}{\partial t}\Delta t^{[k]} \overset{(4.1)}{=} \boldsymbol{B}(t^{[k]}) + \Delta t^{[k]}\boldsymbol{Q}(t^{[k]})$$

as the rule of evolution for the explicit scheme, while we get

$$\boldsymbol{B}(t^{[k+1]}) = \boldsymbol{B}(t^{[k]}) + \frac{\partial \boldsymbol{B}(t^{[k+1]})}{\partial t}\Delta t^{[k]} \overset{(4.1)}{=} \boldsymbol{B}(t^{[k]}) + \Delta t^{[k]}\boldsymbol{Q}(t^{[k+1]}) \tag{4.3}$$

as the evolution law in the implicit case. Both methods are due to LEONHARD EULER, and both have advantages and disadvantages when compared to each other [16]; since the implicit time discretizations exhibit better stability, and, given the fact that in both cases we to have solve the algebraic systems iteratively because of their highly non-linear character, we will use the implicit EULER method (4.3) as time discretization throughout the remainder of this thesis.

It needs to be noted that there are more advanced time discretization methods which exhibit better convergence behavior like the backward differential formula approach [6] and RUNGE-KUTTA methods [16]. In this context, "better" convergence behavior means that the error term of the method is in $O((t - t_{\mathrm{e}})^3)$. Most of these methods are based on the TAYLOR expansion (4.2) but truncate the series differently than the EULER methods.

4.3 Method of NEWTON and RAPHSON

Instead of solving a system of coupled non-linear partial differential equations, we now have to solve a sequence of much larger systems of non-linear algebraic equations. In this work we use the NEWTON-RAPHSON method to accomplish this.

Let us first look at the simplest case: Solving the equation

$$\mathrm{f}(x) = 0$$

featuring a smooth non-linear function $\mathrm{f} : \boldsymbol{R} \to \boldsymbol{R}$. The idea is to start at an arbitrary initial value $x^{[0]}$. Then we linearize the non-linear curve at this position. This means that we need to find the tangent for $\mathrm{f}(x^{[0]})$, and calculate the root of this tangent. We then use the value of this root as start value $x^{[1]}$ of the next iteration. The motivation for this is that $x^{[1]}$ is usually closer to the root of the non-linear function f than $x^{[0]}$. As illustrated in Figure 4.6a, we often can get as close to the root of f as desired by repeating the described procedure.

Now, let us find the root of $\mathrm{g}^{[i]}$, the tangent of f at $x^{[i]}$, defined as

$$\mathrm{g}^{[i]}(x) = m^{[i]}\, x + c^{[i]}, \qquad \text{with } x, m^{[i]}, c^{[i]} \in \boldsymbol{R}\,. \tag{4.4}$$

The slope of the tangent is determined by the derivative of f at the location of the NEWTON-RAPHSON iteration, *i.e.*,

$$m^{[i]} = \frac{\partial\, \mathrm{f}(x^{[i]})}{\partial x}\,.$$

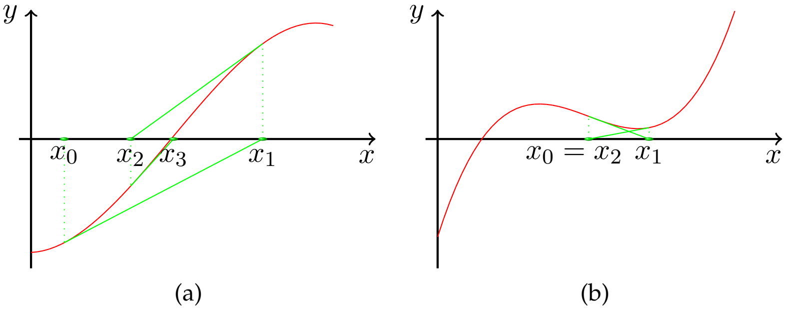

Figure 4.6: Repeated linearization, the idea of the NEWTON-RAPHSON method: **(a)** An example where the approach converges. **(b)** An example where the method oscillates between two values.

Also, $\mathrm{f}(x^{[i]}) = \mathrm{g}(x^{[i]})$ holds so that after resolving to $c^{[i]}$ we get

$$c^{[i]} = \mathrm{f}(x^{[i]}) - m^{[i]}\, x^{[i]} \ .$$

Inserting $m^{[i]}$ and $c^{[i]}$ back into Equation 4.4, requiring that $\mathrm{g}^{[i]}(x^{[i+1]}) = 0$, and resolving for the next iterative value $x^{[i+1]}$ yields

$$x^{[i+1]} = x^{[i]} - \mathrm{f}(x^{[i]}) \left(\frac{\partial \mathrm{f}(x^{[i]})}{\partial x} \right)^{-1} \ . \tag{4.5}$$

We should be aware that the NEWTON-RAPHSON method only exhibits local convergence behavior: This means that the initial value $x^{[0]}$ must be sufficiently close to the root of f. It has been shown though, that in this case, the local convergence rate of the method is quadratic if f is sufficiently smooth [63].

By using the inverse JACOBIAN matrix instead of the reciprocal derivative, we can generalize the idea of Equation 4.5 to vectorial functions $\mathbf{F}(\boldsymbol{x}) : \boldsymbol{R}^n \to \boldsymbol{R}^n$ that are sufficiently smooth in all variables [63]. The iteration rule of the NEWTON-RAPHSON method which we will use is thus

$$\boldsymbol{x}^{[i+1]} = \boldsymbol{x}^{[i]} - \left(\mathbf{grad}\ \mathbf{F}(\boldsymbol{x}^{[i]}) \right)^{-1} \mathbf{F}(\boldsymbol{x}^{[i]}) \ , \tag{4.6}$$

where $\boldsymbol{x}^{[i]}$ is the vector of all variables of the algebraic system of equations which we need to solve after the i-th iteration of the NEWTON-RAPHSON method.

4.3.1 Calculation of the JACOBIAN Matrix

To apply the vectorial form of the NEWTON-RAPHSON method (4.6), the JACOBIAN matrix of the function $\mathbf{F}(\boldsymbol{x})$ for which the root is to be found is required. We can either try to calculate this analytically—as done by, for example GRIEWANK [36] and ZHOU *et al.* [92]—, or we can compute it approximately by using the TAYLOR theorem (4.2): An approximation of the partial derivative $\partial\mathbf{F}(\boldsymbol{x})/\partial x_j$ can be determined by truncating Equation 4.2 after the second term, and resolving for the derivative. Using this approach, we get

$$\mathbf{F}(\boldsymbol{x}_{[x_j \leftarrow x_{j_e}]}) = \mathbf{F}(\boldsymbol{x}) + \frac{\partial\mathbf{F}(\boldsymbol{x})}{\partial x_j}(x_{j_e} - x_j) + O((x_j - x_{j_e})^2) \; .$$

Depending on whether we set the evaluation point x_{j_e} for the j-th row of $\mathbf{F}$ to $x_j + \epsilon$ or $x_j - \epsilon$ (for some arbitrary but fixed small $\epsilon \in \boldsymbol{R}^+$), we get the forward difference scheme

$$\frac{\partial\mathbf{F}(\boldsymbol{x})}{\partial x_j} = \frac{\mathbf{F}(\boldsymbol{x}_{[x_j \leftarrow x_j + \epsilon]}) - \mathbf{F}(\boldsymbol{x})}{\epsilon} + O(\epsilon^2)$$

or the backward difference scheme

$$\frac{\partial\mathbf{F}(\boldsymbol{x})}{\partial x_j} = \frac{\mathbf{F}(\boldsymbol{x}) - \mathbf{F}(\boldsymbol{x}_{[x_j \leftarrow x_j - \epsilon]})}{\epsilon} + O(\epsilon^2) \; .$$

A slightly more accurate method is to truncate the TAYLOR series only after the second term, expand it once at $x_j + \epsilon$ and once at $x_j - \epsilon$, and subtract the equations from each other. This results in the *central difference* scheme

$$\frac{\partial\mathbf{F}(\boldsymbol{x})}{\partial x_j} = \frac{\mathbf{F}(\boldsymbol{x}_{[x_j \leftarrow x_j + \epsilon]}) - \mathbf{F}(\boldsymbol{x}_{[x_j \leftarrow x_j - \epsilon]})}{\epsilon} + O(\epsilon^3) \; ,$$

which exhibits an error term in $O(\epsilon^3)$ because the second order terms of the TAYLOR series cancel each other. Thus, the central difference scheme has a higher accuracy compared to forward or backward differences. Having noted this, the central difference scheme requires a significantly higher computational effort compared to the one-sided variants, since for this scheme $\mathbf{F}$ must be evaluated twice per derivative instead once for per derivative plus one time for the whole JACOBIAN. For the numerical examples shown in Chapter 6, we will thus always use forward differences. Another reason for this is using for one-sided finite difference schemes, we can choose the value of ϵ small enough to achieve a sufficient accuracy.

4.3.2 Discretized Partial Differential Equations

For systems of equations that stem from partial differential equations that where spatially discretized using a grid based method, we can assemble the JACOBIAN matrix efficiently: For this, we take advantage of the observation that each row of $\mathbf{F}$ only interacts with a small number of other rows. This is due to the fact that, for such grid based spatial discretizations, the direct influence of the value of a quantity at a position is limited to the element which contains this position and the neighbors of that element. This leads to a *sparse* JACOBIAN matrix of $\mathbf{F}$ where most entries are zero, *i.e.*, the number of non-zero entries of $\mathbf{grad}\ \mathbf{F}$ is in $O(n)$ with n being the number of rows in $\mathbf{F}$. We can exploit this property by calculating the residual and its gradient for each element locally followed by summing them up to get a sparse JACOBIAN matrix for $\mathbf{F}$.

4.4 Linear Solvers

At this point, we need to solve the sequence of systems of linear equations produced by the NEWTON-RAPHSON method. To simplify the notation of this section, we discuss linear systems of equations in the form

$$\boldsymbol{A}\boldsymbol{x} = \boldsymbol{b}\ , \tag{4.7}$$

where $\boldsymbol{A} \in \boldsymbol{R}^{n\times n}$, $\boldsymbol{b}, \boldsymbol{x} \in \boldsymbol{R}^n$ and $n \in \boldsymbol{N}$. To adapt the iteration rule of the NEWTON-RAPHSON scheme (4.6) to the notation used by the current section, we need to set $\boldsymbol{x}$ to $\boldsymbol{x}^{[i]} - \boldsymbol{x}^{[i+1]}$, $\boldsymbol{b}$ to $\mathbf{F}(\boldsymbol{x}^{[i]})$ and $\boldsymbol{A}$ to $\mathbf{grad}\ \mathbf{F}(\boldsymbol{x}^{[i]})$.

Many ways to solve such systems of equations have been proposed [70], but we can classify all of these into two categories: Direct and iterative linear solvers. In the following, we will outline the basic ideas of both of these classes.

4.4.1 Direct Solution

The canonical method to solve Equation 4.7 is to use GAUSS elimination. It is the "canonical" approach because it is guaranteed to work for all non-degenerate matrices $\boldsymbol{A}$ and all right-hand sides $\boldsymbol{b}$, *i.e.*, we do not need to assume any properties other than $\boldsymbol{A}$ being non-degenerate. The basic approach of GAUSS elimination is to decompose $\boldsymbol{A}$ into

$$\boldsymbol{A} = \boldsymbol{L}\,\boldsymbol{U} \tag{4.8}$$

where $\boldsymbol{U}$ is an upper diagonal matrix and $\boldsymbol{L}$ is a lower diagonal matrix.

This decomposition, which we call LU-decomposition, can be achieved using *equivalence transformations*. The idea of these is that multiplying a line in $\boldsymbol{L}$ by a non-zero scalar value $\gamma \in \boldsymbol{R}$ can be reversed by multiplying the same column in $\boldsymbol{U}$ with $1/\gamma$. Similarly substituting a row by its sum with another row scaled by any factor does not change the solution of a linear system of equations. This way, by starting with $\boldsymbol{L}_0 = \boldsymbol{A}$ and $\boldsymbol{U}_0 = \boldsymbol{I}$ we can eliminate all entries on the upper right of $\boldsymbol{A}$ as well as normalize its main diagonal.

Once we have calculated the LU-decomposition of $\boldsymbol{A}$, we get the inverse using

$$\boldsymbol{A}^{-1} = (\boldsymbol{L}\,\boldsymbol{U})^{-1} = \boldsymbol{U}^{-1}\,\boldsymbol{L}^{-1}\,. \tag{4.9}$$

Here, the factors $\boldsymbol{L}^{-1}$ and $\boldsymbol{U}^{-1}$ can be efficiently calculated using *forward elimination* for triangular matrices.

Cost Analysis

Although direct methods to solve Equation 4.7 are versatile, in practice they are rarely used in unaltered form because of their high computational cost: To solve a linear system of equations with n rows, we require $O(n^3)$ scalar operations and $O(n^2)$ scalars need to be stored [70] if we implement this method naively. Even worse, in the general case these estimates hold even for sparse matrices [70]. For such matrices we have two options to tackle this problem: We may either try to re-order the linear system so that this problem gets reduced and the system can be solved much faster [70, 53, 71], or we can use an iterative solver as described in the next section.

4.4.2 Iterative Solvers

In contrast to directly solving Equation 4.7, iterative solvers require additional properties of the linear system of equations to be solved [70]. This means that, using iterative linear solvers, we cannot guarantee to solve any non-degenerate linear system of equations. However, in practice this constraint is not very relevant since the iterative solvers usually converge for the linear systems of equations stemming from discretized partial differential equations.

The fundamental property upon which all iterative solvers rely, is that the matrix-vector product

$$\boldsymbol{y} = \boldsymbol{A}\,\boldsymbol{x}$$

can be computed using $O(n)$ scalar operations, provided that $\boldsymbol{A}$ is sparse. In the following subsections we will illustrate how some widely used iterative linear solvers work.

4.4.2.1 Steepest Descent

The first solver which we investigate here, is the steepest descent solver. For it, we take advantage of the fact that for symmetric and positive definite matrices $\boldsymbol{A}$, the minimum of the function

$$\mathrm{f}(\boldsymbol{x}) = \frac{1}{2}\boldsymbol{x}^T\boldsymbol{A}\boldsymbol{x} - \boldsymbol{x}^T\boldsymbol{b} + c \tag{4.10}$$

corresponds to the solution of Equation 4.7. To see this, we set the JACOBIAN matrix of f to zero, and get

$$\begin{aligned} 0 &\overset{!}{=} \mathbf{grad}\ \mathrm{f} \qquad (4.11) \\ &= \frac{1}{2}\left(\boldsymbol{x}^T\,\mathbf{grad}(\boldsymbol{A}\boldsymbol{x}) + \mathbf{grad}\big(\boldsymbol{x}^T\big)\,\boldsymbol{A}\boldsymbol{x}\right) - \boldsymbol{b} \\ &= \frac{1}{2}\left(\boldsymbol{x}^T\boldsymbol{A} + \boldsymbol{A}\boldsymbol{x}\right) - \boldsymbol{b}\ . \end{aligned}$$

Since we assumed that $\boldsymbol{A}$ is symmetric, *i.e.*, that

$$\boldsymbol{x}^T\boldsymbol{A} = \boldsymbol{A}^T\boldsymbol{x} = \boldsymbol{A}\boldsymbol{x}$$

holds, we find that Equation 4.7 is satisfied, if and only if, Equation 4.11 holds. Further, the solution must be a minimum of Equation 4.10, because the gradient of Equation 4.11 is

$$\mathbf{grad}(\mathbf{grad}\ \mathrm{f}) = \mathbf{grad}(\boldsymbol{A}\boldsymbol{x} - \boldsymbol{b}) = \boldsymbol{A}$$

which is positive definite by assumption.

We can exploit these properties by starting at an arbitrary value $\boldsymbol{x}^{[0]}$, and repeatedly calculate the minimum along the line in the direction of the strongest decrease of f, *i.e.*, the solver uses

$$\boldsymbol{x}^{[k+1]} = \boldsymbol{x}^{[k]} + \alpha^{[k]} \mathbf{grad}\ \mathrm{f}(\boldsymbol{x}^{[k]}) \tag{4.12}$$

to find the next iterative value. To use this equation, now we need to minimize Equation 4.12 with respect to $\alpha^{[k]}$. This yields

$$\begin{aligned}
0 &\overset{!}{=} \frac{\mathrm{df}(\boldsymbol{x}^{[k+1]})}{\mathrm{d}\alpha^{[k]}} \\
&= \mathbf{grad}\Big(\mathrm{f}(\boldsymbol{x}^{[k+1]})\Big)\, \frac{\mathrm{d}\boldsymbol{x}^{[k+1]}}{\mathrm{d}\alpha^{[k]}} \\
&= -\boldsymbol{r}^{[k+1]} \cdot \boldsymbol{r}^{[k]} \\
&= \Big(\boldsymbol{b} - \boldsymbol{A}\boldsymbol{x}^{[k+1]}\Big) \cdot \boldsymbol{r}^{[k]} \\
&= \ \boldsymbol{b} \cdot \boldsymbol{r}^{[k]} - \boldsymbol{A}\left(\boldsymbol{x}^{[k]} + \alpha^{[k]} \mathbf{grad}\ \mathrm{f}(\boldsymbol{x}^{[k]})\right) \cdot \boldsymbol{r}^{[k]} \\
&= \ \boldsymbol{b} \cdot \boldsymbol{r}^{[k]} - \boldsymbol{A}\left(\boldsymbol{x}^{[k]} + \alpha^{[k]} \boldsymbol{r}^{[k]}\right) \cdot \boldsymbol{r}^{[k]}\ ,
\end{aligned}$$

where $\boldsymbol{r}^{[k]}$ is called the *linear residual*, and is an abbreviation for $\mathbf{grad}\ \mathrm{f}(\boldsymbol{x}^{[k]}) = \boldsymbol{A}\boldsymbol{x}^{[k]} - \boldsymbol{b}$. Resolving for $\alpha^{[k]}$, we get

$$\begin{aligned}
\alpha^{[k]} &= \frac{\big(\boldsymbol{A}\boldsymbol{x}^{[k]} - \boldsymbol{b}\big) \cdot \boldsymbol{r}^{[k]}}{\big(\boldsymbol{A}\boldsymbol{r}^{[k]}\big) \cdot \boldsymbol{r}^{[k]}} \\
&= \frac{\boldsymbol{r}^{[k]} \cdot \boldsymbol{r}^{[k]}}{\boldsymbol{r}^{[k]} \cdot \big(\boldsymbol{A}\boldsymbol{r}^{[k]}\big)}\ .
\end{aligned} \tag{4.13}$$

Using Equation 4.12 in conjunction with Equation 4.13 as iteration rule, we are able to approximate the solution of the linear system of Equations 4.7 arbitrarily closely, as illustrated in Figure 4.7 for the case of two unknowns. Figure 4.7 also illustrates a major shortcoming of the steepest descent method; namely that convergence tends to be slow. This is because, although each two consecutive optimization directions $\mathbf{grad}\ \mathrm{f}(\boldsymbol{x}^{[k]})$ and $\mathbf{grad}\ \mathrm{f}(\boldsymbol{x}^{[k+1]})$ are orthogonal, the method optimizes into "almost" the same direction at steps k and $k + 2$.

4.4.2.2 Conjugate Gradients

If we can make sure that $\boldsymbol{x}^{[k]}$ stays minimal for directions that we optimized for in previous steps, this issue does not occur. Also, if the optimization directions are not linearly dependent on each other, we will reach the exact solution after at most n iterations. For symmetric, positive definite matrices $\boldsymbol{A}$, we can achieve these properties by making the optimization

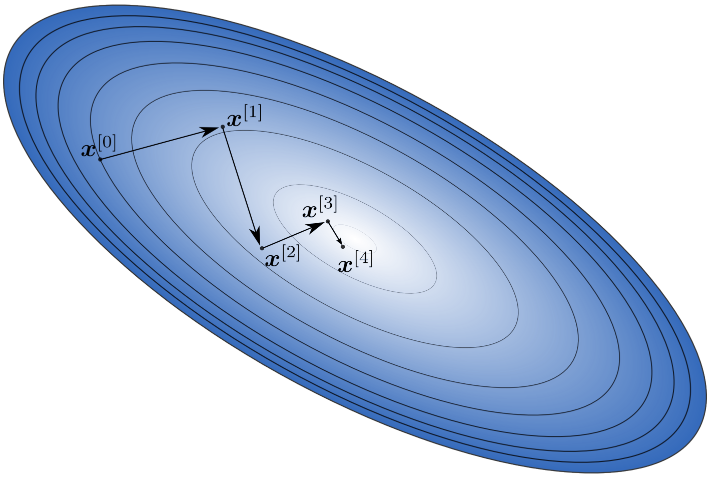

Figure 4.7: Illustration of the steepest descent algorithm: For any point $\boldsymbol{x}^{[k]}$, the minimum of the function f along the negative direction of the gradient $-\mathbf{grad}\ \mathrm{f}(\boldsymbol{x}^{[k]})$ is the value of the next iterative solution $\boldsymbol{x}^{[k+1]}$.

direction pairwise $\boldsymbol{A}$-*orthogonal*, *i.e.*, requiring that

$$\boldsymbol{d}^{[i]}\boldsymbol{A}\boldsymbol{d}^{[j]} = 0$$

holds for any two distinct optimization directions $\boldsymbol{d}^{[i]}$ and $\boldsymbol{d}^{[j]}$. It turns out [70] that we can use

$$\boldsymbol{d}^{[k+1]} = \boldsymbol{r}^{[k+1]} + \frac{\boldsymbol{r}^{[k+1]} \cdot \boldsymbol{r}^{[k+1]}}{\boldsymbol{r}^{[k]} \cdot \boldsymbol{r}^{[k]}}$$

to calculate the next optimization direction $\boldsymbol{d}^{[k+1]}$ at the end of iteration k, with

$$\boldsymbol{d}^{[0]} = \boldsymbol{r}^{[0]}$$

as the initial optimization direction, and

$$\boldsymbol{x}^{[k+1]} = \boldsymbol{x}^{[k]} + \alpha^{[k]}\boldsymbol{d}^{[k]}, \quad \text{with} \quad \alpha^{[k]} = \frac{\boldsymbol{d}^{[k]} \cdot \boldsymbol{r}^{[k]}}{\boldsymbol{d}^{[k]} \cdot \boldsymbol{A}\boldsymbol{d}^{[k]}} \tag{4.14}$$

as the iteration rule. Since $\boldsymbol{A}$-orthogonal vectors are said to be conjugate, the linear solver emerging from using Equation 4.14 as iteration rule is called the conjugate gradient method.

4.4.2.3 Bi-Conjugate Gradients

The conjugate gradient method covered in the previous section only works well for symmetric, positive definite matrices. As an extension to unsymmetric matrices, the bi-conjugate gradient method has been proposed by VAN DER VORST [86]. The basic idea of this method is to find the solution for a dual system

$$\boldsymbol{A}^T\boldsymbol{x}^\star - b = 0$$

in addition to the linear system $\boldsymbol{Ax} = \boldsymbol{b}$ for which we actually seek the solution. The bi-conjugate gradient method works by executing the conjugate gradient algorithm on each of those two systems separately, and ensuring that the search directions $\boldsymbol{d}^{[k]}$ and $\boldsymbol{d}^{\star[k]}$ of each iteration are $\boldsymbol{A}$-orthogonal to each other. Note that this method is equivalent to the conjugate gradient method for symmetric, positive definite matrices, albeit it requires twice the computational cost in this case.

Since the bi-conjugate method cannot guarantee convergence for all matrices $\boldsymbol{A}$, and is quite unstable [70], several stabilized variants have been proposed [70]. The one which we will use for the numerical examples presented in Chapter 6 is BiCGSTAB [70].

4.4.2.4 GMRES

The last iterative linear solver which we will cover in this work is the **G**erneralized **M**inimal **Res**idual (GMRES) method. This solver uses the initial optimization direction $\boldsymbol{r}^{[0]}$ and the optimization direction $\boldsymbol{d}^{[k]}$ of iteration k is found by explicitly orthogonalizing $\boldsymbol{r}^{[k]}$ with respect to all previous optimization directions. The advantage of the GMRES method is that it can be proved that—like bi-conjugate gradient based methods—it converges to the solution of the linear system of equations after at most n iterations [70]. This comes at the disadvantage that the memory requirement is in $O(n^2)$, and the number of scalar operations is in $O(n^3)$ which is not better than if we would use a direct solution method based on GAUSS elimination.

To avoid this issue, the GMRES method is usually restarted after a fixed number of iterations j. This has the effect that the memory consumption is in $O(n \cdot j)$, but has the disadvantage that convergence cannot be guaranteed anymore. In most cases, restarted GMRES is still more stable than a bi-conjugate gradient solver [70].

4.4.3 Preconditioners

Using *preconditioners*, we may get faster convergence of the iterative linear solvers. The idea of preconditioners is to make the linear system of equations better suited for the linear solver by applying a computationally cheap preprocessing step in every iteration. Conceptually, we can use preconditioners with any iterative linear solver using the relation

$$\boldsymbol{x}^{[k+1]} = \boldsymbol{P}(\boldsymbol{y}^{[k]})$$

where $\boldsymbol{x}^{[k+1]}$ is the start vector of iteration $k+1$ of the linear solver, $\boldsymbol{y}^{[k]}$ is the result of iteration k of the linear solver, and $\boldsymbol{P}$ is a computationally cheap function that is approximately the inverse of $\boldsymbol{A}$ in some sense, *i.e.*,

$$\mathbf{grad}\,\boldsymbol{P} \approx \boldsymbol{A}^{-1} .$$

The JACOBI Preconditioner

A simple preconditioner, which outlines the basic idea of preconditioners quite well, is due to CARL GUSTAV JACOB JACOBI. If we assume that all entries of the main-diagonal of $\boldsymbol{A}$ are non-zero, we may use the inverse of the main diagonal of $\boldsymbol{A}$, *i.e.*, we get the preconditioner

$$\boldsymbol{P}(\boldsymbol{y}^{[k]}) = (\mathbf{diag}\ \boldsymbol{A})^{-1}\, \boldsymbol{y}^{[k]}\ .$$

Because of its simplicity, the JACOBI preconditioner does not require significant computational costs. Having said that, it also does not improve convergence much [70].

Other Preconditioners

We note that preconditioners are typically much more elaborate and exhibit much higher computational costs than the JACOBI preconditioner. For example, if we use the LU decomposition presented in Section 4.4.1, but execute it only on the non-zero matrix entries, we get the incomplete LU (ILU) preconditioner [70]. Another approach is to create a hierarchy of matrices by successively merging rows and columns of the matrix $\boldsymbol{A}$. This idea leads to algebraic multi-grid preconditioners [82].

4.5 Parallelization

Now we are in a position to compute approximate solutions for a system of partial differential equations. We will thus proceed briefly at how this process can be sped up by doing the required computations in parallel. We will first discuss one of the fundamental techniques to perform parallel computations, domain decomposition. Then, we will then present how we can use this idea to parallelize the linearization process, and in Section 4.5.3 we will finally look at how iterative linear solvers can be implemented on loosely coupled parallel computers.

4.5.1 Domain Decomposition Methods

Computations involving very large grids are usually performed on parallel computers that feature a large number of processors which are only connected by a network. The mathematical basis which allows to use such machines are domain decomposition methods [75]. The general idea of these methods is to partition the grid for the whole spatial domain into a number of smaller connected subgrids of approximately equal size followed by assigning each subgrid to a processor. This processor then deals with discretizing and linearizing the system of partial differential equations on the subgrid using the methods which we discussed in Section 4.2. After each such step, we get a distributed linear system of equations which we need to solve in a parallel manner.

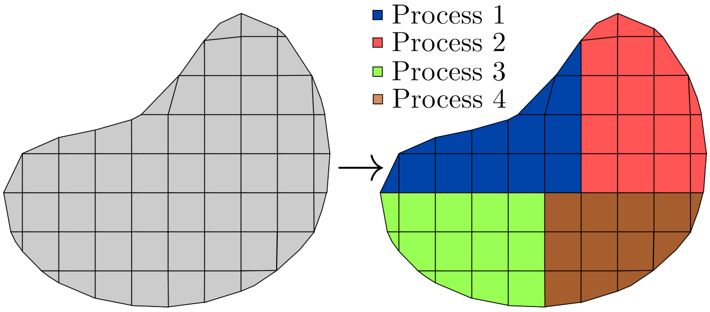

(a) Domain Decomposition

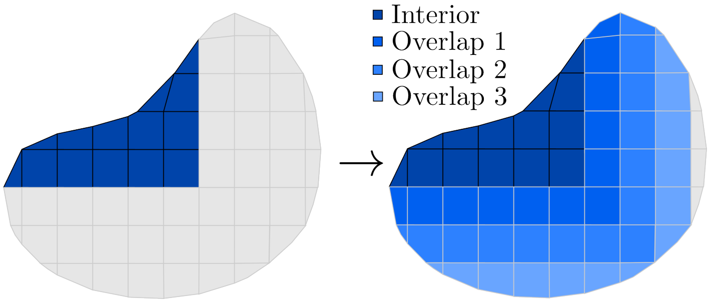

(b) Overlap of First Process

Figure 4.8: **(a)** Decomposition of the grid of a computational domain into four connected, approximately equally large subgrids. Each of the four subgrids can be treated almost independently which allows using loosely coupled parallel computations. **(b)** A domain overlap of three elements of the first process.

One major difficulty of this approach is the partitioning of the grid: In order to obtain good—*i.e.*, compact and approximately equally large—subgrids, we generally have to use complex graph processing algorithms that solve NP-complete problems [43, 66]. Since this partitioning process is not a focus of this work, we refer the interested reader to KARYPIS and KUMAR [43], PELLEGRINI and ROMAN [66], and to BURRI *et al.* [15]. An illustration of the idea of domain decomposition is given in Figure 4.8a where a two-dimensional grid is partitioned into four subgrids.

4.5.2 Distributed Linearization

To linearize the overall system of equations, we first linearize the individual subgrids independently. If there are so-called ghost elements, *i.e.*, elements at the subgrid boundary which are visible a processor but which are located within a neighboring subgrid, nothing else needs to be done. If no ghost elements are present, each processor must sum up the values of the matrix rows and the rows of the residual vector which represent entities adjacent to the boundary of the subgrid of the processor.

In both cases, we get a distributed version of the linearized system of equations

$$\begin{aligned} \boldsymbol{A}\boldsymbol{x} &= \boldsymbol{b}\ , \quad \text{where} \qquad (4.15)\\ \boldsymbol{A} &= \begin{pmatrix} \boldsymbol{A}_1 & 0 & 0 \\ 0 & \ddots & 0 \\ 0 & 0 & \boldsymbol{A}_k \end{pmatrix} ,\\ \boldsymbol{x} &= (\boldsymbol{x}_1, \ldots, \boldsymbol{x}_k)^T \quad \text{and}\\ \boldsymbol{b} &= (\boldsymbol{b}_1, \ldots, \boldsymbol{b}_k)^T \end{aligned}$$

are distributed on k processors, *i.e.*, processor i can only access $\boldsymbol{A}_i$ and the vectors $\boldsymbol{x}_i$ and $\boldsymbol{b}_i$ without communication.

4.5.3 Parallel Iterative Linear Solvers

Now we have to efficiently solve the distributed linear system of equations (4.15) in parallel. For direct solvers this problem is much more complicated than for iterative ones [53, 71], so we will concentrate on the latter. For these solvers, the only operations which we need to provide for the global linear system of equations are matrix-vector products, scalar products, norms, and preconditioners.

Matrix-Vector Products

Parallel matrix-vector products can be implemented by local matrix-vector products, provided that the domains overlap by at least one finite volume. After executing the local operation, rows which correspond to finite volumes that are at the front of the overlap need to be synchronized by retrieving their values from the process which is associated with the subgrid of the finite volume.

Scalar Products

We can compute all common scalar products in parallel by local scalar products followed by a summation of the results of all processors. For example, we can express the EUCLIDEAN scalar product in CARTESIAN coordinates in terms of the local operation

$$\boldsymbol{p}^i \cdot \boldsymbol{q}^i = \sum_{j=1}^{n_i} p_j^i q_j^i \ ,$$

followed by computing the sum of the results of all processes, *i.e.*,

$$\boldsymbol{p} \cdot \boldsymbol{q} = \sum_{i=1}^{k} \boldsymbol{p}^i \cdot \boldsymbol{q}^i \ .$$

Only the last step requires communication between the processes.

Norms

The norms of distributed vectors which we need for iterative linear solvers can be computed using the corresponding scalar products. For example, the two-norm of a distributed vector $\boldsymbol{p}$ is given by

$$\|\boldsymbol{p}\| = \sqrt{\boldsymbol{p} \cdot \boldsymbol{p}}\,.$$

Preconditioners

Preconditioners are the most challenging operations in the context of distributed iterative solvers. This is due to the fact, that the result of the preconditioner may depend on the ordering of the rows and columns of $\boldsymbol{A}$. For ordering independent preconditioners such as the JACOBI method, it is sufficient to apply them locally for each subgrid. Unfortunately, we cannot use these preconditioners in practice, as the convergence rates of the iterative linear solvers is much slower compared to more advanced preconditioners [70]. For preconditioners that dependent on the ordering of the rows, we can provide a parallel version by applying the sequential preconditioner locally, followed by a synchronization of the result on the overlapping rows—if the overlap regions are large enough. The synchronization is done by retrieving the values of the overlapping rows from the processes that are assigned to the subgrids of the finite volumes associated with the rows.

4.6 Chapter Synopsis

In this chapter, we discussed numerical methods for finding approximate solutions of systems of partial differential equations. The conceptual approach which we use is to first transform a relatively small system of partial differential equations

$$\frac{\partial b(\boldsymbol{x}, t)}{\partial t} + \operatorname{div}(b(\boldsymbol{x}, t) \cdot \boldsymbol{v}) = q(\boldsymbol{x}, t)$$

into a much larger system of coupled ordinary differential equations

$$\frac{\partial \boldsymbol{B}(t)}{\partial t} = \boldsymbol{Q}(t)$$

using a space discretization method.

The space discretization methods which we discussed partitioned the spatial domain Ω into a set of smaller subdomains $\{\omega_1, \ldots, \omega_n\}$, and represented any quantity b as piecewise constant functions on the subdomains. The value of an individual subdomain $b(\omega_i)$ we interpreted as the average of the quantity within ω_i.

After the spatial discretization, we transformed the obtained system of ordinary differential equations into a set of coupled non-linear algebraic equations. For this we truncated the TAYLOR series and obtained

$$\boldsymbol{B}(t^{[k+1]}) = \boldsymbol{B}(t^{[k]}) + (t^{k+1} - t^{[k]})\boldsymbol{Q}(t^{[k+1]})$$

as the time stepping rule. At this point, we had to repeatedly solve coupled non-linear systems of algebraic equations. To achieve this, we applied the NEWTON-RAPHSON method which exhibits the iteration rule

$$\boldsymbol{x}^{[i+1]} = \boldsymbol{x}^{[i]} - \Big(\mathbf{grad}\ \mathbf{F}(\boldsymbol{x}^{[i]})\Big)^{-1}\ \mathbf{F}(\boldsymbol{x}^{[i]})\ ,$$

i.e., for each time step, we now needed to repeatedly linearize the non-linear algebraic system of equations, and solve the corresponding linear systems of equations until the error was smaller than the allowed tolerance.

The final piece of the numerical puzzle were ways to solve such linear systems of equations. For this, we discussed several direct and iterative approaches as well as preconditioners for the iterative linear solvers.

To conclude this chapter, we briefly discussed how the steps of discretizing the partial differential equations, linearization of the resulting algebraic systems and solving the linear systems of equations can be efficiently implemented on loosely coupled parallel computers.

5 Implementation Aspects

For this thesis, the methods which we discussed in the previous chapters have been implemented using the numerical C++ framework eWoms [30]. In this chapter, we will look at some of the technical aspects of this implementation.

5.1 DUNE

The eWoms framework is based on the **D**istributed and **U**nified **N**umerics **E**nvironment (DUNE) [28]. As illustrated in Figure 5.1, DUNE provides a set of basic C++ classes which simplify the development of numerical schemes, but DUNE itself does not implement any of those. Instead, such methods have to be implemented by additional modules like eWoms. Currently, DUNE comprises the following core modules:

dune-common implements very basic abstractions like, for example, dense vector and matrix classes, helper routines for parsing configuration files, exception handling, and low-level macros for compiler abstraction.

dune-geometry provides a set of reference elements and the associated transformations to convert these into the actual geometries required by the grid. Currently, the dune-geometry module supports line segments for one spatial dimension, triangles, and rectangles for two spatial dimensions, and tetrahedra, cubes, prisms, and pyramids for three dimensional grids. In addition, simplices and cubes are provided for higher spatial dimensions.

dune-grid defines an abstract interface for partitioning the spatial domain into a grid as described in Section 4.1. The DUNE grid interface also supports parallel computations based on the domain decomposition concept which we discussed in Section 4.5. Besides defining a parallel programming interface for grids, this module also provides a few sample implementations for CARTESIAN grids, and wrappers for external unstructured grid management libraries, such as ALUGrid [4], ALBERTA [3], and UG [85].

dune-localfunctions supplies finite-element shape functions based on the infrastructure of the grid and the geometry modules. The only shape functions used by eWoms are those of linear finite elements. The reason for this is that these functions are used to calculate the gradients of quantities on the dual-grid of vertex-centered finite volume methods which we discussed in Section 4.1.

dune-istl stands for **I**terative **S**olvers **T**emplate **L**ibrary, and implements a superset of the iterative linear solvers and preconditioners which we described in Section 4.4.

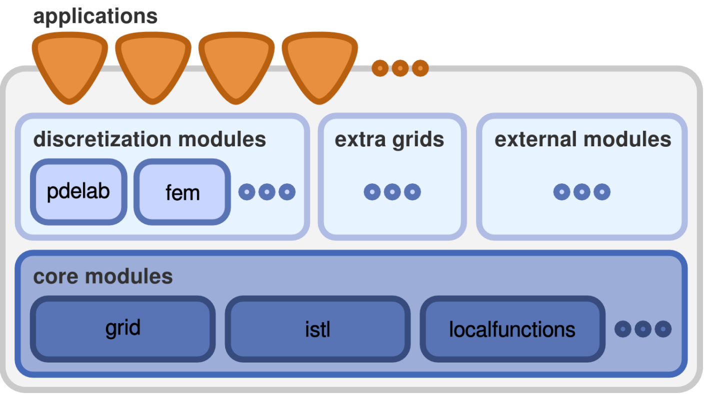

Figure 5.1: The software architecture of the DUNE C++ framework [28]. The core of eWoms represents an *external module* which implements discretization schemes and the numerical problems which will be presented in Chapter 6 fall into the *applications* category.

All DUNE modules use the C++ template mechanism extensively. The reason for this is to keep the run-time overhead of the abstractions low, but it comes at the price of increased compilation time, and a relatively steep learning curve.

5.2 eWoms

Based on these DUNE modules, the eWoms framework implements discretization schemes and physical models which we will cover in greater detail in the following. But before we can discuss these models, a rough overview of the general software architecture of eWoms is required.

5.2.1 General Structure

Conceptually, eWoms currently consists of the following parts:

The Time Loop deals with adapting time step sizes, simplifies implementing time-dependent problems, and runs the simulation from the initial time to the specified end time. To actually advance the time level from $t^{[k]}$ to $t^{[k+1]}$, it calls the non-linear solver.

The NEWTON-RAPHSON Solver implements the non-linear solver for algebraic systems of equations as discussed in Section 4.3. This part of the code calls the discretization scheme to linearize the system of equations, and subsequently calls a linear solver to find the solution of the linearized system of equations.

Discretization Schemes: Implement the fully implicit vertex-centered finite volume space discretization discussed in Section 4.1, and the implicit EULER time discretization of Section 4.2. It is also the part of eWoms which uses the DUNE grid interface most extensively.

Flow Models: This part of eWoms is called by the discretization schemes, and specifies the conservation equations, *i.e.*, it determines the function $\mathbf{F}$ of Equation 4.6. The flow model also specifies the interpretation of its primary variables, and it provides some auxiliary methods like scaling parameters of the primary variables and of the conservation equations.

Problems: In eWoms, the purpose of problems is to describe the setup of a physical system. This includes the grid used by the simulation, boundary and initial conditions, as well as spatially dependent parameters like the intrinsic permeability of the porous medium or the value of the gravitational acceleration. The parameters of the problem are mostly queried by the flow model.

Material Framework: The purpose of the eWoms material framework is to provide material specific relations. Such relations include the thermodynamic relations of multi-phase multi-component systems of fluids, capillary pressure and relative permeability relationships.

Parallelization: This part of eWoms implements distributed overlapping linear systems of equations with the required operations and synchronization algorithms for preconditioners of the iterative linear solvers. These linear systems of equations are then solved using one of the iterative linear solvers of dune-istl.

Auxiliary Infrastructure: eWoms also provides auxiliary code. Amongst other things, this code is used to specify simulation-wide parameters, comprises routines simplifying the startup procedure, and classes providing checkpointing functionality as well as classes for writing the solutions into file formats suitable for visualization.

5.2.2 Flow Models

Now that we have covered the general software design of eWoms, we will have a closer look at the implementation aspects of the eWoms flow models in the following paragraphs. First, we will discuss how the flow models work in general, then we will consider the specific aspects of the individual flow models.

General Mode of Operation

The central part of all flow models is the code which defines of the local residual function, *i.e.*, a class to compute the residual for a single element of the grid. After linearizing these local residuals for each element, the local linearized system of equations is transferred to the linear system of equations for the full subgrid of the respective process. This process involves mapping the element-local indices of each finite volume to its respective index in the subgrid, and summing them into a large vector. In eWoms, the local linearization and the transfer from the element-local to the global system of equations is implemented generically by infrastructural code, so the only part which needs to be provided by a flow model is the element-local residual.

The flow models presented in this thesis use a multi-stage approach to define the local residual of an element: First, the *primary variables*—which are defined as the quantities which are contained in the solution vector $\boldsymbol{x}^{[i]}$ of the NEWTON-RAPHSON method (4.6)—are transformed into so-called *volume variables*. In eWoms, volume variables are quantities that are independent of the state of the spatial neighborhood of a given point in the spatial domain like, for example, temperature, pressures, and saturations.

The volume variables are then used to calculate *flux variables*. The flux variables represent all quantities which depend on the spatial neighborhood of a finite volume. They are mainly required to calculate the divergence term of Equation 2.6. Quantities represented by the flux variables are, for example, the gradients of pressure and temperature.

Based on the flux and the volume variables, the local residual of a flow model then specifies the volumetric rate of each conservation quantity that is incorrectly added to or removed from the system for a given solution. For mass, eWoms uses either Equation 2.42 or Equation 2.47, and if energy is conserved, the local residual of the flow model also includes Equation 2.46.

The Immiscible Model

As covered in Section 3.5.1, the immiscible model assumes that the components do not mix, and that, as a consequence, each fluid phase comprises exactly one component. This model uses Equation 2.42 as the equation for the conservation of mass in conjunction with the multi-phase version of DARCY's law (2.37), *i.e.*, the residual function F_α for the conservation of the mass of a component reads

$$\frac{\partial \phi \rho_\alpha S_\alpha}{\partial t} - \mathrm{div}\left(\rho_\alpha \frac{k_{\mathrm{r},\alpha}}{\mu_\alpha} \boldsymbol{K} \left(\mathbf{grad}\, p_\alpha - \boldsymbol{g} \rho_\alpha \right) \right) - q_\alpha = \mathrm{F}_\alpha \stackrel{!}{=} 0 \;,$$

where α is the fluid phase corresponding to the component.

The primary variables for this model are the pressure of the fluid phase with the lowest index and the $M-1$ saturations of the fluid phases associated with the lowest indices.

The PVS Model

The PVS model for M-phase, N-component flow in porous media which uses the primary variable switching conditions (3.31) as model assumptions is based on Equation 2.47, the molar formulation of the component-wise mass conservation equation. The residual function F^κ for the conservation of the mass of component κ is thus given by

$$\sum_\alpha \frac{\partial \phi x_\alpha^\kappa \rho_{\mathrm{mol},\alpha} S_\alpha}{\partial t} - \sum_\alpha \mathrm{div}\left(x_\alpha^\kappa \rho_{\mathrm{mol},\alpha} \frac{k_{\mathrm{r},\alpha}}{\mu_\alpha} \boldsymbol{K} \left(\mathbf{grad}\, p_\alpha - \boldsymbol{g} \rho_\alpha \right) + D_{\mathrm{pm}.\alpha}^\kappa \,\mathbf{grad}\, x_\alpha^\kappa \right) - q^\kappa = \mathrm{F}^\kappa \stackrel{!}{=} 0 \;.$$

Compared to the immiscible model, the interpretation of the N primary variables is much more complicated:

- The first primary variable always represents the pressure of the phase with the lowest index.
- The next $M-1$ primary variables represent the saturations of the phases if the respective phase is present, or else the mole fraction of the component with the same index as the primary variable in the corresponding to with the phase lowest index that in the set of present phases.
- The final $N - M$ primary variables represent the mole fractions of the $N - M$ last components in the phase associated with the lowest index that is assumed to be present.

In this model, in addition to the N "real" primary variables, M boolean *pseudo primary variables* $\{\hat{p}_1, \ldots, \hat{p}_M\}$ are required to specify the set of fluid phases which are present at a given spatial location. They are determined at the end of each NEWTON-RAPHSON iteration according to the following rules:

- If fluid phase α was assumed not to be present at the beginning of the current NEWTON-RAPHSON iteration and if the sum of the mole fractions of the phase is larger than or equal to 1 after updating the solution, for the next iteration we assume that phase α is present.
- If fluid phase α was assumed to be present for the current NEWTON-RAPHSON iteration and the saturation of phase α is smaller than 0, we assume that phase α is not present in the next iteration.

After updating the pseudo primary variables, we need to adapt all "real" primary variables to make the model consistent.

The NCP Model

Like the primary variable switching model, the model which directly embeds non-linear complementarity functions, uses Equation 2.47 as mass conservation equation. This means that it also uses the component-wise molar formulation of the conservation of mass in conjunction with DARCY's law. In other words, the residual function F^κ which describes the conservation of component κ is also given by

$$\sum_\alpha \frac{\partial \phi x_\alpha^\kappa \rho_{\mathrm{mol},\alpha} S_\alpha}{\partial t} - \sum_\alpha \mathrm{div}\left(x_\alpha^\kappa \rho_{\mathrm{mol},\alpha} \frac{k_{\mathrm{r},\alpha}}{\mu_\alpha} \boldsymbol{K} \left(\mathbf{grad}\, p_\alpha - \boldsymbol{g} \rho_\alpha \right) + D_{\mathrm{pm}.\alpha}^\kappa \,\mathbf{grad}\, x_\alpha^\kappa \right) - q^\kappa = \mathrm{F}^\kappa \overset{!}{=} 0 \ .$$

In addition to the mass conservation equations, the model explicitly includes the M non-linear complementarity functions of Equation 3.33.

Compared to the primary variable switching model, the set of primary variables for this model is quite simple:

- The first primary variable is the pressure of the phase associated with the lowest index.
- The next $M - 1$ primary variables are the saturations of the $M - 1$ phases with the lowest indices.

Model	SLOC	Core SLOC
Immiscible	720	297
Black-Oil	1013	434
NCP	1046	551
PVS	1260	720

Table 5.1: Comparison of the number of source lines of C++ code (SLOC) implementing the discussed model approaches in eWoms as determined by the SLOCCount tool [74]. The first number represents the total number of source code lines of the implementation of each model in eWoms, while the "Core SLOC" column excludes auxiliary code like the one for writing the solutions to the hard disk, making checkpoints *et cetera*.

- The final N primary variables represent the fugacities f^κ of all components.

The Black-Oil Model

In addition to the generic models discussed in the previous model, the eWoms back-oil model implements the specialized approach covered in Section 3.5.4. From the software engineering point of view, it is very similar to the model which assumes immiscibility. This is due to the fact that two of the three fluid phases are assumed to be immiscible. This allows the eWoms implementation of the black-oil model to use the same primary variables as the immiscible model, *i.e.*, the pressure and the saturation of the gas phase, in addition to the saturation of the water phase.

Compared to the immiscible model, the main differences of the black-oil model are that the quantities required for the mass conservation equations are calculated by directly using the black-oil parameters, and that undersaturated oil phase needs special attention if we use the aforementioned primary variables: Such oil is described by negative saturations of the gas phase, where the amount of "negative" gas is subtracted from the amount of the gas component which is dissolved in the oil phase. In this respect, the eWoms implementation of the black-oil model is similar to the negative saturations approach proposed by, for example, ABADPOUR and PANFILOV [2], with the differences that the composition of the gas and water phases are known *a priori*, and that the black-oil model considers three instead of two fluid phases.

5.2.3 Implementational Complexity

When estimating the effort required to implement the discussed models in software, we can use the number of lines of code required for each as a very rough indication. We have to be aware though, that the complexity of the implementation is not linear to the number of lines of code. This is due to the facts that tightly written source code packs much more functionality into the same number of lines than loosely written source code and that highly convoluted algorithms are much more difficult to implement than straightforward ones. In the case of the numerical models featured by eWoms, the density of the source code can be assumed to be similar for all models, but the inherent complexity of the primary-variable switching model is higher than that of the other models.

These numbers of lines of source code needed to implement the individual models in eWoms are compared in Table 5.1. As this table indicates, the model which assumes immiscibility is by far the simplest, followed by the black-oil model. Also clearly represented is the fact that the effort required to implement the model based on primary variable switching is much higher than for the model which directly incorporates non-linear complementarity functions.

From the point of view of the implementation, the main simplifying factor of the NCP model compared to the PVS model is the fact that the semantics of all primary variables are independent of the state of the solution, *i.e.*, no pseudo primary variables are required.

6 Numerical Applications

After briefly sketching the software implementation in the previous chapter, we will now compare the physical accuracy and the computational performance of the presented numerical models for fluid flow in porous media.

We roughly proceed in order of complexity of the examples: First, we compare the physical and numerical performance of the primary-variable switching (PVS) approach with the one based on non-linear complementarity problems (NCP) using a one-dimensional non-isothermal setup for which a semi-analytical solution is known. Then we discuss the results and the computational performance of the immiscible, PVS, and NCP models for an isothermal, radially symmetric CO_2 injection problem. In this section, we will also briefly examine the scalability of the domain decomposition parallelization approaches, and we analyze the viability of using two-dimensional simulations for radially symmetric problems.

We then proceed with the ninth [45] and the fifth [46] benchmark problems specified by the society of petroleum engineers. The ninth benchmark problem is used to estimate merrits and drawbacks of the black-oil model versus fully compositional models and demonstrates the computational instability of the PVS model. In contrast, the primary intention of the fifth SPE benchmark problem is to show the viability of the generic compositional multi-phase models for the complex cubic equations of state which we discussed in Sections 3.3.1 and 3.3.2. We conclude the chapter with a brief discussion of geological-scale simulations for the CO_2 injection research project in Ketzin/Havel, Germany.

6.1 The Heat-Pipe Problem

In this section, we will discuss the heat-pipe setup as proposed by UDELL [84]. The problem uses the spatial domain depicted in Figure 6.1: In the beginning, the domain is fully saturated by liquid distilled water, and the domain is fully closed for mass flows except on the left side, where it is open. Initially, and on the left boundary of the domain, the domain is fully saturated by liquid exhibiting a pressure p_l of one bar. For energy, the domain is fully closed except on the left side, where it is assumed to be open, and on the right side, which is heated at a constant rate. The initial temperature and the permanent temperature on the left boundary is $70\,^\circ\mathrm{C}$.

In steady-state, this setup leads to a region that is only occupied by the liquid on the left where the temperature is too low to evaporate the liquid water, and the heat is thus exclusively transported by means of heat conduction. On the right side of the domain, the temperature is high enough to create a zone where only steam is present so that in this region energy can

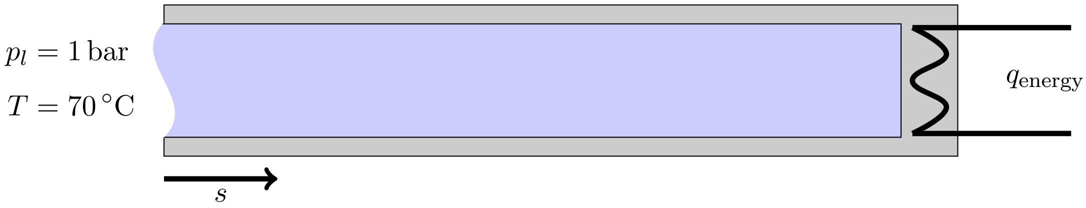

Figure 6.1: The spatial domain of the heat-pipe problem: The experiment consists of a tube of $2\,\mathrm{m}$ length filled by a fully water-saturated porous medium. On the left side, the tube is open and exposed to atmospheric pressure; on the right, it is closed but heated. Initially the temperature within the domain is $T = 70\,^\circ\mathrm{C}$.

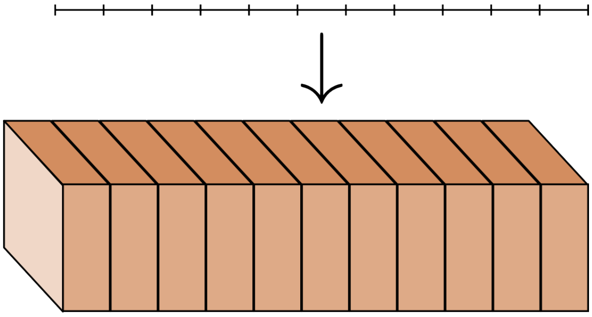

Figure 6.2: Uniform extrusion of a one-dimensional grid to three spatial dimensions.

also only be transported by means of heat conduction. The most interesting part of this setup lies in between these two extremes: There, liquid water as well as steam is present. The liquid is drawn from left to right by the capillary pressure where the liquid is evaporated. Then, the material gets transported back to the left by a pressure gradient in the gas phase and it condenses to liquid again.

6.1.1 Uniform Domain Extrusion

Since the mass and energy conservation equations (2.10, 2.23) are only valid for three spatial dimensions, we first have to become aware of their interpretation in the case of one space-dimension. The answer turns out to be quite simple: In order to apply Equations 2.10 and 2.46, the spatial domain can be extruded uniformly to three dimensions as depicted in Figure 6.2 and the usual conservation equations thus apply.

6.1.2 Semi-Analytical Solution

Besides this small glitch in the interpretation of the results, the quasi one-dimensional nature of this setup allows us to derive a semi-analytical solution. To obtain it, we first suppose the system to be in steady-state. This means that there cannot be any net flux of mass along the axis s of the tube, *i.e.*,

$$\rho_l \frac{k_{\mathrm{r},l}}{\mu_l} K \frac{\partial p_l}{\partial s} = -\rho_g \frac{k_{\mathrm{r},g}}{\mu_g} K \frac{\partial p_g}{\partial s} \tag{6.1}$$

holds.

Since the intrinsic permeability K is equal on both sides, it can be eliminated. If we also include the definition of capillary pressure $p_g = p_l + p_{\mathrm{c},gl}$, and if we use kinematic viscosities $\nu_\alpha = {}^{\mu_\alpha}/_{\rho_\alpha}$ instead of dynamic ones, we can transform Equation 6.1 to

$$\frac{k_{\mathrm{r},l}}{\nu_l}\frac{\partial\, p_l}{\partial s} = -\frac{k_{\mathrm{r},g}}{\nu_g}\frac{\partial\left(p_l + p_{\mathrm{c},gl}\right)}{\partial s} \; .$$

Reordering, we get

$$\frac{\partial\, p_l}{\partial s} = -\frac{\frac{k_{\mathrm{r},g}}{\nu_g}\frac{\partial\, p_{\mathrm{c},gl}}{\partial s}}{\frac{k_{\mathrm{r},l}}{\nu_l} + \frac{k_{\mathrm{r},g}}{\nu_g}} \; . \tag{6.2}$$

We can now multiply the numerator as well as the denominator of Equation 6.2 with ${}^{\nu_g}/_{k_{\mathrm{r},g}}$, and apply the chain rule. We get

$$\frac{\partial p_l}{\partial S_l}\frac{\partial S_l}{\partial s} = -\frac{\frac{\partial\, p_{\mathrm{c},gl}}{\partial S_l}\frac{\partial S_l}{\partial s}}{1 + \frac{k_{\mathrm{r},g}}{k_{\mathrm{r},l}}\frac{\nu_l}{\nu_g}} \; . \tag{6.3}$$

Finally, multiplying both sides of Equation 6.3 with $\partial s/\partial S_l$, we get

$$\frac{\partial p_l}{\partial S_l} = -\frac{\frac{\partial p_{\mathrm{c},gl}}{\partial S_l}}{1 + \frac{k_{\mathrm{r},g}}{k_{\mathrm{r},l}}\frac{\nu_l}{\nu_g}} \; . \tag{6.4}$$

For the next part of the semi-analytical solution we take advantage of the fact that the energy flux is a given constant for the whole length of the tube. This means that

$$h_l \rho_l v_l + h_g \rho_g v_g + \lambda_{\mathrm{pm}}\frac{\partial T}{\partial s} = q_{\mathrm{energy}} \tag{6.5}$$

holds, where λ_{pm} is the overall heat conductivity of the medium. In this context, we also know that

$$\rho_l v_l = -\rho_g v_g$$

holds, since the net mass flux must be zero. This allows us to transform Equation 6.5 to

$$\rho_g v_g \left(h_g - h_l\right) + \lambda_{\mathrm{pm}}\frac{\partial T}{\partial s} = q_{\mathrm{energy}} \; .$$

Further, using DARCY's relation (2.39) for the velocity of the liquid phase, and using kinematic instead of dynamic viscosities, we get

$$h_{\mathrm{vap}}\frac{k_{\mathrm{r},g}}{\nu_g}K\frac{\partial p_g}{\partial s} + \lambda_{\mathrm{pm}}\frac{\partial T}{\partial s} = q_{\mathrm{energy}} \; ,$$

where $h_{\mathrm{vap}} = h_g - h_l$ is the *specific enthalpy of vaporization* of liquid water. Next, we use the chain rule and the definition of capillary pressure, so we get

$$h_{\mathrm{vap}} \frac{k_{\mathrm{r},g}}{\nu_g} K \left(\frac{p_l}{\partial s} + \frac{\partial p_{\mathrm{c},gl}}{\partial S_l} \frac{\partial S_l}{\partial S_l} \frac{\partial S_l}{\partial s} \right) + \lambda_{\mathrm{pm}} \frac{\partial T}{\partial s} = q_{\mathrm{energy}} \ .$$

Multiplying both sides with $\partial s / \partial S_l$ leads us to

$$h_{\mathrm{vap}} \frac{k_{\mathrm{r},g}}{\nu_g} K \left(\frac{\partial p_l}{\partial S_l} + \frac{\partial p_{\mathrm{c},gl}}{\partial S_l} \right) + \lambda_{\mathrm{pm}} \frac{\partial T}{\partial S_l} = q_{\mathrm{energy}} \frac{\partial s}{\partial S_l} \ . \tag{6.6}$$

In Equation 6.6 we now observe that, since we expressed p_g in terms of p_l and $p_{\mathrm{c},gl}$, the term $\partial p_l / \partial S_l$ is identical to zero, so that we get

$$h_{\mathrm{vap}} \frac{k_{\mathrm{r},g}}{\nu_g} K \frac{\partial p_{\mathrm{c},gl}}{\partial S_l} + \lambda_{\mathrm{pm}} \frac{\partial T}{\partial S_l} = q_{\mathrm{energy}} \frac{\partial s}{\partial S_l} \ .$$

Now, we apply the chain rule to the temperature term. We get

$$h_{\mathrm{vap}} \frac{k_{\mathrm{r},g}}{\nu_g} K \frac{\partial p_{\mathrm{c},gl}}{\partial S_l} + \lambda_{\mathrm{pm}} \frac{\partial T}{\partial p_g} \frac{\partial (p_l + p_{\mathrm{c},gl})}{\partial S_l} = q_{\mathrm{energy}} \frac{\partial s}{\partial S_l} \ .$$

After some reordering, we get

$$\frac{\partial s}{\partial S_l} = \frac{\partial p_{\mathrm{c},gl}}{\partial S_l} \frac{h_{\mathrm{vap}} K \frac{k_{\mathrm{r},g}}{\nu_g} + \lambda_{\mathrm{pm}} \frac{\partial T}{\partial p_g}}{q_{\mathrm{energy}}} \ .$$

Finally, we take advantage of

$$p_g = p_{\mathrm{vap}}(T) \ ,$$

i.e., the fact that the pressure of the gas phase is identical to the vapor pressure of water [88] at a given temperature in the two-phase, one-component case. This leads us to the second equation of the semi-analytical solution

$$\frac{\partial s}{\partial S_l} = \frac{\partial p_{\mathrm{c},gl}}{\partial S_l} \frac{h_{\mathrm{vap}} K \frac{k_{\mathrm{r},g}}{\nu_g} + \lambda_{\mathrm{pm}} \left(\frac{\partial p_{\mathrm{vap}}}{\partial T} \right)^{-1}}{q_{\mathrm{energy}}} \ . \tag{6.7}$$

Together, Equations 6.4 and 6.7 form a coupled system of two ordinary differential equations which can be solved using the methods presented in Section 4.2.

6.1.3 Results

For the results presented in this section, the capillary pressure relation proposed by LEVERETT [51]

$$p_{\mathrm{c},gl} = p_{\mathrm{c},gl,0} \, \gamma (1.263 \, S_g^3 - 2.120 \, S_g^2 + 1.417 \, S_g),$$

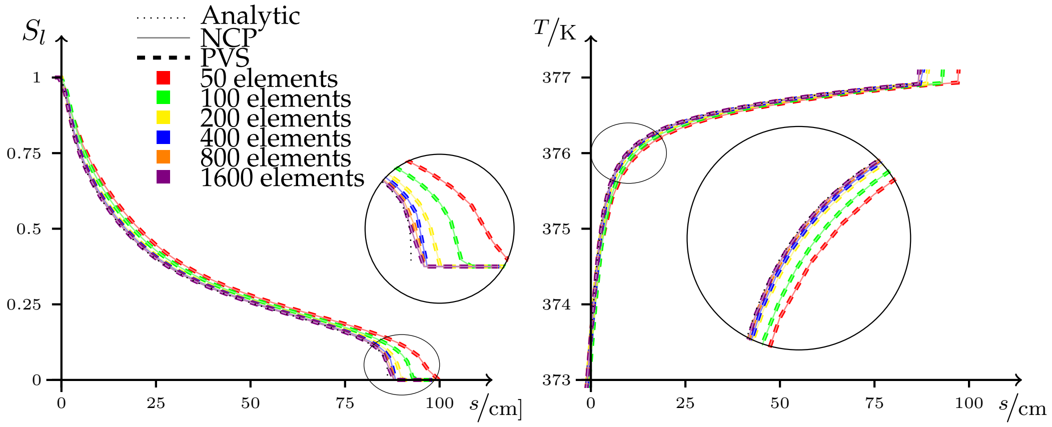

(a) Liquid Saturation

(b) Temperature

Figure 6.3: Comparison of the semi-analytical solution calculated using Equations 6.4 and 6.7 (dotted) with results obtained by the numerical models using primary variable switching (PVS, dashed) and non-linear complementary functions (NCP, non-dashed). The numerical models were run until $t = 10^9\,\mathrm{s}$ with a uniform spatial resolution along the tube axis of 50, 100 200, 400, 800, and 1600 elements.

was applied, where $\gamma = 0.05878\,{}^{\mathrm{N}}\!/\!{}_{\mathrm{m}}$ represents the surface tension, and $p_{c,gl,0} = \sqrt{{}^{\phi}\!/\!{}_{K}}$ is the *scaling pressure*. Further, the porosity ϕ is 0.4, and the intrinsic permeability K is $10^{-12}\,\mathrm{m}^2$.

The overall heat conductivity λ_{pm} is approximated by the SOMERTON [76] relation

$$\lambda_{\mathrm{pm}} = \lambda_{\mathrm{pm,dry}} + \sqrt{S_l}\,(\lambda_{\mathrm{pm,wet}} - \lambda_{\mathrm{pm,dry}}) \ ,$$

where $\lambda_{\mathrm{pm,dry}}$ is the heat conductivity of the porous medium fully saturated by steam and $\lambda_{\mathrm{pm,wet}}$ is the heat conductivity of the porous medium when it is fully saturated by liquid water. For these parameters, we assume

$$\lambda_{\mathrm{pm},dry} = 1.85\,{}^{\mathrm{W}}\!/\!{}_{\mathrm{K\,m^2}} \qquad \text{and}$$
$$\lambda_{\mathrm{pm},wet} = 2.67\,{}^{\mathrm{W}}\!/\!{}_{\mathrm{K\,m^2}} \ .$$

Finally, the energy influx at the right side of the domain is $q_{\mathrm{energy}} = 200\,{}^{\mathrm{W}}\!/\!{}_{\mathrm{m^2}}$.

Figure 6.3 shows the obtained results for the steady-state saturation of liquid water and the temperature for the semi-analytical solution calculated using Equations 6.4 and 6.7 in comparison to the results of the finite-volume based numerical models. In this figure, the origin of the spatial domain is set to the leftmost point where the saturation of the gas phase deviates from zero.

Generally, it can be observed that both numerical solutions are identical up to rounding errors, and that both converge to the semi-analytical solution when the grid gets refined. From these results, we can conclude that both numerical models and their implementation are correct in the sense that the discretization is convergent and that both models lead to

	NCP (200 elements)	NCP (1600 elements)	PVS (200 elements)	PVS (1600 elements)
$n\,[-]$	48	232	344	1629
t_{CPU} [s]	1.056	79.99	12.212	469.603
$n_{\mathrm{NEWTON}}\,[-]$	234	2161	3858	17750
$n_{\mathrm{NEWTON}}/t_{\mathrm{CPU}}$ [1/s]	221.59	27.01	315.91	37.79

Table 6.1: Comparison of the performance of the numerical models using primary variable switching (PVS) and non-linear complementarity functions (NCP) for the heat-pipe problem. Here, n corresponds to the number of time steps required to reach steady state, t_{CPU} is the CPU time required to reach steady state and n_{NEWTON} is the total number of iterations of the NEWTON-RAPHSON method required for the whole simulation.

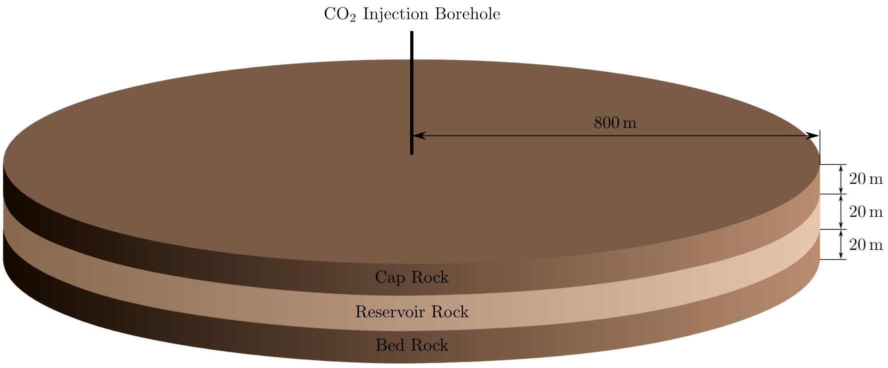

Figure 6.4: The spatial domain of the radially symmetric CO_2 injection problem.

physically meaningful results.

Table 6.1 compares the number of time steps, NEWTON-RAPHSON iterations, and the CPU time which both numerical models required to reach the simulation time of 10^9 s on a computer equipped with an Intel® Core™ i7-3770K processor at 3.5 GHz. These results clearly demonstrate that the model which directly incorporates the non-linear complementarity functions exhibits much better stability, *i.e.*, the number of time steps required is about an order of magnitude lower compared to the model which uses primary variable switching. This effect more than amortizes the slightly higher computational cost required for each iteration of the NEWTON-RAPHSON scheme.

6.2 A Radially Symmetric CO_2 Injection Problem

Having evaluated the physical quality and the numerical performance of the numerical models using the heat-pipe problem, we now slightly increase the complexity of the investigated problem by drawing our attention to a problem which is inspired by an artificial CO_2 injection problem proposed by DARCIS [25]. The physical setup is illustrated in Figure 6.4: The domain consists of a layer of high-permeability and high porosity rock sandwiched

Layer	Parameter	Value
Cap rock	$\boldsymbol{K}$	$10^{-17}\,\boldsymbol{I}\,\mathrm{m}^2$
Reservoir	$\boldsymbol{K}$	$1.97 \cdot 10^{-13}\,\boldsymbol{I}\,\mathrm{m}^2$
Bed rock	$\boldsymbol{K}$	$10^{-17}\,\boldsymbol{I}\,\mathrm{m}^2$
Cap rock	ϕ	$4.6\,\%$
Reservoir	ϕ	$20\,\%$
Bed rock	ϕ	$4.6\,\%$
All	p_e	$5\,\mathrm{kPa}$
All	λ_bc	2
All	$S_{\mathrm{r},l}$	$25\,\%$
All	$S_{\mathrm{r},g}$	$2.5\,\%$

Table 6.2: Parameters used for the radially symmetric CO_2 injection problem. The quantity p_e represents the entry pressure, and λ_bc stands for the shape parameter of the BROOKS-COREY capillary pressure relation (3.18). Further, $S_{\mathrm{r},l}$ and $S_{\mathrm{r},g}$ specify the residual saturations of the liquid and gas phases [39].

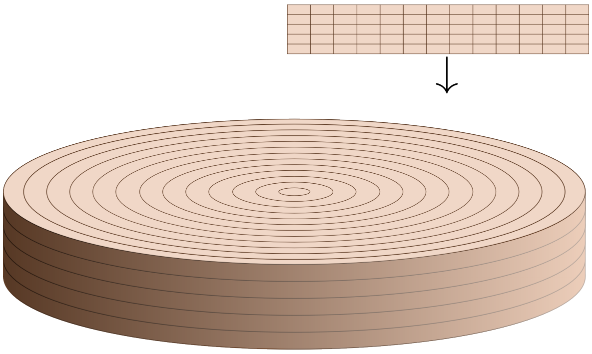

Figure 6.5: Radial extrusion of a two-dimensional grid to three spatial dimensions.

between two layers of rock with low permeability and porosity. In the center of the domain, CO_2 is injected into the reservoir layer for 20 years at a rate of $0.17\,\mathrm{kg/s}$ while on the outer boundary we assume the reservoir to be fully saturated with brine and that all fluids can flow freely. Finally, the material parameters used for this problem are given in Table 6.2.

6.2.1 Radial Domain Extrusion

One thing we notice immediately about this problem is that it is radially symmetric, so we are able to discretize the conservation equations (2.42, 2.46) using only two dimensions, provided that we extrude the domain radially along the horizontal axis. In this case, we define the extrusion factor as

$$\gamma = 2\,\pi r\ ,$$

where r is the distance to the center of the bore hole of the well, *i.e.*, the distance from the left boundary of the spatial domain plus the radius of the bore hole of the injection well. This concept is illustrated in Figure 6.5.

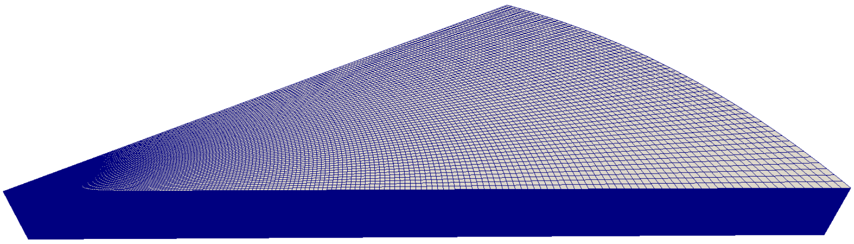

(a) 3D Grid

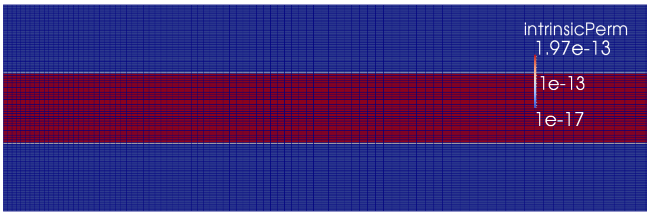

(b) Zoom on the Tip of the 2D Grid with Intrinsic Permeability

(c) Gas Saturation

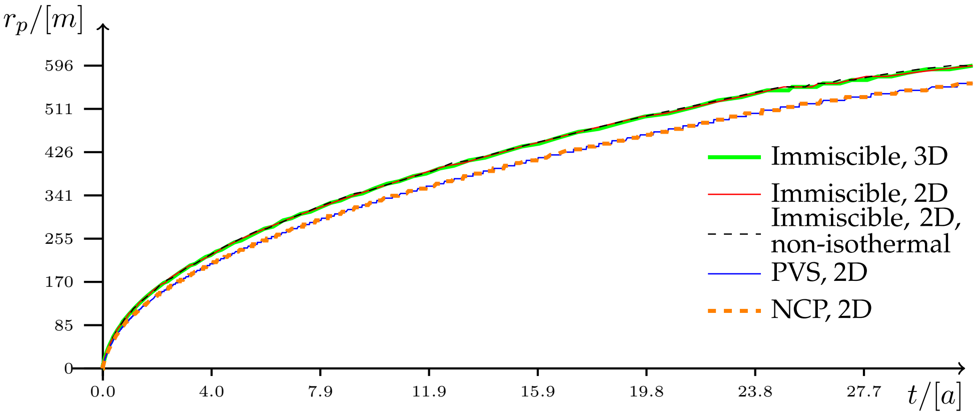

(d) CO_2 Plume Radius Versus Simulation Time

Figure 6.6: The radially symmetric CO_2 injection problem. (a) Grid used for the full three-dimensional simulations. The domain extends $800\,\mathrm{m}$ in radial, $60\,\mathrm{m}$ in vertical and $45°$ in angular direction. The radial direction is discretized using 200 cells exhibiting a prolongation factor of 1.01 while the vertical dimension is discretized uniformly via 120 cells and the angular one by 60 cells. (b) Zoom to the injection area on the left of the two-dimensional grid which was used in conjunction with radial domain extrusion. The two-dimensional grid is a cut through the three-dimensional one. (c) Gas saturation after 32 years obtained using the two-dimensional grid and the immiscible model. (d) Comparison of the results for this problem using various approaches.

6.2.2 Results

Now we are in a position to discuss results for this problem. In Figure 6.6, we outline the results obtained using both, the radial domain extrusion method as well as the direct three-dimensional simulation approaches. As we can conclude from Figure 6.6d, the difference of the radius of the CO_2 plume for a full three dimensional simulation compared to that of the two-dimensional simulation is quite small, and probably below the discretization error if we consider the fact that the sizes of the time steps are generally slightly smaller for the three-dimensional grid compared to the two-dimensional one.

Further, we observe that the results do not differ significantly if energy is conserved compared to neglecting this equation. Quite likely, we can attribute this to the fact that the CO_2 is injected at reservoir temperature.

Finally, the results obtained using the NCP model agree very well with the ones obtained using the PVS approach. This means that for this problem, the only significant differences are between the results of models which incorporate miscibility and the results of the model which assumes immiscibility.

Besides the quality of the results, the parallel performance of a simulator is of major interest for large-scale problems. To investigate it, this problem was used in conjunction with the three dimensional grid. The reason for this choice is that, on one hand, the problem is large enough to keep the communication overhead of the processors reasonably low compared to the local computational work of each processor in parallel simulations, but on the other hand, it is still small enough to compute results on a single processor within a reasonable time frame. Figure 6.7a shows the wall time required to linearize the non-linear system of equations and the time to solve the resulting linear system of equations depending on the number of processors used. The linear solver used to obtain these results was a stabilized BiCG method [86] in conjunction with an incomplete LU decomposition preconditioner [70]. Also, the overlap of the linearization was chosen to be 10 cells.

The results of this are depicted in Figure 6.7 which shows the wall time of the simulations and the *parallel efficiency* of the individual parts depending on the number of involved processors. There, the parallel efficiency α_par is defined as the CPU time required by a single processor to finish the simulation t_seq divided by time the required by the parallel run t_par and by the number of processors n_cores:

$$\alpha_\mathrm{par} = \frac{t_\mathrm{seq}}{t_\mathrm{par} \cdot n_\mathrm{cores}} \; .$$

A remarkable aspect of Figure 6.7b is the fact that the efficiency of the linearization process is not dependent on the number of processors and is even sightly better for parallel runs than for sequential ones. The latter observation can probably be attributed to cache effects.

As clearly visible in Figure 6.7, the part of the simulations that does not scale well is the linear solver: We can observe that the wall time required for the linear solver even *increases* for 8 processes compared to 4. For more than 8 cores, the linear solver scales again, albeit its parallel efficency asymptotically decreases to zero. Quite likely, we can explain the former behavior by the fact that the memory bandwidth of a single node of the used computer system is

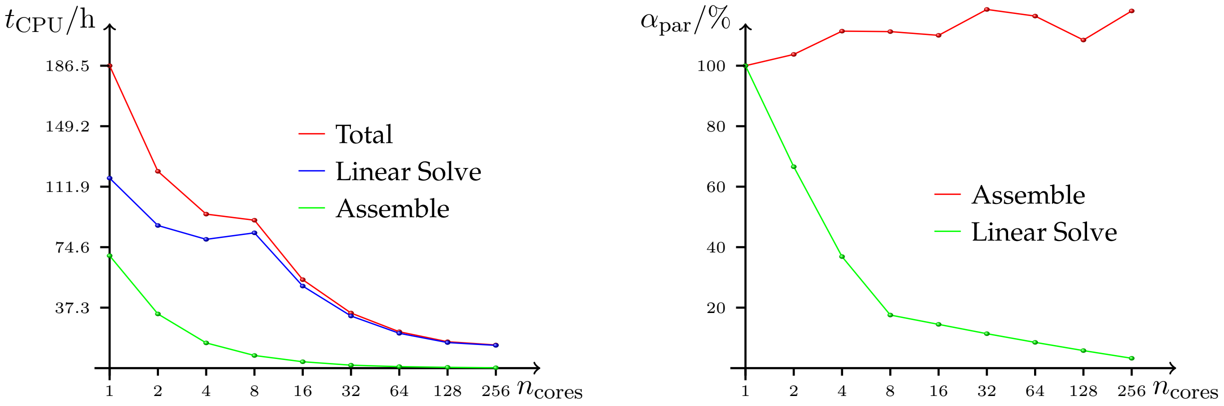

(a) Wall Time

(b) Parallel Efficiency

Figure 6.7: Parallel performance of the CO_2 injection problem simulated in three spatial dimensions using an isothermal model that assumes immiscibility. The problem was simulated on a compute cluster equipped with dual-socket 2.83 GHz Intel® Xeon$^{\mathrm{TM}}$ E5440 CPUs. The simulation used a hexahedron grid featuring about 1.45 million elements (200 cells in radial, 60 elements in angular, and 120 elements in vertical direction).

shared amongst all eight processors on a single compute node. For more than four concurrent processes, the limiting factor of the linear solver thus becomes the available bandwidth to the main memory. Using more than eight processors then leads to a distribution of the simulation to more than one compute node, which increases the overall bandwidth to the main memory. If we continue to use more processors, the need for inter-node communication during the linear solution process increases proportionally. In turn, this leads to the asymptotic decrease of the parallel efficiency which is featured in Figure 6.7b.

The gist of Figure 6.7b is that, in the case of the synthetic CO_2 injection problem, using more than approximately 64 processors does not lead to sufficient performance improvements to justify the additional computational resources. This situation might change if we could improve the parallel efficiency of the linear solution part of the simulation, for example by using more sophisticated linear solvers like multi-grid methods [82]; these are not investigated in the context of this thesis, though.

Finally, Table 6.3 shows the CPU time required on a single core of a 3.5 GHz Intel® Core$^{\mathrm{TM}}$ i7-3770K CPU for various simulation approaches to this problem. As expected, the two-dimensional simulations which use radial domain extrusion are much faster than the fully three-dimensional one. From this table, we can also conclude that in contrast to the heat-pipe problem discussed in Section 6.1, the model which directly solves non-linear complementarity functions does not profit much from its increased robustness regarding changes of the phase presence, but is obviously hit by increased costs for linearizing the non-linear system of equations and solving the resulting linear systems of equations: If energy is conserved via an additional equation, the model based on primary variable switching requires approximately 70 % more time steps than the model which solves the non-linear complementarity

Model	Grid	Time Steps	NEWTON-Iterations	Wall Time /[h]
Immiscible	3D	133	1114	69.54
Immiscible	2D	115	929	0.24
Immiscible, non-isothermal	2D	115	932	0.49
PVS	2D	1066	12278	7.21
PVS, non-isothermal	2D	1744	20569	20.34
NCP	2D	1032	11817	12.22
NCP, non-isothermal	2D	1012	11503	17.43

Table 6.3: Performance metrics for various approaches on a single core of an 3.5 GHz Intel® Core™ i7-3770K CPU.

functions directly, although this is only barely enough to compensate the additional costs of the additional equations required by the NCP model.

Summarizing this example, we can conclude that the most effective approach to model radially symmetric problems is to use a two-dimensional grid in conjunction with radial domain extrusion. Further, Figure 6.6d shows that the results obtained using models that include miscibility are easily distinguishable from the ones neglecting it, even if miscibility is quite low as is the case for CO_2 injection scenarios. At the same time, it indicates that we do not need to consider energy as a conservation quantity for CO_2 injection scenarios if the temperature of the injected CO_2 is close to the temperature of the reservoir. Finally, we observe that the scalability of parallel runs of such simulations usually is not very good, and that this is primarily caused by the part which solves the linear systems of equations.

6.3 The Ninth SPE Benchmark Problem

The next setup which we will discuss is a slightly simplified version of the ninth benchmark problem of the society of petroleum engineers [45] (SPE-9): Instead of the 27 wells of the original specification, the problem which we discuss has only one injection and one production well. The spatial domain is outlined in Figure 6.8. In planar direction, it is a rectangle of $2.2\,\mathrm{km}$ by $2.2\,\mathrm{km}$, and exhibits a thickness of $110\,\mathrm{m}$. The domain is skewed by 16 degrees with its deepest point being at a depth of $3200\,\mathrm{m}$. This domain is discretized using 24 times 24 rectangles in planar direction and 16 layers of varying thicknesses in depth direction. The intrinsic permeability $\boldsymbol{K}$ varies widely within the spatial domain as outlined in Figure 6.8b. Initially, the pressure in the domain is $248\,\mathrm{bar}$. Elements deeper than $3030\,\mathrm{m}$ are initially set to be fully water saturated, while elements above that threshold exhibit an initial oil saturation of $100\,\%$.

While all borders of the reservoir are assumed to be completely impermeable, the reservoir is penetrated by the two boreholes mentioned above: The one used for the production of oil and gas is located at the center of the topmost and most north-eastern element. The well which injects water is assumed to be located at the center of the bottommost, most south-western element of the grid. Both wells are implemented as source terms using the PEACEMAN well

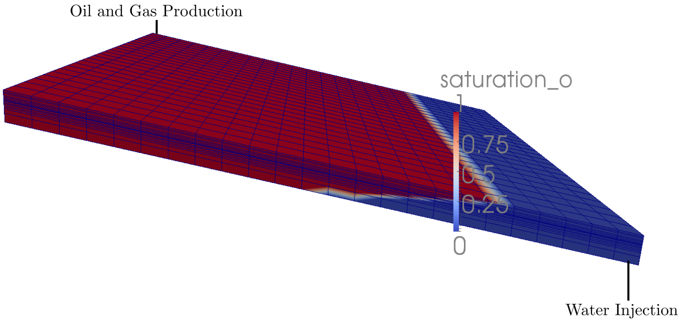

(a) The Grid, Initial Oil Saturation S_o and Well Locations

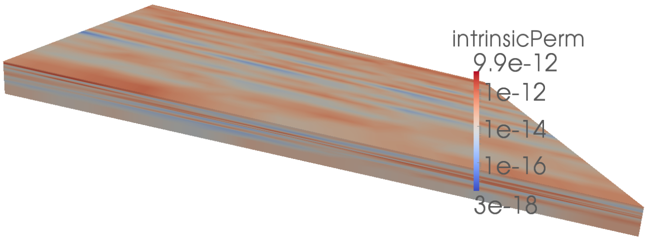

(b) Intrinsic Permeability $\|\boldsymbol{K}\|/\mathrm{m}^2$

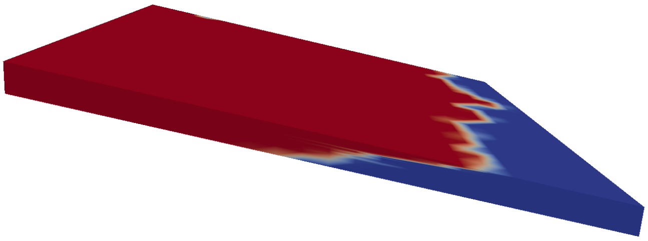

(c) Oil Saturation After 9000 Days

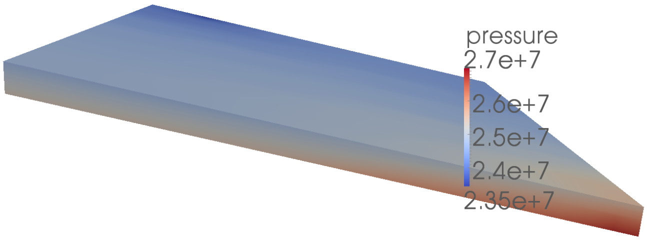

(d) Oil Pressure p_o/Pa After 9000 Days

Figure 6.8: The simplified SPE-9 benchmark problem.

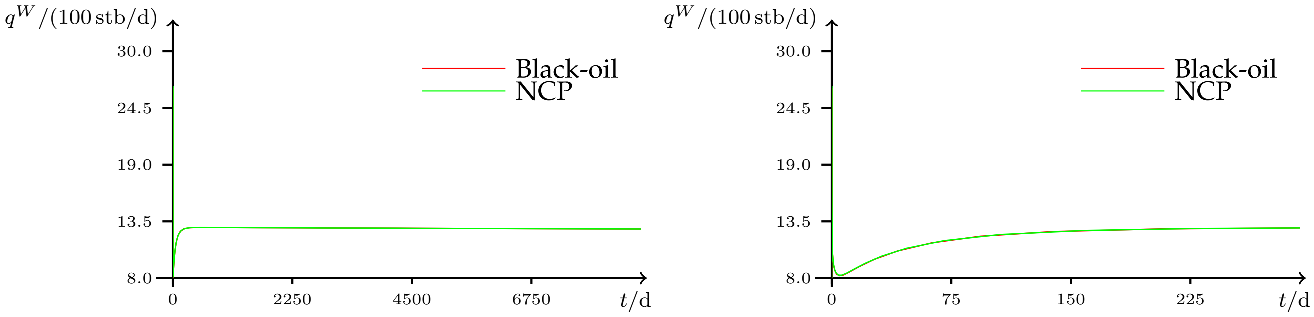

(a) Water Injection Rates

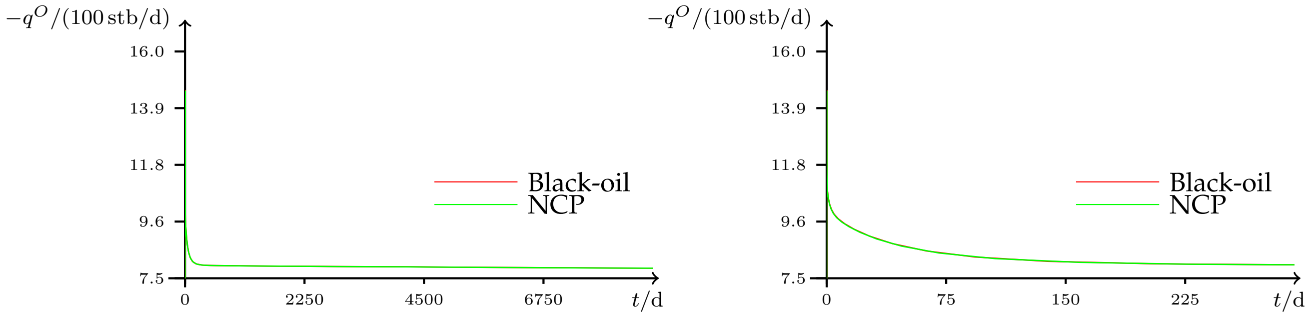

(b) Oil Production Rates

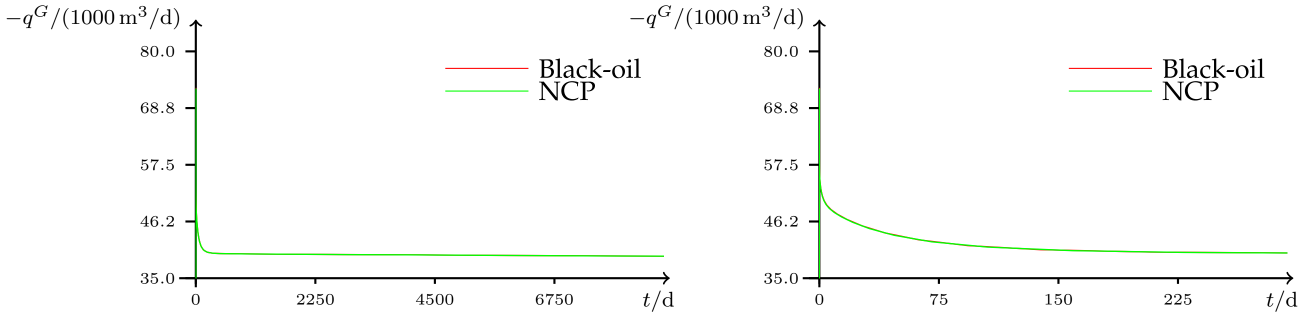

(c) Gas Production Rates

Figure 6.9: Predicted production and injection rates for the simplified SPE-9 benchmark: The left side shows the production and injection curves for the whole simulated period of 9000 days, the graphs on the right show the same curves for the first 300 days. The unit stb stands for *stock tank barrel*, and it is the amount of mass which is contained within one barrel at atmospheric pressure, *i.e.*, $0.159\,\mathrm{m}^3$; the gas production rates are given in terms of the volume of the produced gas at atmospheric pressure.

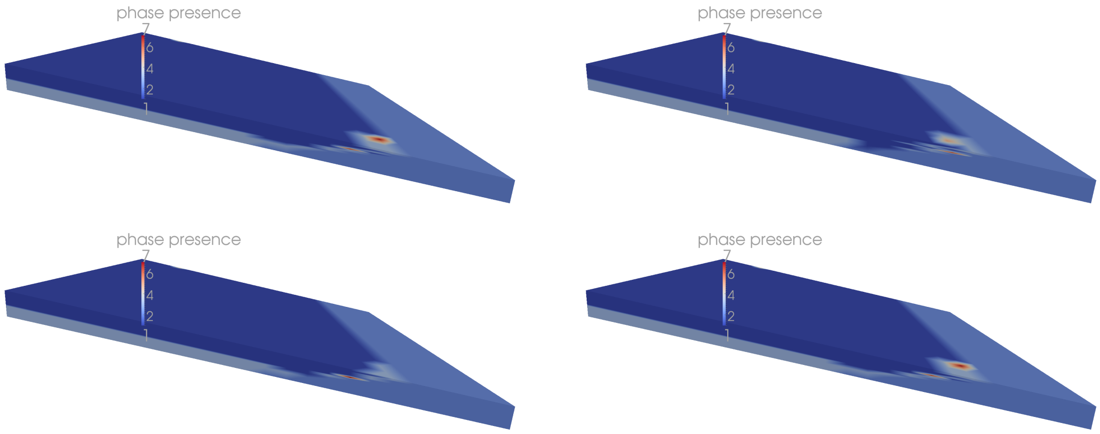

Figure 6.10: Typical behavior of the NEWTON-RAPHSON method for the SPE-9 problem if using the PVS model: The phase presence pseudo variables oscillate. The value displayed χ_{pp} is calculated using

$$\chi_{\mathrm{pp}} := 2^0 \cdot \bar{p}_o + 2^1 \cdot \bar{p}_w + 2^2 \cdot \bar{p}_g$$

where $\bar{p}_\alpha$ is 1 if fluid phase α is present at a given spatial location, and zero otherwise. The phase presence initially displayed on the upper left is changed to the one on the upper right in the next NEWTON-RAPHSON iteration, then it assumes the value on the lower left, and finally goes back to the initial state as displayed on the lower right.

	NCP	Black-Oil
$n\,[-]$	84	60
$n_{\mathrm{NEWTON}}\,[-]$	536	327
$t_{\mathrm{CPU}}\,[\mathrm{h}]$	0.77	0.19

Table 6.4: Comparison of the performance of the numerical models using the specialized black-oil model and the NCP model incorperating non-linear complementarity functions for the SPE-9 problem. Here, n corresponds to the number of time steps required to simulate the setup for 9000 days, t_{CPU} is the required computation time of a single core of an Intel® Core™ i7-3770K CPU, and n_{NEWTON} is the total number of iterations of the NEWTON-RAPHSON method required for the whole simulation.

model [19]. The parameters used are a skin factor of zero, a borehole radius of $7.5\,\mathrm{cm}$, and a bottom-hole pressure of $275\,\mathrm{bar}$ for the injection well and $206\,\mathrm{bar}$ for the production well.

This setup was simulated using the PVS and the NCP models as well as with the black-oil model. The obtained results for the water injection rate as well as for the oil and gas production rates agree very well as we can see in Figure 6.9. Inspecting this figure, we also note that the production and injection rates for the PVS model are not included. The reason for this is that the NEWTON-RAPHSON algorithm is very unstable for the SPE-9 problem when using the PVS model. This caused a non-recoverable breakdown at the beginning

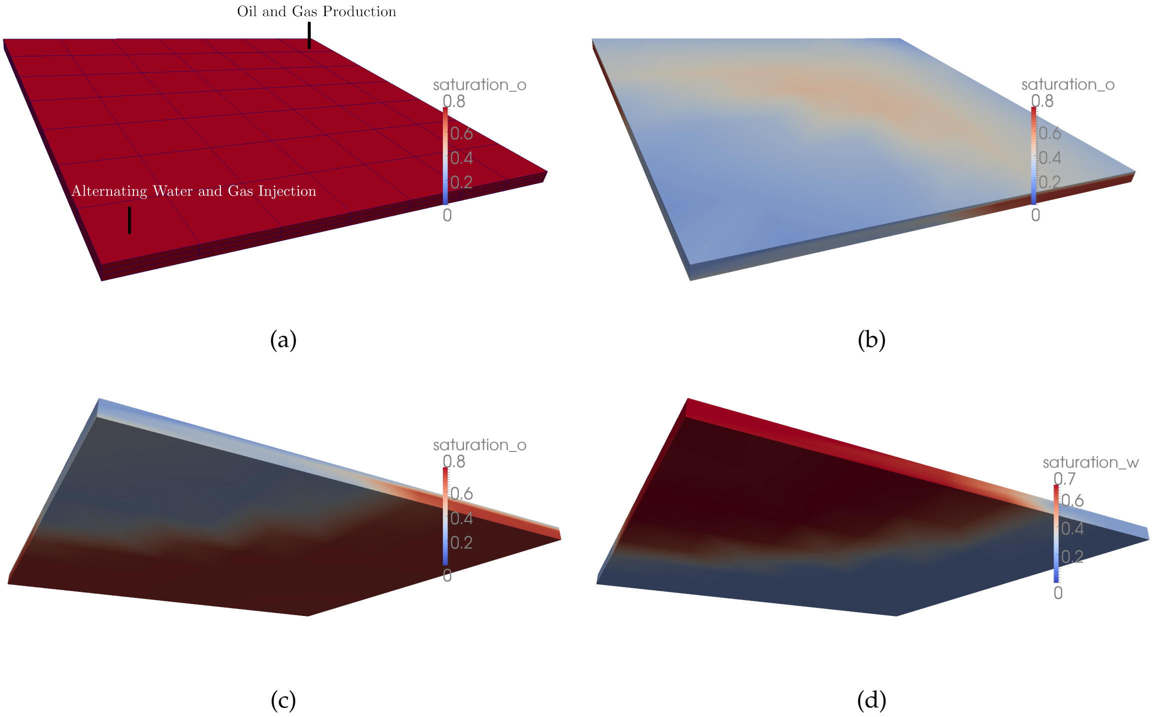

(a) (b) (c) (d)

Figure 6.11: The SPE-5 benchmark problem: **(a)** The grid, initial oil phase saturation, and the locations of the wells. **(b)** Oil phase saturation after three years of production as seen from above. **(c)** The oil phase saturation after three years of production as seen from below. **(d)** The water phase saturation after three years of only oil production and one subsequent year of water injection plus oil production as seen from below.

of the simulation. The reason for this is illustrated in Figure 6.10. It displays the values of the phase-presence pseudo primary variables for successive iterations of the NEWTON-RAPHSON algorithm of a failing time step: The presence of the phases keeps oscillating between iterations instead of reaching a stable state. This behavior is likely caused by the similar values of the fugacity coefficients for components which are not preferred by the gas and the water phases. Since the NCP model directly embeds the presence of the fluid phases in the non-linear system of equations to be solved, it is less vulnerable to this issue and does not suffer a breakdown.

Moreover, we can infer from Figure 6.9 that the production and the injection rates calculated using the specialized black-oil model agree quite well with the ones computed using the generic NCP model. As outlined in Table 6.4, the computational effort for the generic NCP model is higher, though.

Component $\langle\cdot\rangle^\kappa$	p^κ_{crit} [bar]	T^κ_{crit}[K]	ω^κ
Water (H_2O)	220.64	647.10	0.344
Methane (C_1)	460.43	190.56	0.013
Propane (C_3)	424.92	369.83	0.1524
Hexane (C_6)	301.23	507.44	0.3007
Decane (C_{10})	209.60	617.67	0.489
Pentadecane (C_{15})	137.89	705.56	0.65
Icosane (C_{20})	111.69	766.67	0.85

Table 6.5: PENG-ROBINSON parameters used for the fifth SPE benchmark problem. All binary interaction coefficients $\bar{k}^{\kappa\lambda}_\alpha$ are zero, except for C_1 interacting with C_{15} or C_{20}, and C_3 interacting with C_{15} or C_{20}. In the former case, the interaction coefficient is assumed to be 0.05 while in the latter case $\bar{k}^{\kappa\lambda}_\alpha = 0.005$ is used.

6.4 The Fifth SPE Benchmark Problem

Let us now consider the problem specified by the fifth comparative solution project of the Society of Petroleum Engineers [46]. This problem is the subject of Figure 6.11 and features a simple three-dimensional CARTESIAN grid exhibiting 7 by 7 by 3 elements with a total extend of $1067\,\mathrm{m}$ by $1067\,\mathrm{m}$ by $30.5\,\mathrm{m}$, as outlined. The bottom of the domain is assumed to be at a depth of $2750\,\mathrm{m}$ which yields an initial pressure of $275\,\mathrm{bar}$. Like for the simplified ninth benchmark problem, the boundary of the domain is fully closed, and production and injection are handled by vertical boreholes using the PEACEMAN well model [19]. For this problem, the injection well is located in the highest, most south-western cell, while the production well is located in the deepest north-eastern cell, with a bottom hole pressure of $310\,\mathrm{bar}$ for the injection well and $69\,\mathrm{bar}$ for the production well. Initially, the reservoir exhibits a uniform water saturation of $20\,\%$ and an oil saturation of $80\,\%$. Of the three scenarios described in the benchmark specification [46], only the first is considered: This scenario specifies a period of three years where oil and gas is produced without any injection occuring. After that, water and gas injections are alternated yearly. In this scenario, oil production and water injection is capped at 12000 stock-tank barrels per day, while the injection rate of gas is limited to 12 thousand cubic feet at standard conditions per day.

The interesting part of the problem are the thermodynamics of the involved fluids: Like the black-oil model, this problem assumes the potential presence of the three fluid phases gas, oil, and water, but it specifies the thermodynamic properties using seven components, and the PENG-ROBINSON parameterization of the cubic equation of state. The parameters used for these thermodynamic relations are outlined in Table 6.5. Also, the problem applies the standard mixing rule (3.4). With this, we calculate the mass densities ρ_o and ρ_g of the oil and the gas phases. The fugacity coefficients for all components are calculated using Equation 3.15 for the initial state and are then used throughout the simulations.

For this thesis, this problem was simulated using the PVS and NCP models. As we can infer from Figure 6.12, the predicted injection and production rates as well as the average pressure within the reservoir are virtually indistinguishable. Moreover, the computed rates and the

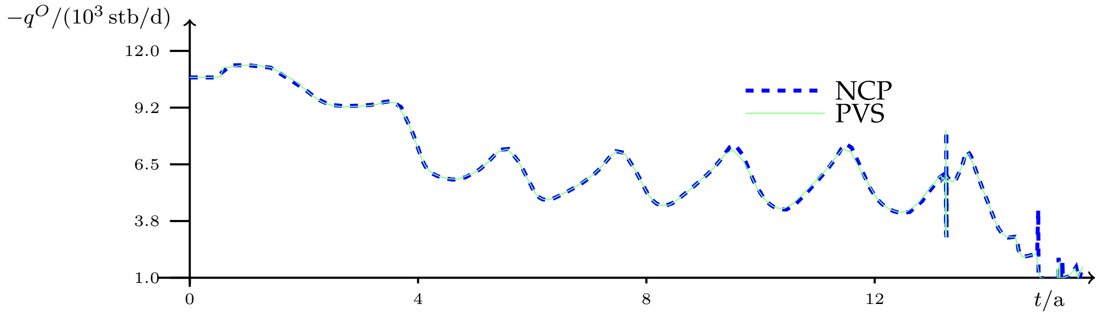

(a) Oil Production Rates

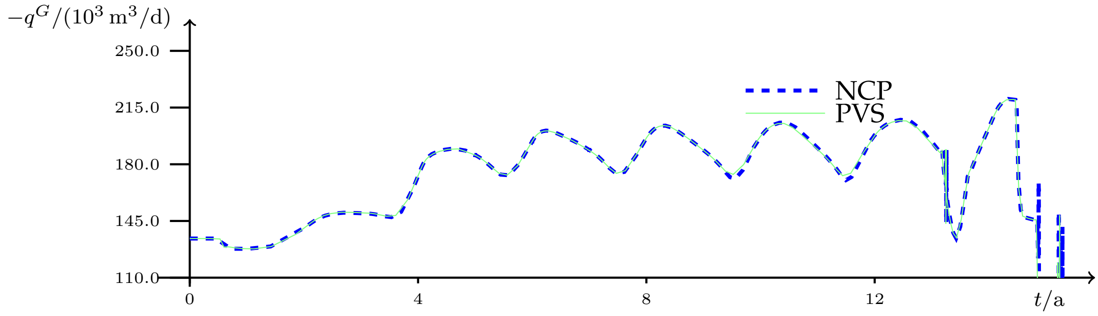

(b) Gas Production Rates

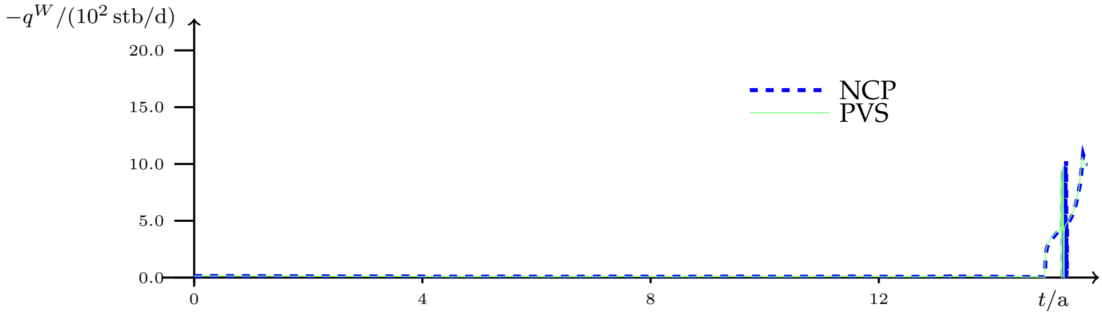

(c) Water Production Rates

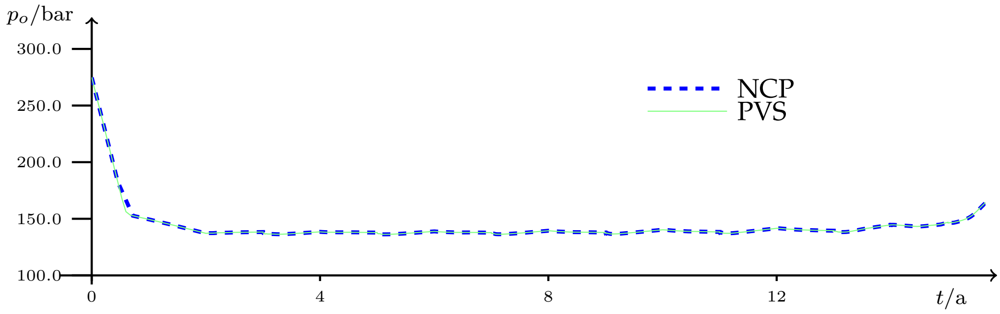

(d) Average Reservoir Pressure

Figure 6.12: Predicted production and injection rates for the SPE-5 benchmark. The rates for oil production and water injection are given in stock tank barrels per day (stb/d), the gas production rate is plotted in thousands of cubic feet per day (MCF/d).

	NCP	PVS
$n\,[-]$	858	826
$n_{\text{Newton}}\,[-]$	5334	4840
$t_{\text{CPU}}\,[\text{h}]$	0.67	0.50
$n_{\text{Newton}}/t_{\text{CPU}}\,[1/\text{s}]$	2.20	2.67

Table 6.6: Comparison of the performance of the numerical models using primary variable switching (PVS) and non-linear complementarity functions (NCP) for the SPE-5 benchmark problem. Like for the previously presented problems, n corresponds to the number of time steps required to simulate the problem for 17 years, t_{CPU} is the CPU time required for the simulation using an Intel® Core™ i7-3770K CPU running at a clock speed of $3.50\,\text{GHz}$. Further, n_{Newton} is the total number of iterations of the NEWTON-RAPHSON method.

average reservoir pressure agree very well with the results of most simulators published in the original specification [46]. If we consider the computational effort required for our simulations as presented in Table 6.6. One aspect worth mentioning here is that the ratio of the computational costs per NEWTON-RAPHSON iteration for the PVS and the NCP models is smaller for the SPE-5 problem than for the setups discussed before. This is due to the fact that solving the local systems of equations for the PVS model is much more elaborate in the three-phase case than if only two phases are involved. In conjunction with the large number of components, this leads to the PVS-based simulation to exhibit high computational costs per NEWTON-RAPHSON iteration. Unlike for the previously presented examples, the number of NEWTON-RAPHSON iterations required is higher for the NCP model than for the PVS model.

6.5 The Ketzin CO_2 Storage Project

After investigating the physical accuracy and comparing the computational performance of the flow models amongst each other, let us now have a brief look at a setup which describes a large-scale real-world experiment – the German CO_2 injection pilot site near Ketzin/Havel [55, 44, 49]. The geology of the site of this project features a dome-shaped reservoir formation which exhibits relatively a high permeability as well as high porosity, that is “sandwiched” between highly impermeable salt layers. Together with the intrinsic permeability field of the reservoir, the shape of the reservoir formation is displayed in Figure 6.13. The capillary-pressure and relative permeability curves used for the simulation are presented in Figure 6.14.

The planar extend of this domain is a square of $5\,\text{km}$ by $5\,\text{km}$, and the reservoir layer is about $130\,\text{m}$ thick. This domain is discretized by roughly 4 million tetrahedra using the DUNE-ALUGrid manager [4, 15]. The resulting grid is depicted in Figure 6.13.

Figure 6.15 shows the shape of CO_2 plumes after injecting roughly 55 thousand tons of CO_2 over a period of slightly more than three years while Figure 6.16 shows the predicted share

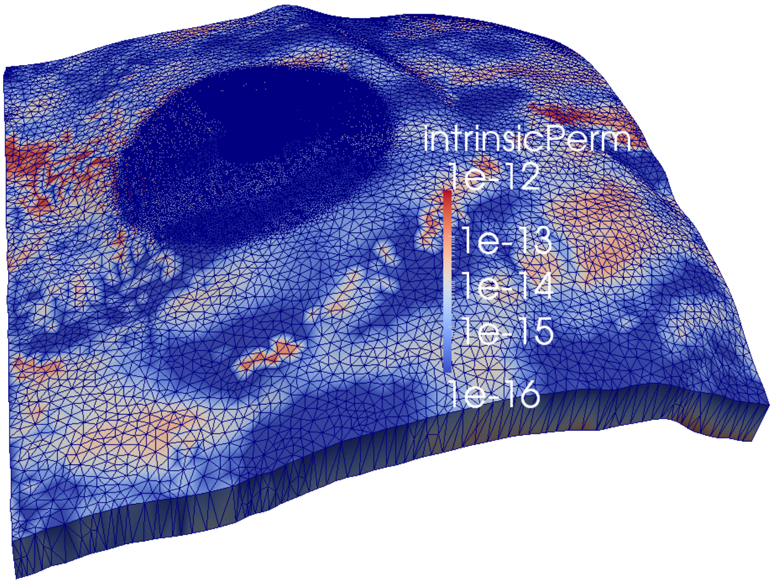

(a) Grid and Intrinsic Permeability $\|\boldsymbol{K}\|/\mathrm{Pa}$

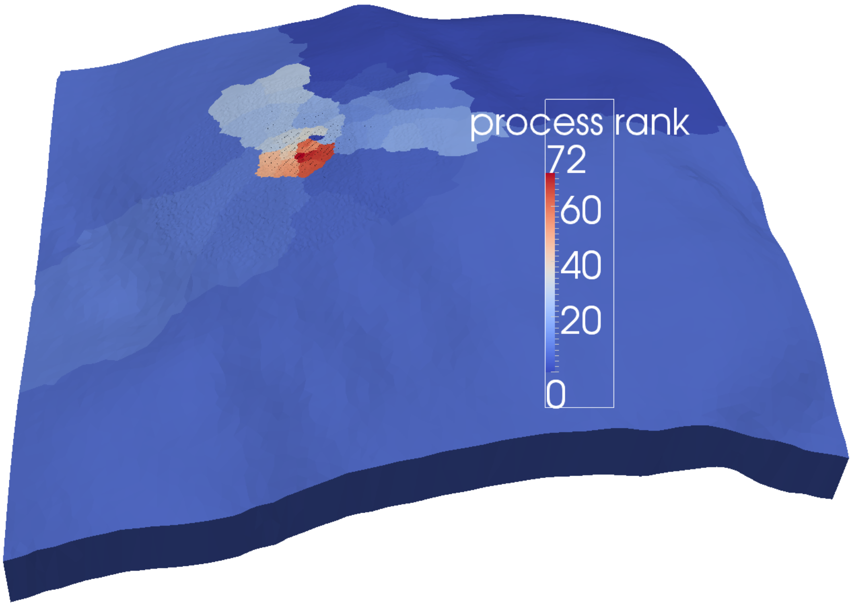

(b) The Partition of the Grid Used for the Parallel Simulation

Figure 6.13: Discretization the Ketzin CO$_2$ injection site.

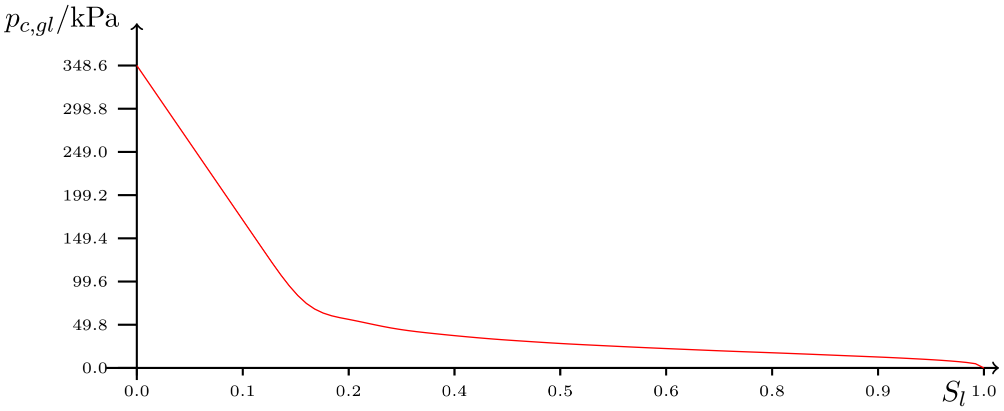

(a) Capillary Pressure $p_{c,gl}$

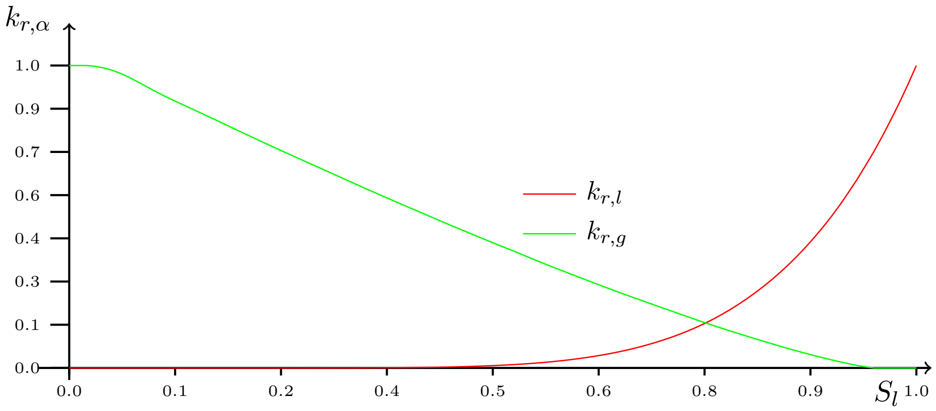

(b) Relative Permeabilities

Figure 6.14: The material parameters used by the simulations of the Ketzin CO_2 storage project. It is assumed that these parameters only depend on the saturation of the liquid phase.

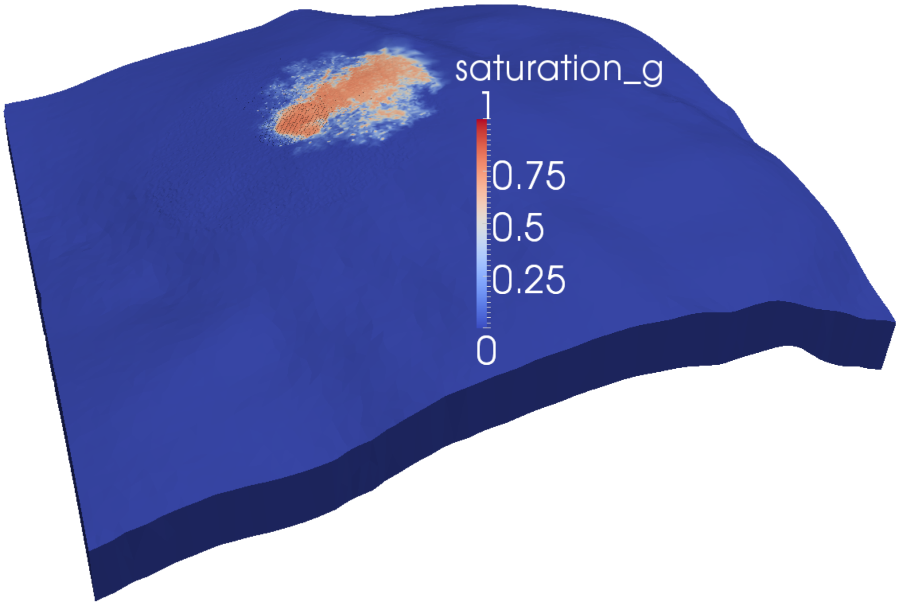

(a) Gas Saturation Predicted by the Model Assuming Immiscibility

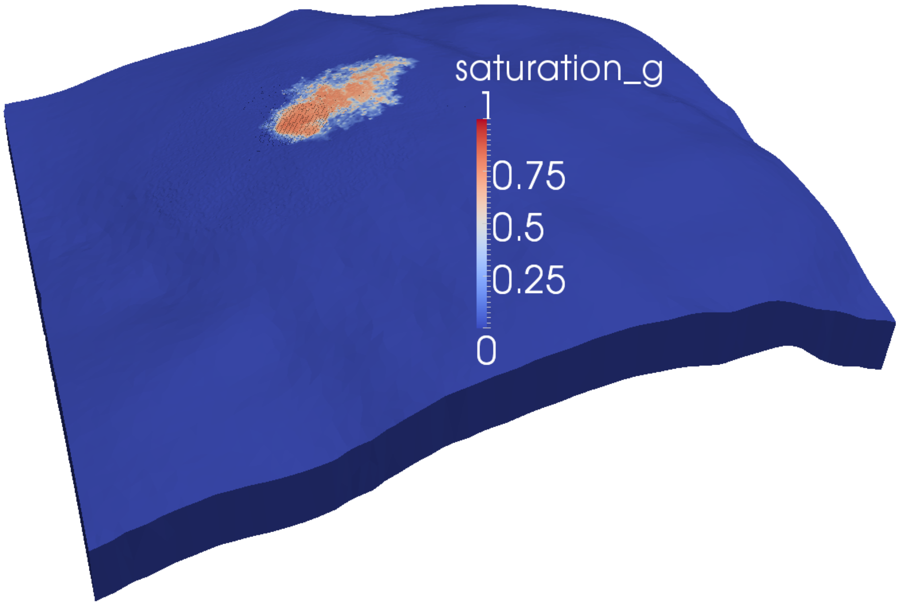

(b) Gas Saturation Predicted by the NCP Model

Figure 6.15: The simulated gas-phase saturation for the Ketzin CO_2 injection experiment after injecting about 55 thousand tons of CO_2 during a three year period. The extend of the CO_2 plume for the NCP case which includes miscibility is clearly smaller than for the case where miscibility is neglected. Both simulations assume the potential presence of the two phases “liquid” and “gas”, and use the two components brine and CO_2 which are described using the relations provided by IAPWS [88], and SPAN and WAGNER [77]. Based on the conclusions of Section 6.2, energy is not considered as a conservation quantity in these simulations.

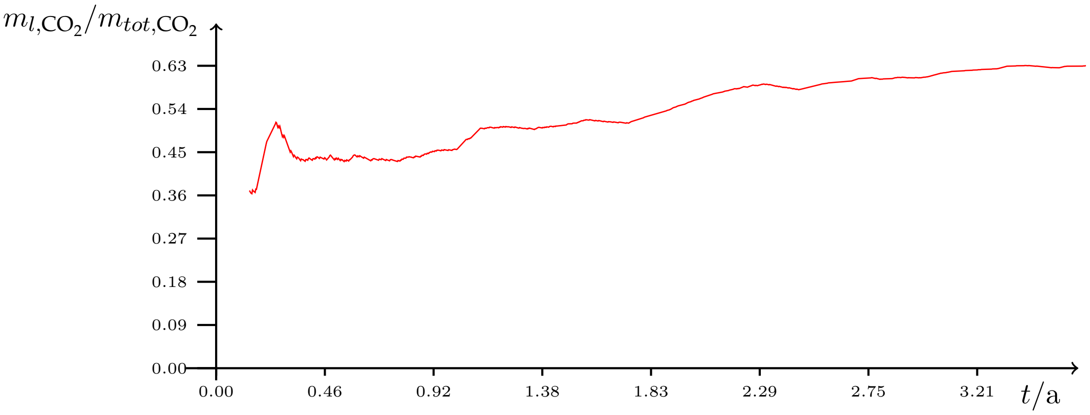

Figure 6.16: Predicted share of CO_2 dissolved in the brine phase for the Ketzin CO_2 injection experiment. The brine-CO_2 miscibility relations used in this simulation have been proposed by SPYCHER and PRUESS [78].

of CO_2 dissolved in the brine phase if using a model that considers miscibility (in this case using the NCP model).

In comparison to the synthetic CO_2 injection problem which we discussed in Section 6.2, miscibility effects play a much more important role in this scenario, as $40\,\%$ to $60\,\%$ of the injected CO_2 are predicted to be dissolved in the brine. We can also clearly observe the relevance of miscibility by comparing the shape of the CO_2 plume of Figure 6.15a to that of Figure 6.15b. In this context we should be aware that—due to using finite volume methods as spatial discretizations for these simulations—the amount of dissolved CO_2 is overestimated systematically. The reason for this is that finite volume discretizations use only a single value to represent the conditions within an individual element. For large finite volumes, this leads to CO_2 being assumed to be present in regions of the elements where it cannot be present in reality. This implies that the amount of brine which CO_2 is assumed dissolve in is overestimated. In turn, this over-estimation of the amount of dissolved CO_2 leads to an underestimation of the gas phase saturation. In the case of the Ketzin project, this supposition is supported by seismic evidence [55]. For this setup, we should also be aware that the input parameters, like the intrinsic permeability $\boldsymbol{K}$ exhibit large uncertainties, so that the results presented in Figures 6.15 and 6.16 should be used with care.

Nevertheless, these simulations prove that the methods presented in this thesis can be used for large-scale geological applications and that miscibility is a factor which needs to be considered in many real-world applications.

7 Summary and Conclusion

In this thesis, we first motivated the continuum mechanical approach and derived the conservation equations for the physical quantities mass, momentum, and energy on this scale. After adapting the momentum conservation equations to the special case of NEWTONIAN fluids, we used the obtained relations to derive the conservation equations for macro-scale fluid flow in porous media. We then discussed how we can close the system of equations in a mathematical sense. It turned out that one relation per fluid phase needs to be defined using *model assumptions*. For this purpose, we presented the assumptions of the well established immiscibility model [39], primary variable switching model [23], and black-oil model [19] and introduced a new set of model assumptions which are based on directly including non-linear complementarity problems into the system of equations to be solved [48].

Following this coverage of all relevant equations, we discussed how the resulting systems of equations can be discretized and how the resulting algebraic non-linear systems of equations can be solved. After briefly looking at the software which was used to implement the aforementioned concepts, we finally discussed some numerical examples.

The first of these was the heat-pipe setup proposed by UDELL [84]. This problem features a one-dimensional spatial domain occupied by water that evaporates and condenses. For this problem, we could derive a semi-analytical solution for the steady-state with which we compared to results obtained using the numerical models based on primary variable switching (PVS) and non-linear complementarity problems (NCP) and observed that the numerical results obtained using both models are identical up to rounding errors. We further observed that the numerical solutions converged to the semi-analytical one as we increased the spatial resolution of the grid. This led us to the conclusion that from the point of view of physical and numerical accuracy, both the NCP and the PVS models produce correct results, and that thus the computational cost is the main factor for deciding which one to use. Analyzing this computational performance of both approaches, we found that for this problem, the NCP model required an order of magnitude fewer time steps than the PVS approach. This increased robustness more than amortized higher costs per time-step of the NCP model.

After the heat-pipe problem, we compared the NCP and the PVS models with the immiscible model for a synthetic CO_2 injection problem. For this problem we used a radially symmetric domain which allowed us to compare the numerical results obtained using a three-dimensional simulation with the ones computed using radial domain extrusion in conjunction with a two-dimensional spatial domain. We found that the results of both approaches are comparable, but that the approach using radial domain extrusion is much cheaper from the point of view of computational effort. We deduced that we should choose a 2D approach in conjunction with radial domain extrusion if possible. For this problem, we also compared the immiscible model with the ones that consider miscibility, and found that the results differed significantly. Having said that, the results obtained using the immiscible model should still be accurate enough for many purposes.

Since the three-dimensional grid used by this problem featured approximately 1.4 million elements, it was large enough to apply domain decomposition methods on a parallel machine. Simultaneously, it was small enough to complete sequential simulations in an acceptable time frame. For this reason, we used this problem to analyze the efficiency of the parallelization. In this context, we found that the computational time required for this simulation is clearly dominated by the procedure of solving the linearized systems of equations, and, even worse, that this procedure typically does not scale well with the number or processors involved.

Next, we compared the computational effort required for the three models for this problem. We found that the effort in terms of the number of time steps and NEWTON-RAPHSON iterations is much lower for the immiscible model compared to the other two. For the two models that include miscibility, the NCP model requires fewer time steps and fewer NEWTON-RAPHSON iterations, but in terms of processing time, it is still slower than the PVS approach. The reason for this is the fact that the discretization and linearization as well as the linear solution processes are more elaborate for the NCP model. This is the case because it includes one additional equation and primary variable per phase compared to the PVS model. Further, in contrast to the heat-pipe problem, the determination of the presence of the fluid phases does not seem to be a major limiting factor of this problem when it comes to numerical performance, so the higher costs of each NEWTON-RAPHSON iteration are not amortized by the fewer required time-steps.

After the synthetic CO_2 injection problem, we considered a slightly simplified version of the ninth benchmark problem of the society of petroleum engineers [45]. For this setup, we compared the PVS and NCP models with the black-oil model. We found, that the PVS model is incapable of simulating this setup, but that the NCP model and the black-oil model could be used. For this setup, we observed that the injection and production rates calculated using the two models agreed very well, but we also noted that the computational effort required for the black-oil model was much lower.

This was followed by an investigation of the first scenario of the fifth benchmark problem of the society of petroleum engineers [46]. Like the ninth SPE benchmark problem, this specification originates from the field of oil reservoir engineering, and thus features the three fluid phases oil, gas, and water. Compared to the ninth benchmark problem, it uses a simpler CARTESIAN grid with uniform material properties. The interesting part of this problem are its complicated thermodynamic relations which involve cubic equations of state. The predicted production and injection rates as well as the average pressure of the reservoir which we obtained for this problem using the PVS and NCP models were very similar. From the point of view of the required computational effort, the NCP model was worse than the PVS model, but the on a per NEWTON-RAPHSON iteration basis the NCP model difference to the PVS model was smaller than in the other examples. We attributed the latter observation to the relatively large number of components of this problem and to the observation that the systems of equations which need to be solved locally are relatively large for three-phase problems when using the PVS model compared to those which need to be solved for the NCP model.

Finally, we compared the results of the immiscible model and the ones of the NCP model for the CO_2 injection experiment in Ketzin/Havel, Germany. For these simulations, an unstructured tetrahedral grid featuring roughly four million elements, and spatially varying permeability and porosity fields were used. The results obtained using a model which assumes immiscibility differed considerably from the results produced by the NCP model. We found that the reason for this is that the share of CO_2 which is predicted to dissolve in the liquid phase is quite significant in this case. However, in this context we noted that this is probably an overestimation which is due to the spatial discretization used. Even so, miscibility is often a relevant effect in large-scale geological applications, and should thus not be neglected at the outset.

In summary, the NCP model has proven to be the most versatile as it performed reasonably well for all problems presented in the context of this thesis. Further, from a computational point of view, it is generally advisable to use a model that directly takes advantage of additional knowledge available for a given setting. For example, if miscibility of components can be neglected, using the immiscible model often leads to a large improvement of the computational performance. Another example is if the setup to be simulated can be assumed to be radially symmetric: Then, using a two-dimensional simulation in conjunction with radial domain extrusion exhibits much lower computational costs while the quality of the results is basically identical compared to fully three-dimensional simulations.

Future Research

Like all scientific works, this thesis has only a limited scope, so there are plenty of topics of interest which could not be covered. In the following, we will outline a few of those.

Model Coupling

For many problems, we may benefit using different numerical models for parts of the simulation that feature diverse characteristics. For example, we could use a model which assumes immiscibility for periods of time where miscibility of components is unimportant, and use a more elaborate model for the remaining time [25].

Another situation for which coupling multiple models might be beneficial are multi-physics situations [34]. For these problems, most of the spatial domain can be described well by a simple model, for example a model neglecting energy or only considering a subset of all fluid phases, while a small part of the domain needs to be simulated using a more comprehensive model. For the fully implicit methods which we covered in this thesis, the implementational effort required for such schemes is quite high [34],and for this reason multi-physics approaches currently mostly use semi-implicit methods [34].

Also, we need to use several models for the spatial domain if the the flow characteristic is vastly different in various parts of the domain. For example, problems that incorporate a part occupied by a porous medium and a part which features turbulent flows, like river-groundwater systems [37] or the soil-atmosphere interactions [57], require us to use a coupling between the models for the individual spatial subdomains.

Finally, we can also think of coupling the models for flow and transport in porous media which we discussed in this thesis with geomechanical models [25] or with large-scale models for global phenomena like climate.

Parameter Uncertainty

In the context of this work, we assumed the external parameters—like the intrinsic permeability $\boldsymbol{K}$—as quantities precisely known *a priori*. This is rarely the case for real-world applications. There, only rough indications about the distribution of these parameters, and a limited set of measured values are usually available for practical and economic reasons. This means that in reality all parameters used in our models feature an uncertainty which we would need to quantify in order to obtain predictive results. This is a fulminant challenge, and we refer the interested reader to OLADYSHKIN *et al.* [62], CIRPKA *et al.* [21], and to BÁRDOSSY *et al.* [17].

Advanced Discretizations

For this thesis, only finite volume were used as spatial discretizations. While conceptually finite volume schemes are easy to understand, locally conservative [31] as well as numerically stable [31], they also exhibit severe disadvantages. Amongst those are slow grid convergence rates and a large impact of the numerical dispersion effect [31]. It would thus be beneficial to investigate more sophisticated spatial discretizations like discontinuous GALERKIN methods [5] or mimetic finite difference methods [12].

Also, as time discretization scheme, the implicit EULER method was exclusively used. Like in the case of finite volume schemes for spatial discretization, this scheme is simple and exhibits good numerical stability [6], but its convergence rate tends to be low because of the relatively large error term. We could thus benefit from investigating better time discretization schemes like implicit RUNGE-KUTTA methods [16] or backward differential formula methods [6].

Adaptivity

Adaptive methods are related to the advanced discretizations and multi-physics approaches [26]. mentioned above. Generally speaking, there are two different approaches to adaptivity: For h-adaptive methods, more elements are added to (or removed from) the grid as soon as the estimated error in the obtained solution is too large (or low enough). For p-adaptive schemes [26], a spatial discretization with a better error term is used for regions of the domain for which a large error is detected.

Finally, h-p-adaptive schemes [26] are combining these two concepts. For them, a higher-order space discretization is used if it is computationally cheaper than refining the grid, else the resolution of the grid is locally increased. Typically, h-p-discretization schemes are challanging to implement [26] since, in addition to error estimates for the refined grid and for the solution with a locally better discretization, we need to find a balance between the two approaches in order to decide which one is better in a given situation.

Further Applications

The final item of this non-exhaustive list of topics that are not covered by this thesis is a closer investigation of additional applications of multi-phase flows in porous media. Amongst these applications we find ground decontamination methods [22, 39], measures to control subsurface coal fires [24], polymer-electrolyte membrane fuel cells [7], and many other chemical engineering applications [42].

A Reproducibility and Raw Data

For the interested and sufficiently determined reader, all results presented in this thesis are available at `http://www.hydrosys.uni-stuttgart.de/institut/hydrosys/publikationen/phd_data/` in their raw and refined forms. The only exception is the data for the Ketzin CO_2 storage project discussed in Section 6.5, which is not included in its raw form due to licensing reasons.

The source code of the software packages which were used to produce these results are also provided. In addition to the raw data and the source code of the simulations which we discussed within this thesis, the LaTeX sources of this document, and editable versions of all pictures used within it, are available at this site.

The source code of the software is provided under the terms of the GNU General Public License (GPL), version two—or, at your option—any newer version of the license. The sources of this document and the raw data of the presented results are licensed under the Creative Commons Attribution Share-Alike 3.0 license. Further information on the used licenses can be found at
`http://www.gnu.org/licenses/gpl-2.0.html`
and at
`http://creativecommons.org/licenses/by-sa/3.0/`

Bibliography

[1] I. Aavatsmark. An Introduction to Multipoint Flux Approximations for Quadrilateral Grids. *Computational Geosciences*, 6:405–432, 2002.

[2] A. Abadpour and M. Panfilov. Method of Negative Saturations for Modeling Two-Phase Compositional Flow with Oversaturated Zones. *Transport in Porous Media*, 79:197–214, 2009.

[3] The ALBERTA Website: `http://www.alberta-fem.de/`.

[4] The ALU-Grid Website:
`http://www.mathematik.uni-freiburg.de/IAM/Research/alugrid/`.

[5] D. N. Arnold, F. Brezzi, B. Cockburn, and L. D. Marini. Unified Analysis of Discontinuous Galerkin Methods for Elliptic Problems. *SIAM Journal on Numerical Analysis*, 39(5):1749–1779, 2002.

[6] U. M. Ascher and L. R. Petzold. *Computer Methods for Ordinary Differential Equations and Differential-Algebraic Equations*. Society for Industrial and Applied Mathematics, 1997.

[7] F. Barbir. *PEM Fuel Cells - Theory and Practice*. Elsevier, second edition, 2012.

[8] C. Bartels. Analyzing Biased Monte Carlo and Molecular Dynamics Simulations. *Chemical Physics Letters*, 331(5-6):446–454, 2000.

[9] G. K. Batchelor. *An Introduction to Fluid Dynamics*. Cambridge University Press, 2000.

[10] A. Y. Beliaev and S. M. Hassanizadeh. A Theoretical Model of Hysteresis and Dynamic Effects in the Capillary Relation for Two-Phase Flow in Porous Media. *Transport in Porous Media*, 43(3):487–510, 2001.

[11] P. Bobeck. *The Public Fountains of the City of Dijon*. Kendall/Hunt Publishing Company, 2009. English Translation of H. Darcy's 1856 Book *Les Fontaines Publiques de la Ville de Dijon*.

[12] F. Brezzi, K. Lipnikov, and V. Simoncini. A Family of Mimetic Finite Difference Methods on Polygonal and Polyhedral Meshes. *Mathematical Models and Methods in Applied Sciences*, 15(10):1533–1551, 2005.

[13] R. H. Brooks and A. T. Corey. Hydraulic Properties of Porous Media. *Hydrology Papers, Colorado State University*, 1964.

[14] E. Buckingham. Studies on the Movement of Soil Moisture. *United States Bureau of Soils Bulletin*, 38:1–61, 1907.

[15] A. Burri, A. Dedner, R. Klöfkorn, and M. Ohlberger. An Efficient Implementation of an Adaptive and Parallel Grid in DUNE. *Proceedings of the Russian-German Advanced Research Workshop on Computational Science and High Performance Computing*, 2:67–82, 2006.

[16] J. C. Butcher. *Numerical Methods for Ordinary Differential Equations*. Wiley, 2003.

[17] A. Bárdossy, I. I. Bogardi, and W. E. Kelly. Imprecise (Fuzzy) Information in Geostatistics. *Mathematical Geology*, 20:287–311, 1988.

[18] R. Car and M. Parrinello. Unified Approach for Molecular Dynamics and Density-Functional Theory. *Physical Review Letters*, 55:2471–2474, 1985.

[19] Z. Chen, G. Huan, and Y. Ma. *Computational Methods for Multiphase Flows in Porous Media*. Society for Industrial and Applied Mathematics, 2006.

[20] T. J. Chung. *General Continuum Mechanics*. Cambridge University Press, second edition, 2007.

[21] O. A. Cirpka, F. P. J. de Barros, G. Chiogna, M. Rolle, and W. Nowak. Stochastic Flux-Related Analysis of Transverse Mixing in Two-Dimensional Heterogeneous Porous Media. *Water Resources Research*, 47(6), 2011.

[22] H. Class and R. Helmig. Numerical Simulation of Non-Isothermal Multiphase Multicomponent Processes in Porous Media: 2. Applications for the Injection of Steam and Air. *Advances in Water Resources*, 25(5):551–564, 2002.

[23] H. Class, R. Helmig, and P. Bastian. Numerical Simulation of Non-Isothermal Multiphase Multicomponent Processes in Porous Media: 1. An Efficient Solution Technique. *Advances in Water Resources*, 25(5):533–550, 2002.

[24] G. J. Colaizzi. Prevention, Control and/or Extinguishment of Coal Seam Fires Using Cellular Grout. *International Journal of Coal Geology*, 59(1–2):75 – 81, 2004.

[25] M. Darcis. *Coupling Models of Different Complexity for the Simulation of CO_2 Storage in Deep Saline Aquifers*. PhD thesis, University of Stuttgart, 2012.

[26] L. Demkowicz. *Computing with h-p Adaptive Finite Elements: One and Two-Dimensional Elliptic and Maxwell Problems*. CRC Press, 2006.

[27] A. H. Demond, F. N. Desai, and K. F. Hayes. Effect of Cationic Surfactants on Organic Liquid-Water Capillary Pressure-Saturation Relationships. *Water Resources Research*, 30(2):333–342, 1994.

[28] The DUNE Website: `http://www.dune-project.org/`.

[29] K. Eriksson, D. Estep, P. Hansbo, and C. Johnson. *Computational Differential Equations*, volume 7. Cambridge University Press, 1996.

[30] The eWoms Website: `http://opm-project.org/ewoms`.

[31] R. Eymard, T. Gallou, and R. Herbin. *Finite Volume Methods*, volume 7. Elsevier, 2000.

[32] A. Fischer. A Special Newton-Type Optimization Method. *Optimization*, 24(3-4):269–284, 1992.

[33] P. A. Forsyth and R. B. Simpson. A Two-Phase, Two-Component Model for Natural Convection in a Porous Medium. *International Journal for Numerical Methods in Fluids*, 12(7):655–682, 1991.

[34] J. Fritz, B. Flemisch, and R. Helmig. Decoupled and Multiphysics Models for Non-Isothermal Compositional Two-Phase Flow in Porous Media. *International Journal of Numerical Analysis & Modeling*, 9(1):17–28, 2011.

[35] W. G. Gray. A Derivation of the Equations for Multi-Phase Transport. *Chemical Engineering Science*, 30(2):229–233, 1975.

[36] A. Griewank. *Mathematical Programming: Recent Developments and Applications*, pages 83–108. Kluwer Academic Publishers, 1989.

[37] O. Gunduz and M. M. Aral. River Networks and Groundwater Flow: A Simultaneous Solution of a Coupled System. *Journal of Hydrology*, 301(1–4):216–234, 2005.

[38] S. M. Hassanizadeh, M. A. Celia, and H. K. Dahle. Dynamic Effect in the Capillary Pressure–Saturation Relationship and its Impacts on Unsaturated Flow. *Vadose Zone*, 1(1):38–57, 2002.

[39] R. Helmig. *Multiphase Flow and Transport Processes in the Subsurface: A Contribution to the Modeling of Hydrosystems*. Springer, first edition, 1997.

[40] R. Helmig and R. Huber. Comparison of Galerkin-Type Discretization Techniques for Two-Phase Flow in Heterogeneous Porous Media. *Advances in Water Resources*, 21(8):697–711, 1998.

[41] J. Jaffré and A. Sboui. Henry' Law and Gas Phase Disappearance. *Transport in Porous Media*, 82:521–526, 2010.

[42] H. A. Jakobsen. *Chemical Reactor Modeling: Multiphase Reactive Flows*. Springer, 2008.

[43] G. Karypis and V. Kumar. METIS - Unstructured Graph Partitioning and Sparse Matrix Ordering System, Version 2.0. Technical report, 1995.

[44] T. Kempka, M. Kühn, H. Class, P. Frykman, A. Kopp, C. M. Nielsen, and P. Probst. Modelling of CO_2 Arrival Time at Ketzin – Part I. *International Journal of Greenhouse Gas Control*, 4(6):1007–1015, 2010.

[45] J. E. Killough. Ninth Comparative Solution Project: A Reexamination of Black-Oil Simulation. *Society of Petroleum Engineers*, SPE 29110, 1995.

[46] J. E. Killough and C. A. Kossack. Fifth Comparative Solution Project: Evaluation of Miscible Flood Simulators. *Society of Petroleum Engineers*, SPE 16000, 1987.

[47] J. Kool, J. C. Parker, and M. T. van Genuchten. Parameter Estimation for Unsaturated Flow and Transport Models - A Review. *Journal of Hydrology*, 91:255–293, 1987.

[48] A. Lauser, C. Hager, R. Helmig, and B. Wohlmuth. A new Approach for Phase Transitions in Miscible Multi-Phase Flow in Porous Media. *Advances in Water Resources*, 34(8):957–966, 2011.

[49] U. Lengler, M. D. Lucia, and M. Kühn. The Impact of Heterogeneity on the Distribution of CO_2: Numerical Simulation of CO_2 Storage at Ketzin. *International Journal of Greenhouse Gas Control*, 4(6):1016–1025, 2010.

[50] R. J. Lenhard, J. C. Parker, and S. Mishra. On the Correspondence Between Brooks-Corey and van Genuchten Models. *Journal of Irrigation and Drainage Engineering*, 115(4):744–751, 1989.

[51] M. C. Leverett. Capillary Behavior in Porous Solids. Technical report, AIME, 1940.

[52] M. C. Leverett and W. B. Lewis. Steady Flow of Gas-Oil-Water Mixtures Through Unconsolidated Sands. *Transactions of AIME*, 142(107):14, 1941.

[53] X. S. Li. An Overview of SuperLU: Algorithms, Implementation, and User Interface. *ACM Transactions on Mathematical Software*, 31(3):302–325, 2005.

[54] O. Lia, H. Omre, H. Tjelmeland, L. Holden, and T. Egeland. Uncertainties in Reservoir Production Forecasts. *AAPG Bulletin*, 82(5):775–803, 1997.

[55] S. Martens, T. Kempka, A. Liebscher, S. Lüth, F. Möller, A. Myrttinen, B. Norden, C. Schmidt-Hattenberger, M. Zimmer, and M. Kühn. Europe's Longest-Operating On-shore CO_2 Storage Site at Ketzin, Germany: A Progress Report After Three Years of Injection. *Environmental Earth Sciences*, 67(2):323–334, 2012.

[56] G. J. Martyna, D. J. Tobias, and M. L. Klein. Constant Pressure Molecular Dynamics Algorithms. *Journal of Chemical Physics*, 101(5):4177 – 4189, 1994.

[57] K. Mosthaf, K. Baber, B. Flemisch, R. Helmig, T. Leijnse, I. Rybak, and B. Wohlmuth. A Coupling Concept for Two-Phase Compositional Porous-Medium and Single-Phase Compositional Free Flow. *Water Resources Research*, 47(10), 2011.

[58] R. Neumann, P. Bastian, and O. Ippisch. Modeling and Simulation of Two-Phase Two-Component Flow with Disappearing Nonwetting Phase. *Computational Geosciences*, 17:139–149, 2013.

[59] J. Niessner and S. M. Hassanizadeh. A Model for Two-Phase Flow in Porous Media Including Fluid-Fluid Interfacial Area. *Water Resources Research*, 44(8), 2008.

[60] J. Nolen. Numerical Simulation of Compositional Phenomena in Petroleum Reservoirs. *Society of Petroleum Engineers*, SPE 4274, 1973.

[61] S. O. Ochs. *Steam Injection into Saturated Porous Media: Process Analysis Including Experimental and Numerical Investigations*. PhD thesis, University of Stuttgart, 2006.

[62] S. Oladyshkin, H. Class, R. Helmig, and W. Nowak. An Integrative Approach to Robust Design and Probabilistic Risk Assessment for CO_2 Storage in Geological Formations. *Computational Geosciences*, 15:565–577, 2011.

[63] J. M. Ortega and W. C. Rheinboldt. *Iterative Solution of Nonlinear Equations in Several Variables*. Society for Industrial and Applied Mathematics, 2000.

[64] A. M. Otten, A. Alphenaar, C. Pijls, F. Spuij, and H. de Wit. *In Situ Soil Remediation*. Springer, 1997.

[65] J. C. Parker, R. J. Lenhard, and T. Kuppusamy. A Parametric Model for Constitutive Properties Governing Multiphase Flow in Porous Media. *Water Resources Research*, 23(4):618–624, 1987.

[66] F. Pellegrini and J. Roman. Scotch: A Software Package for Static Mapping by Dual Recursive Bipartitioning of Process and Architecture Graphs. In *High-Performance Computing and Networking*, volume 1067 of *Lecture Notes in Computer Science*, pages 493–498. Springer, 1996.

[67] M. Quintard and S. Whitaker. Transport in Ordered and Disordered Porous Media II: Generalized Volume Averaging. *Transport in Porous Media*, 14:179–206, 1994.

[68] R. C. Reid, J. M. Prausnitz, and B. E. Poling. *The Properties of Gases and Liquids*. McGraw-Hill, fourth edition, 1987.

[69] E. Rubin and H. de Coninck. *IPCC Special Report on Carbon Dioxide Capture and Storage*. Cambridge University Press, 2005.

[70] Y. Saad. *Iterative Methods for Sparse Linear Systems*. PWS Publishing, first edition, 1996.

[71] O. Schenk and K. Gärtner. Solving Unsymmetric Sparse Systems of Linear Equations with PARDISO. *Future Generation Computer Systems*, 20(3):475–487, 2004.

[72] A. A. Shabana. *Computational Continuum Mechanics*. Cambridge University Press, second edition, 2012.

[73] H. Y. She and B. E. Sleep. The Effect of Temperature on Capillary Pressure-Saturation Relationships for Air-Water and Perchloroethylene-Water Systems. *Water Resources Research*, 34(10):2587–2597, 1998.

[74] D. M. Wheeler's SLOCCount Website: `http://www.dwheeler.com/sloccount`.

[75] B. Smith, P. Bjørstad, and W. Gropp. *Domain Decomposition: Parallel Multilevel Methods for Elliptic Partial Differential Equations*. Cambridge University Press, 2004.

[76] W. H. Somerton, A. H. El-Shaarani, and S. M. Mobarak. *High Temperature Behavior of Rocks Associated with Geothermal Type Reservoirs*, volume SPE 4897. Society of Petroleum Engineers, 1974.

[77] R. Span and W. Wagner. A New Equation of State for Carbon Dioxide Covering the Fluid Region from the Triple-Point Temperature to 1100 K at Pressures up to 800 MPa. *Journal of Chemical and Physical Reference Data*, 25(6):1509–1596, 1996.

[78] N. Spycher and K. Pruess. CO_2-H_2O Mixtures in the Geological Sequestration of CO_2. II. Partitioning in Chloride Brines at 12–100°C and Up to 600 bar. *Geochimica et Cosmochimica Acta*, 69(13):3309 – 3320, 2005.

[79] H. L. Stone. Probability Model for Estimating Three-Phase Relative Permeability. *Journal of Petroleum Technology*, 22(2):214–218, 1970.

[80] H. L. Stone. Estimation of Three-Phase Relative Permeability and Residual Oil Data. *Journal of Petroleum Technology*, 12(4), 1973.

[81] W. G. Strang and G. J. Fix. *An Analysis of the Finite Element Method*. Prentice-Hall, 1973.

[82] K. Stüben. *Algebraic Multigrid (AMG). An Introduction with Applications*. GMD Forschungszentrum Informationstechnik, 1999.

[83] J. A. Trangenstein and J. B. Bell. Mathematical Structure of the Black-Oil Model for Petroleum Reservoir Simulation. *SIAM Journal on Applied Mathematics*, 49(3), 1989.

[84] K. S. Udell. Heat Transfer in Porous Media Considering Phase Change and Capillarity – The Heat-Pipe Effect. *International Journal of Heat and Mass Transfer*, 28(2):485–495, 1985.

[85] The UG Website: `http://atlas.gcsc.uni-frankfurt.de/~ug/`.

[86] H. A. van der Vorst. BI-CGSTAB: A Fast and Smoothly Converging Variant of BI-CG for the Solution of Non-symmetric Linear Systems. *SIAM Journal on Scientific and Statistical Computing*, 13(2):631–644, 1992.

[87] M. T. van Genuchten. A Closed-Form Equation for Predicting the Hydraulic Conductivity of Unsaturated Soils. *Journal of the Soil Science Society of America*, 44(5):892–898, 1980.

[88] W. Wagner and A. Pruß. The IAPWS Formulation 1995 for the Thermodynamic Properties of Ordinary Water Substance for General and Scientific Use. *Journal of Chemical and Physical Reference Data*, 31(2):387–535, 2002.

[89] S. Whitaker. Flow in Porous Media I: A Theoretical Derivation of Darcy's Law. *Transport in Porous Media*, 1(1):3–25, 1985.

[90] Wikipedia Article on Carbon Capture and Storage: `http://en.wikipedia.org/wiki/Carbon_capture_and_storage`. Article Date: January 18, 2013.

[91] Wikipedia Article on Petroleum Reservoirs: `http://en.wikipedia.org/wiki/Petroleum_reservoir`. Article Date: March 23, 2013.

[92] Y. Zhou, H. A. Tchelepi, and B. T. Mallison. Automatic Differentiation Framework for Compositional Simulation on Unstructured Grids with Multi-Point Discretization Schemes. *Society of Petroleum Engineers*, SPE 141592, 2011.

Institut für Wasser- und
Umweltsystemmodellierung
Universität Stuttgart

Pfaffenwaldring 61
70569 Stuttgart (Vaihingen)
Telefon (0711) 685 - 64717/64749/64752/64679
Telefax (0711) 685 - 67020 o. 64746 o. 64681
E-Mail: iws@iws.uni-stuttgart.de
http://www.iws.uni-stuttgart.de

Direktoren
Prof. Dr. rer. nat. Dr.-Ing. András Bárdossy
Prof. Dr.-Ing. Rainer Helmig
Prof. Dr.-Ing. Silke Wieprecht

Vorstand *(Stand 19.08.2013)*
Prof. Dr. rer. nat. Dr.-Ing. A. Bárdossy
Prof. Dr.-Ing. R. Helmig
Prof. Dr.-Ing. S. Wieprecht
Prof. Dr. J.A. Sander Huisman
Jürgen Braun, PhD
apl. Prof. Dr.-Ing. H. Class
Dr.-Ing. H.-P. Koschitzky
Dr.-Ing. M. Noack
Jun.-Prof. Dr.-Ing. W. Nowak, M.Sc.
Dr. rer. nat. J. Seidel
Dr.-Ing. K. Terheiden

Emeriti
Prof. Dr.-Ing. habil. Dr.-Ing. E.h. Jürgen Giesecke
Prof. Dr.h.c. Dr.-Ing. E.h. Helmut Kobus, PhD

Lehrstuhl für Wasserbau und Wassermengenwirtschaft
Leiter: Prof. Dr.-Ing. Silke Wieprecht
Stellv.: Dr.-Ing. Kristina Terheiden
Versuchsanstalt für Wasserbau
Leiter: Dr.-Ing. Markus Noack

Lehrstuhl für Hydromechanik und Hydrosystemmodellierung
Leiter: Prof. Dr.-Ing. Rainer Helmig
Stellv.: apl. Prof. Dr.-Ing. Holger Class
Jungwissenschaftlergruppe: Stochastische Modellierung von Hydrosystemen
Leiter: Jun.-Prof. Dr.-Ing. Wolfgang Nowak, M.Sc.

Lehrstuhl für Hydrologie und Geohydrologie
Leiter: Prof. Dr. rer. nat. Dr.-Ing. András Bárdossy
Stellv.: Dr. rer. nat. Jochen Seidel
Hydrogeophysik der Vadosen Zone
(mit Forschungszentrum Jülich)
Leiter: Prof. Dr. J.A. Sander Huisman

***VEGAS*, Versuchseinrichtung zur Grundwasser- und Altlastensanierung**
Leitung: Jürgen Braun, PhD, AD
Dr.-Ing. Hans-Peter Koschitzky, AD

Verzeichnis der Mitteilungshefte

1 Röhnisch, Arthur: *Die Bemühungen um eine Wasserbauliche Versuchsanstalt an der Technischen Hochschule Stuttgart*, und
Fattah Abouleid, Abdel: *Beitrag zur Berechnung einer in lockeren Sand gerammten, zweifach verankerten Spundwand*, 1963

2 Marotz, Günter: *Beitrag zur Frage der Standfestigkeit von dichten Asphaltbelägen im Großwasserbau*, 1964

3 Gurr, Siegfried: *Beitrag zur Berechnung zusammengesetzter ebener Flächentragwerke unter besonderer Berücksichtigung ebener Stauwände, mit Hilfe von Randwert- und Lastwertmatrizen*, 1965

4 Plica, Peter: *Ein Beitrag zur Anwendung von Schalenkonstruktionen im Stahlwasserbau*, und Petrikat, Kurt: *Möglichkeiten und Grenzen des wasserbaulichen Versuchswesens*, 1966

5 Plate, Erich: *Beitrag zur Bestimmung der Windgeschwindigkeitsverteilung in der durch eine Wand gestörten bodennahen Luftschicht*,
und
Röhnisch, Arthur; Marotz, Günter: *Neue Baustoffe und Bauausführungen für den Schutz der Böschungen und der Sohle von Kanälen, Flüssen und Häfen; Gestehungskosten und jeweilige Vorteile*, sowie Unny, T.E.: *Schwingungsuntersuchungen am Kegelstrahlschieber*, 1967

6 Seiler, Erich: *Die Ermittlung des Anlagenwertes der bundeseigenen Binnenschiffahrtsstraßen und Talsperren und des Anteils der Binnenschiffahrt an diesem Wert*, 1967

7 *Sonderheft anläßlich des 65. Geburtstages von Prof. Arthur Röhnisch mit Beiträgen von* Benk, Dieter; Breitling, J.; Gurr, Siegfried; Haberhauer, Robert; Honekamp, Hermann; Kuz, Klaus Dieter; Marotz, Günter; Mayer-Vorfelder, Hans-Jörg; Miller, Rudolf; Plate, Erich J.; Radomski, Helge; Schwarz, Helmut; Vollmer, Ernst; Wildenhahn, Eberhard; 1967

8 Jumikis, Alfred: *Beitrag zur experimentellen Untersuchung des Wassernachschubs in einem gefrierenden Boden und die Beurteilung der Ergebnisse*, 1968

9 Marotz, Günter: *Technische Grundlagen einer Wasserspeicherung im natürlichen Untergrund*, 1968

10 Radomski, Helge: *Untersuchungen über den Einfluß der Querschnittsform wellenförmiger Spundwände auf die statischen und rammtechnischen Eigenschaften*, 1968

11 Schwarz, Helmut: *Die Grenztragfähigkeit des Baugrundes bei Einwirkung vertikal gezogener Ankerplatten als zweidimensionales Bruchproblem*, 1969

12 Erbel, Klaus: *Ein Beitrag zur Untersuchung der Metamorphose von Mittelgebirgsschneedecken unter besonderer Berücksichtigung eines Verfahrens zur Bestimmung der thermischen Schneequalität*, 1969

13 Westhaus, Karl-Heinz: *Der Strukturwandel in der Binnenschiffahrt und sein Einfluß auf den Ausbau der Binnenschiffskanäle*, 1969

14 Mayer-Vorfelder, Hans-Jörg: *Ein Beitrag zur Berechnung des Erdwiderstandes unter Ansatz der logarithmischen Spirale als Gleitflächenfunktion*, 1970

15 Schulz, Manfred: *Berechnung des räumlichen Erddruckes auf die Wandung kreiszylindrischer Körper*, 1970

16 Mobasseri, Manoutschehr: *Die Rippenstützmauer. Konstruktion und Grenzen ihrer Standsicherheit*, 1970

17 Benk, Dieter: *Ein Beitrag zum Betrieb und zur Bemessung von Hochwasserrückhaltebecken*, 1970

18 Gàl, Attila: *Bestimmung der mitschwingenden Wassermasse bei überströmten Fischbauchklappen mit kreiszylindrischem Staublech*, 1971, vergriffen

19 Kuz, Klaus Dieter: *Ein Beitrag zur Frage des Einsetzens von Kavitationserscheinungen in einer Düsenströmung bei Berücksichtigung der im Wasser gelösten Gase*, 1971, vergriffen

20 Schaak, Hartmut: *Verteilleitungen von Wasserkraftanlagen*, 1971

21 *Sonderheft zur Eröffnung der neuen Versuchsanstalt des Instituts für Wasserbau der Universität Stuttgart mit Beiträgen von* Brombach, Hansjörg; Dirksen, Wolfram; Gàl, Attila; Gerlach, Reinhard; Giesecke, Jürgen; Holthoff, Franz-Josef; Kuz, Klaus Dieter; Marotz, Günter; Minor, Hans-Erwin; Petrikat, Kurt; Röhnisch, Arthur; Rueff, Helge; Schwarz, Helmut; Vollmer, Ernst; Wildenhahn, Eberhard; 1972

22 Wang, Chung-su: *Ein Beitrag zur Berechnung der Schwingungen an Kegelstrahlschiebern*, 1972

23 Mayer-Vorfelder, Hans-Jörg: *Erdwiderstandsbeiwerte nach dem Ohde-Variationsverfahren*, 1972

24 Minor, Hans-Erwin: *Beitrag zur Bestimmung der Schwingungsanfachungsfunktionen überströmter Stauklappen*, 1972, vergriffen

25 Brombach, Hansjörg: *Untersuchung strömungsmechanischer Elemente (Fluidik) und die Möglichkeit der Anwendung von Wirbelkammerelementen im Wasserbau*, 1972, vergriffen

26 Wildenhahn, Eberhard: *Beitrag zur Berechnung von Horizontalfilterbrunnen*, 1972

27 Steinlein, Helmut: *Die Eliminierung der Schwebstoffe aus Flußwasser zum Zweck der unterirdischen Wasserspeicherung, gezeigt am Beispiel der Iller*, 1972

28 Holthoff, Franz Josef: *Die Überwindung großer Hubhöhen in der Binnenschiffahrt durch Schwimmerhebewerke*, 1973

29 Röder, Karl: *Einwirkungen aus Baugrundbewegungen auf trog- und kastenförmige Konstruktionen des Wasser- und Tunnelbaues*, 1973

30 Kretschmer, Heinz: *Die Bemessung von Bogenstaumauern in Abhängigkeit von der Talform*, 1973

31 Honekamp, Hermann: *Beitrag zur Berechnung der Montage von Unterwasserpipelines*, 1973

32 Giesecke, Jürgen: *Die Wirbelkammertriode als neuartiges Steuerorgan im Wasserbau*, und Brombach, Hansjörg: *Entwicklung, Bauformen, Wirkungsweise und Steuereigenschaften von Wirbelkammerverstärkern*, 1974

33 Rueff, Helge: *Untersuchung der schwingungserregenden Kräfte an zwei hintereinander angeordneten Tiefschützen unter besonderer Berücksichtigung von Kavitation*, 1974

34 Röhnisch, Arthur: *Einpreßversuche mit Zementmörtel für Spannbeton - Vergleich der Ergebnisse von Modellversuchen mit Ausführungen in Hüllwellrohren*, 1975

35 *Sonderheft anläßlich des 65. Geburtstages von Prof. Dr.-Ing. Kurt Petrikat mit Beiträgen von*: Brombach, Hansjörg; Erbel, Klaus; Flinspach, Dieter; Fischer jr., Richard; Gàl, Attila; Gerlach, Reinhard; Giesecke, Jürgen; Haberhauer, Robert; Hafner Edzard; Hausenblas, Bernhard; Horlacher, Hans-Burkhard; Hutarew, Andreas; Knoll, Manfred; Krummet, Ralph; Marotz, Günter; Merkle, Theodor; Miller, Christoph; Minor, Hans-Erwin; Neumayer, Hans; Rao, Syamala; Rath, Paul; Rueff, Helge; Ruppert, Jürgen; Schwarz, Wolfgang; Topal-Gökceli, Mehmet; Vollmer, Ernst; Wang, Chung-su; Weber, Hans-Georg; 1975

36 Berger, Jochum: *Beitrag zur Berechnung des Spannungszustandes in rotationssymmetrisch belasteten Kugelschalen veränderlicher Wandstärke unter Gas- und Flüssigkeitsdruck durch Integration schwach singulärer Differentialgleichungen*, 1975

37 Dirksen, Wolfram: *Berechnung instationärer Abflußvorgänge in gestauten Gerinnen mittels Differenzenverfahren und die Anwendung auf Hochwasserrückhaltebecken*, 1976

38 Horlacher, Hans-Burkhard: *Berechnung instationärer Temperatur- und Wärmespannungsfelder in langen mehrschichtigen Hohlzylindern*, 1976

39 Hafner, Edzard: *Untersuchung der hydrodynamischen Kräfte auf Baukörper im Tiefwasserbereich des Meeres*, 1977, ISBN 3-921694-39-6

40 Ruppert, Jürgen: *Über den Axialwirbelkammerverstärker für den Einsatz im Wasserbau*, 1977, ISBN 3-921694-40-X

41 Hutarew, Andreas: *Beitrag zur Beeinflußbarkeit des Sauerstoffgehalts in Fließgewässern an Abstürzen und Wehren*, 1977, ISBN 3-921694-41-8, vergriffen

42 Miller, Christoph: *Ein Beitrag zur Bestimmung der schwingungserregenden Kräfte an unterströmten Wehren*, 1977, ISBN 3-921694-42-6

43 Schwarz, Wolfgang: *Druckstoßberechnung unter Berücksichtigung der Radial- und Längsverschiebungen der Rohrwandung*, 1978, ISBN 3-921694-43-4

44 Kinzelbach, Wolfgang: *Numerische Untersuchungen über den optimalen Einsatz variabler Kühlsysteme einer Kraftwerkskette am Beispiel Oberrhein*, 1978, ISBN 3-921694-44-2

45 Barczewski, Baldur: *Neue Meßmethoden für Wasser-Luftgemische und deren Anwendung auf zweiphasige Auftriebsstrahlen*, 1979, ISBN 3-921694-45-0

46 Neumayer, Hans: *Untersuchung der Strömungsvorgänge in radialen Wirbelkammerverstärkern*, 1979, ISBN 3-921694-46-9

47 Elalfy, Youssef-Elhassan: *Untersuchung der Strömungsvorgänge in Wirbelkammerdioden und -drosseln*, 1979, ISBN 3-921694-47-7

48 Brombach, Hansjörg: *Automatisierung der Bewirtschaftung von Wasserspeichern*, 1981, ISBN 3-921694-48-5

49 Geldner, Peter: *Deterministische und stochastische Methoden zur Bestimmung der Selbstdichtung von Gewässern*, 1981, ISBN 3-921694-49-3, vergriffen

50 Mehlhorn, Hans: *Temperaturveränderungen im Grundwasser durch Brauchwassereinleitungen*, 1982, ISBN 3-921694-50-7, vergriffen

51 Hafner, Edzard: *Rohrleitungen und Behälter im Meer*, 1983, ISBN 3-921694-51-5

52 Rinnert, Bernd: *Hydrodynamische Dispersion in porösen Medien: Einfluß von Dichteunterschieden auf die Vertikalvermischung in horizontaler Strömung*, 1983, ISBN 3-921694-52-3, vergriffen

53 Lindner, Wulf: *Steuerung von Grundwasserentnahmen unter Einhaltung ökologischer Kriterien*, 1983, ISBN 3-921694-53-1, vergriffen

54 Herr, Michael; Herzer, Jörg; Kinzelbach, Wolfgang; Kobus, Helmut; Rinnert, Bernd: *Methoden zur rechnerischen Erfassung und hydraulischen Sanierung von Grundwasserkontaminationen*, 1983, ISBN 3-921694-54-X

55 Schmitt, Paul: *Wege zur Automatisierung der Niederschlagsermittlung*, 1984, ISBN 3-921694-55-8, vergriffen

56 Müller, Peter: *Transport und selektive Sedimentation von Schwebstoffen bei gestautem Abfluß*, 1985, ISBN 3-921694-56-6

57 El-Qawasmeh, Fuad: *Möglichkeiten und Grenzen der Tropfbewässerung unter besonderer Berücksichtigung der Verstopfungsanfälligkeit der Tropfelemente*, 1985, ISBN 3-921694-57-4, vergriffen

58 Kirchenbaur, Klaus: *Mikroprozessorgesteuerte Erfassung instationärer Druckfelder am Beispiel seegangsbelasteter Baukörper*, 1985, ISBN 3-921694-58-2

59 Kobus, Helmut (Hrsg.): *Modellierung des großräumigen Wärme- und Schadstofftransports im Grundwasser*, Tätigkeitsbericht 1984/85 (DFG-Forschergruppe an den Universitäten Hohenheim, Karlsruhe und Stuttgart), 1985, ISBN 3-921694-59-0, vergriffen

60 Spitz, Karlheinz: *Dispersion in porösen Medien: Einfluß von Inhomogenitäten und Dichteunterschieden*, 1985, ISBN 3-921694-60-4, vergriffen

61 Kobus, Helmut: *An Introduction to Air-Water Flows in Hydraulics*, 1985, ISBN 3-921694-61-2

62 Kaleris, Vassilios: *Erfassung des Austausches von Oberflächen- und Grundwasser in horizontalebenen Grundwassermodellen*, 1986, ISBN 3-921694-62-0

63 Herr, Michael: *Grundlagen der hydraulischen Sanierung verunreinigter Porengrundwasserleiter*, 1987, ISBN 3-921694-63-9

64 Marx, Walter: *Berechnung von Temperatur und Spannung in Massenbeton infolge Hydratation*, 1987, ISBN 3-921694-64-7

65 Koschitzky, Hans-Peter: *Dimensionierungskonzept für Sohlbelüfter in Schußrinnen zur Vermeidung von Kavitationsschäden*, 1987, ISBN 3-921694-65-5

66 Kobus, Helmut (Hrsg.): *Modellierung des großräumigen Wärme- und Schadstofftransports im Grundwasser*, Tätigkeitsbericht 1986/87 (DFG-Forschergruppe an den Universitäten Hohenheim, Karlsruhe und Stuttgart) 1987, ISBN 3-921694-66-3

67 Söll, Thomas: *Berechnungsverfahren zur Abschätzung anthropogener Temperaturanomalien im Grundwasser*, 1988, ISBN 3-921694-67-1

68 Dittrich, Andreas; Westrich, Bernd: *Bodenseeufererosion, Bestandsaufnahme und Bewertung*, 1988, ISBN 3-921694-68-X, vergriffen

69 Huwe, Bernd; van der Ploeg, Rienk R.: *Modelle zur Simulation des Stickstoffhaushaltes von Standorten mit unterschiedlicher landwirtschaftlicher Nutzung*, 1988, ISBN 3-921694-69-8, vergriffen

70 Stephan, Karl: *Integration elliptischer Funktionen*, 1988, ISBN 3-921694-70-1

71 Kobus, Helmut; Zilliox, Lothaire (Hrsg.): *Nitratbelastung des Grundwassers, Auswirkungen der Landwirtschaft auf die Grundwasser- und Rohwasserbeschaffenheit und Maßnahmen zum Schutz des Grundwassers*. Vorträge des deutsch-französischen Kolloquiums am 6. Oktober 1988, Universitäten Stuttgart und Louis Pasteur Strasbourg (Vorträge in deutsch oder französisch, Kurzfassungen zweisprachig), 1988, ISBN 3-921694-71-X

72 Soyeaux, Renald: *Unterströmung von Stauanlagen auf klüftigem Untergrund unter Berücksichtigung laminarer und turbulenter Fließzustände*,1991, ISBN 3-921694-72-8

73 Kohane, Roberto: *Berechnungsmethoden für Hochwasserabfluß in Fließgewässern mit überströmten Vorländern*, 1991, ISBN 3-921694-73-6

74 Hassinger, Reinhard: *Beitrag zur Hydraulik und Bemessung von Blocksteinrampen in flexibler Bauweise*, 1991, ISBN 3-921694-74-4, vergriffen

75 Schäfer, Gerhard: *Einfluß von Schichtenstrukturen und lokalen Einlagerungen auf die Längsdispersion in Porengrundwasserleitern*, 1991, ISBN 3-921694-75-2

76 Giesecke, Jürgen: *Vorträge, Wasserwirtschaft in stark besiedelten Regionen; Umweltforschung mit Schwerpunkt Wasserwirtschaft*, 1991, ISBN 3-921694-76-0

77 Huwe, Bernd: *Deterministische und stochastische Ansätze zur Modellierung des Stickstoffhaushalts landwirtschaftlich genutzter Flächen auf unterschiedlichem Skalenniveau*, 1992, ISBN 3-921694-77-9, vergriffen

78 Rommel, Michael: *Verwendung von Kluftdaten zur realitätsnahen Generierung von Kluftnetzen mit anschließender laminar-turbulenter Strömungsberechnung*, 1993, ISBN 3-92 1694-78-7

79 Marschall, Paul: *Die Ermittlung lokaler Stofffrachten im Grundwasser mit Hilfe von Einbohrloch-Meßverfahren*, 1993, ISBN 3-921694-79-5, vergriffen

80 Ptak, Thomas: *Stofftransport in heterogenen Porenaquiferen: Felduntersuchungen und stochastische Modellierung*, 1993, ISBN 3-921694-80-9, vergriffen

81 Haakh, Frieder: *Transientes Strömungsverhalten in Wirbelkammern,* 1993, ISBN 3-921694-81-7

82 Kobus, Helmut; Cirpka, Olaf; Barczewski, Baldur; Koschitzky, Hans-Peter: *Versucheinrichtung zur Grundwasser und Altlastensanierung VEGAS, Konzeption und Programmrahmen*, 1993, ISBN 3-921694-82-5

83 Zang, Weidong: *Optimaler Echtzeit-Betrieb eines Speichers mit aktueller Abflußregenerierung*, 1994, ISBN 3-921694-83-3, vergriffen

84 Franke, Hans-Jörg: *Stochastische Modellierung eines flächenhaften Stoffeintrages und Transports in Grundwasser am Beispiel der Pflanzenschutzmittelproblematik*, 1995, ISBN 3-921694-84-1

85 Lang, Ulrich: *Simulation regionaler Strömungs- und Transportvorgänge in Karstaquiferen mit Hilfe des Doppelkontinuum-Ansatzes: Methodenentwicklung und Parameteridentifikation*, 1995, ISBN 3-921694-85-X, vergriffen

86 Helmig, Rainer: *Einführung in die Numerischen Methoden der Hydromechanik*, 1996, ISBN 3-921694-86-8, vergriffen

87 Cirpka, Olaf: *CONTRACT: A Numerical Tool for Contaminant Transport and Chemical Transformations - Theory and Program Documentation* -, 1996, ISBN 3-921694-87-6

88 Haberlandt, Uwe: *Stochastische Synthese und Regionalisierung des Niederschlages für Schmutzfrachtberechnungen*, 1996, ISBN 3-921694-88-4

89 Croisé, Jean: *Extraktion von flüchtigen Chemikalien aus natürlichen Lockergesteinen mittels erzwungener Luftströmung*, 1996, ISBN 3-921694-89-2, vergriffen

90 Jorde, Klaus: *Ökologisch begründete, dynamische Mindestwasserregelungen bei Ausleitungskraftwerken*, 1997, ISBN 3-921694-90-6, vergriffen

91 Helmig, Rainer: *Gekoppelte Strömungs- und Transportprozesse im Untergrund - Ein Beitrag zur Hydrosystemmodellierung-*, 1998, ISBN 3-921694-91-4, vergriffen

92 Emmert, Martin: *Numerische Modellierung nichtisothermer Gas-Wasser Systeme in porösen Medien,* 1997, ISBN 3-921694-92-2

93 Kern, Ulrich: *Transport von Schweb- und Schadstoffen in staugeregelten Fließgewässern am Beispiel des Neckars*, 1997, ISBN 3-921694-93-0, vergriffen

94 Förster, Georg: *Druckstoßdämpfung durch große Luftblasen in Hochpunkten von Rohrleitungen 1997*, ISBN 3-921694-94-9

95 Cirpka, Olaf: *Numerische Methoden zur Simulation des reaktiven Mehrkomponententransports im Grundwasser*, 1997, ISBN 3-921694-95-7, vergriffen

96 Färber, Arne: *Wärmetransport in der ungesättigten Bodenzone: Entwicklung einer thermischen In-situ-Sanierungstechnologie*, 1997, ISBN 3-921694-96-5

97 Betz, Christoph: *Wasserdampfdestillation von Schadstoffen im porösen Medium: Entwicklung einer thermischen In-situ-Sanierungstechnologie*, 1998, ISBN 3-921694-97-3

98 Xu, Yichun: *Numerical Modeling of Suspended Sediment Transport in Rivers*, 1998, ISBN 3-921694-98-1, vergriffen

99 Wüst, Wolfgang: *Geochemische Untersuchungen zur Sanierung CKW-kontaminierter Aquifere mit Fe(0)-Reaktionswänden,* 2000, ISBN 3-933761-02-2

100 Sheta, Hussam: *Simulation von Mehrphasenvorgängen in porösen Medien unter Einbeziehung von Hysterese-Effekten*, 2000, ISBN 3-933761-03-4

101 Ayros, Edwin: *Regionalisierung extremer Abflüsse auf der Grundlage statistischer Verfahren*, 2000, ISBN 3-933761-04-2, vergriffen

102 Huber, Ralf: *Compositional Multiphase Flow and Transport in Heterogeneous Porous Media*, 2000, ISBN 3-933761-05-0

103 Braun, Christopherus: *Ein Upscaling-Verfahren für Mehrphasenströmungen in porösen Medien*, 2000, ISBN 3-933761-06-9

104 Hofmann, Bernd: *Entwicklung eines rechnergestützten Managementsystems zur Beurteilung von Grundwasserschadensfällen*, 2000, ISBN 3-933761-07-7

105 Class, Holger: *Theorie und numerische Modellierung nichtisothermer Mehrphasenprozesse in NAPL-kontaminierten porösen Medien,* 2001, ISBN 3-933761-08-5

106 Schmidt, Reinhard: *Wasserdampf- und Heißluftinjektion zur thermischen Sanierung kontaminierter Standorte*, 2001, ISBN 3-933761-09-3

107 Josef, Reinhold:, *Schadstoffextraktion mit hydraulischen Sanierungsverfahren unter Anwendung von grenzflächenaktiven Stoffen*, 2001, ISBN 3-933761-10-7

108 Schneider, Matthias: *Habitat- und Abflussmodellierung für Fließgewässer mit unscharfen Berechnungsansätzen*, 2001, ISBN 3-933761-11-5

109 Rathgeb, Andreas: *Hydrodynamische Bemessungsgrundlagen für Lockerdeckwerke an überströmbaren Erddämmen*, 2001, ISBN 3-933761-12-3

110 Lang, Stefan: *Parallele numerische Simulation instätionärer Probleme mit adaptiven Methoden auf unstrukturierten Gittern*, 2001, ISBN 3-933761-13-1

111 Appt, Jochen; Stumpp Simone: *Die Bodensee-Messkampagne 2001, IWS/CWR Lake Constance Measurement Program 2001*, 2002, ISBN 3-933761-14-X

112 Heimerl, Stephan: *Systematische Beurteilung von Wasserkraftprojekten,* 2002, ISBN 3-933761-15-8, vergriffen

113 Iqbal, Amin: *On the Management and Salinity Control of Drip Irrigation,* 2002, ISBN 3-933761-16-6

114 Silberhorn-Hemminger, Annette: *Modellierung von Kluftaquifersystemen: Geostatistische Analyse und deterministisch-stochastische Kluftgenerierung,* 2002, ISBN 3-933761-17-4

115 Winkler, Angela: *Prozesse des Wärme- und Stofftransports bei der In-situ-Sanierung mit festen Wärmequellen,* 2003, ISBN 3-933761-18-2

116 Marx, Walter: *Wasserkraft, Bewässerung, Umwelt - Planungs- und Bewertungsschwerpunkte der Wasserbewirtschaftung,* 2003, ISBN 3-933761-19-0

117 Hinkelmann, Reinhard: *Efficient Numerical Methods and Information-Processing Techniques in Environment Water,* 2003, ISBN 3-933761-20-4

118 Samaniego-Eguiguren, Luis Eduardo: *Hydrological Consequences of Land Use / Land Cover and Climatic Changes in Mesoscale Catchments*, 2003, ISBN 3-933761-21-2

119 Neunhäuserer, Lina: *Diskretisierungsansätze zur Modellierung von Strömungs- und Transportprozessen in geklüftet-porösen Medien*, 2003, ISBN 3-933761-22-0

120 Paul, Maren: *Simulation of Two-Phase Flow in Heterogeneous Poros Media with Adaptive Methods*, 2003, ISBN 3-933761-23-9

121 Ehret, Uwe: *Rainfall and Flood Nowcasting in Small Catchments using Weather Radar*, 2003, ISBN 3-933761-24-7

122 Haag, Ingo: *Der Sauerstoffhaushalt staugeregelter Flüsse am Beispiel des Neckars - Analysen, Experimente, Simulationen -,* 2003, ISBN 3-933761-25-5

123 Appt, Jochen: *Analysis of Basin-Scale Internal Waves in Upper Lake Constance,* 2003, ISBN 3-933761-26-3

124 Hrsg.: Schrenk, Volker; Batereau, Katrin; Barczewski, Baldur; Weber, Karolin und Koschitzky, Hans-Peter: *Symposium Ressource Fläche und VEGAS - Statuskolloquium 2003, 30. September und 1. Oktober 2003,* 2003, ISBN 3-933761-27-1

125 Omar Khalil Ouda: *Optimisation of Agricultural Water Use: A Decision Support System for the Gaza Strip,* 2003, ISBN 3-933761-28-0

126 Batereau, Katrin: *Sensorbasierte Bodenluftmessung zur Vor-Ort-Erkundung von Schadensherden im Untergrund*, 2004, ISBN 3-933761-29-8

127 Witt, Oliver: *Erosionsstabilität von Gewässersedimenten mit Auswirkung auf den Stofftransport bei Hochwasser am Beispiel ausgewählter Stauhaltungen des Oberrheins*, 2004, ISBN 3-933761-30-1

128 Jakobs, Hartmut: *Simulation nicht-isothermer Gas-Wasser-Prozesse in komplexen Kluft-Matrix-Systemen*, 2004, ISBN 3-933761-31-X

129 Li, Chen-Chien: *Deterministisch-stochastisches Berechnungskonzept zur Beurteilung der Auswirkungen erosiver Hochwasserereignisse in Flussstauhaltungen,* 2004, ISBN 3-933761-32-8

130 Reichenberger, Volker; Helmig, Rainer; Jakobs, Hartmut; Bastian, Peter; Niessner, Jennifer: *Complex Gas-Water Processes in Discrete Fracture-Matrix Systems: Upscaling, Mass-Conservative Discretization and Efficient Multilevel Solution,* 2004, ISBN 3-933761-33-6

131 Hrsg.: Barczewski, Baldur; Koschitzky, Hans-Peter; Weber, Karolin; Wege, Ralf: *VEGAS - Statuskolloquium 2004,* Tagungsband zur Veranstaltung am 05. Oktober 2004 an der Universität Stuttgart, Campus Stuttgart-Vaihingen, 2004, ISBN 3-933761-34-4

132 Asie, Kemal Jabir: *Finite Volume Models for Multiphase Multicomponent Flow through Porous Media*. 2005, ISBN 3-933761-35-2

133 Jacoub, George: *Development of a 2-D Numerical Module for Particulate Contaminant Transport in Flood Retention Reservoirs and Impounded Rivers,* 2004, ISBN 3-933761-36-0

134 Nowak, Wolfgang: *Geostatistical Methods for the Identification of Flow and Transport Parameters in the Subsurface,* 2005, ISBN 3-933761-37-9

135 Süß, Mia: *Analysis of the influence of structures and boundaries on flow and transport processes in fractured porous media*, 2005, ISBN 3-933761-38-7

136 Jose, Surabhin Chackiath: *Experimental Investigations on Longitudinal Dispersive Mixing in Heterogeneous Aquifers,* 2005, ISBN: 3-933761-39-5

137 Filiz, Fulya: *Linking Large-Scale Meteorological Conditions to Floods in Mesoscale Catchments,* 2005, ISBN 3-933761-40-9

138 Qin, Minghao: *Wirklichkeitsnahe und recheneffiziente Ermittlung von Temperatur und Spannungen bei großen RCC-Staumauern*, 2005, ISBN 3-933761-41-7

139 Kobayashi, Kenichiro: *Optimization Methods for Multiphase Systems in the Subsurface - Application to Methane Migration in Coal Mining Areas*, 2005, ISBN 3-933761-42-5

140 Rahman, Md. Arifur: *Experimental Investigations on Transverse Dispersive Mixing in Heterogeneous Porous Media,* 2005, ISBN 3-933761-43-3

141 Schrenk, Volker: *Ökobilanzen zur Bewertung von Altlastensanierungsmaßnahmen,* 2005, ISBN 3-933761-44-1

142 Hundecha, Hirpa Yeshewatesfa: *Regionalization of Parameters of a Conceptual Rainfall-Runoff Model*, 2005, ISBN: 3-933761-45-X

143 Wege, Ralf: *Untersuchungs- und Überwachungsmethoden für die Beurteilung natürlicher Selbstreinigungsprozesse im Grundwasser,* 2005, ISBN 3-933761-46-8

144 Breiting, Thomas: *Techniken und Methoden der Hydroinformatik - Modellierung von komplexen Hydrosystemen im Untergrund*, 2006, 3-933761-47-6

145 Hrsg.: Braun, Jürgen; Koschitzky, Hans-Peter; Müller, Martin: *Ressource Untergrund: 10 Jahre VEGAS: Forschung und Technologieentwicklung zum Schutz von Grundwasser und Boden,* Tagungsband zur Veranstaltung am 28. und 29. September 2005 an der Universität Stuttgart, Campus Stuttgart-Vaihingen, 2005, ISBN 3-933761-48-4

146 Rojanschi, Vlad: *Abflusskonzentration in mesoskaligen Einzugsgebieten unter Berücksichtigung des Sickerraumes,* 2006, ISBN 3-933761-49-2

147 Winkler, Nina Simone: *Optimierung der Steuerung von Hochwasserrückhaltebecken-systemen,* 2006, ISBN 3-933761-50-6

148 Wolf, Jens: *Räumlich differenzierte Modellierung der Grundwasserströmung alluvialer Aquifere für mesoskalige Einzugsgebiete*, 2006, ISBN: 3-933761-51-4

149 Kohler, Beate: *Externe Effekte der Laufwasserkraftnutzung*, 2006, ISBN 3-933761-52-2

150 Hrsg.: Braun, Jürgen; Koschitzky, Hans-Peter; Stuhrmann, Matthias: *VEGAS-Statuskolloquium 2006,* Tagungsband zur Veranstaltung am 28. September 2006 an der Universität Stuttgart, Campus Stuttgart-Vaihingen, 2006, ISBN 3-933761-53-0

151 Niessner, Jennifer: *Multi-Scale Modeling of Multi-Phase - Multi-Component Processes in Heterogeneous Porous Media*, 2006, ISBN 3-933761-54-9

152 Fischer, Markus: *Beanspruchung eingeerdeter Rohrleitungen infolge Austrocknung bindiger Böden,* 2006, ISBN 3-933761-55-7

153 Schneck, Alexander: *Optimierung der Grundwasserbewirtschaftung unter Berücksichtigung der Belange der Wasserversorgung, der Landwirtschaft und des Naturschutzes*, 2006, ISBN 3-933761-56-5

154 Das, Tapash: *The Impact of Spatial Variability of Precipitation on the Predictive Uncertainty of Hydrological Models,* 2006, ISBN 3-933761-57-3

155 Bielinski, Andreas: *Numerical Simulation of CO_2 sequestration in geological formations*, 2007, ISBN 3-933761-58-1

156 Mödinger, Jens: *Entwicklung eines Bewertungs- und Entscheidungsunterstützungssystems für eine nachhaltige regionale Grundwasserbewirtschaftung*, 2006, ISBN 3-933761-60-3

157 Manthey, Sabine: *Two-phase flow processes with dynamic effects in porous media - parameter estimation and simulation,* 2007, ISBN 3-933761-61-1

158 Pozos Estrada, Oscar: *Investigation on the Effects of Entrained Air in Pipelines,* 2007, ISBN 3-933761-62-X

159 Ochs, Steffen Oliver: *Steam injection into saturated porous media – process analysis including experimental and numerical investigations*, 2007, ISBN 3-933761-63-8

160 Marx, Andreas: *Einsatz gekoppelter Modelle und Wetterradar zur Abschätzung von Niederschlagsintensitäten und zur Abflussvorhersage, 2007,* ISBN 3-933761-64-6

161 Hartmann, Gabriele Maria: *Investigation of Evapotranspiration Concepts in Hydrological Modelling for Climate Change Impact Assessment*, 2007, ISBN 3-933761-65-4

162 Kebede Gurmessa, Tesfaye: *Numerical Investigation on Flow and Transport Characteristics to Improve Long-Term Simulation of Reservoir Sedimentation*, 2007, ISBN 3-933761-66-2

163 Trifković, Aleksandar: *Multi-objective and Risk-based Modelling Methodology for Planning, Design and Operation of Water Supply Systems*, 2007, ISBN 3-933761-67-0

164 Götzinger, Jens: *Distributed Conceptual Hydrological Modelling - Simulation of Climate, Land Use Change Impact and Uncertainty Analysis*, 2007, ISBN 3-933761-68-9

165 Hrsg.: Braun, Jürgen; Koschitzky, Hans-Peter; Stuhrmann, Matthias: *VEGAS – Kolloquium 2007,* Tagungsband zur Veranstaltung am 26. September 2007 an der Universität Stuttgart, Campus Stuttgart-Vaihingen, 2007, ISBN 3-933761-69-7

166 Freeman, Beau: *Modernization Criteria Assessment for Water Resources Planning; Klamath Irrigation Project, U.S.*, 2008, ISBN 3-933761-70-0

167 Dreher, Thomas: *Selektive Sedimentation von Feinstschwebstoffen in Wechselwirkung mit wandnahen turbulenten Strömungsbedingungen*, 2008, ISBN 3-933761-71-9

168 Yang, Wei: *Discrete-Continuous Downscaling Model for Generating Daily Precipitation Time Series*, 2008, ISBN 3-933761-72-7

169 Kopecki, Ianina: *Calculational Approach to FST-Hemispheres for Multiparametrical Benthos Habitat Modelling,* 2008*,* ISBN 3-933761-73-5

170 Brommundt, Jürgen: *Stochastische Generierung räumlich zusammenhängender Niederschlagszeitreihen*, 2008, ISBN 3-933761-74-3

171 Papafotiou, *Alexandros: Numerical Investigations of the Role of Hysteresis in Heterogeneous Two-Phase Flow Systems*, 2008, ISBN 3-933761-75-1

172 He, Yi: *Application of a Non-Parametric Classification Scheme to Catchment Hydrology*, 2008, ISBN 978-3-933761-76-7

173 Wagner, Sven: *Water Balance in a Poorly Gauged Basin in West Africa Using Atmospheric Modelling and Remote Sensing Information*, 2008, ISBN 978-3-933761-77-4

174 Hrsg.: Braun, Jürgen; Koschitzky, Hans-Peter; Stuhrmann, Matthias; Schrenk, Volker: *VEGAS-Kolloquium 2008 Ressource Fläche III*, Tagungsband zur Veranstaltung am 01. Oktober 2008 an der Universität Stuttgart, Campus Stuttgart-Vaihingen, 2008, ISBN 978-3-933761-78-1

175 Patil, Sachin: *Regionalization of an Event Based Nash Cascade Model for Flood Predictions in Ungauged Basins*, 2008, ISBN 978-3-933761-79-8

176 Assteerawatt, Anongnart: *Flow and Transport Modelling of Fractured Aquifers based on a Geostatistical Approach,* 2008, ISBN 978-3-933761-80-4

177 Karnahl, Joachim Alexander: *2D numerische Modellierung von multifraktionalem Schwebstoff- und Schadstofftransport in Flüssen*, 2008, ISBN 978-3-933761-81-1

178 Hiester, Uwe: *Technologieentwicklung zur In-situ-Sanierung der ungesättigten Bodenzone mit festen Wärmequellen,* 2009, ISBN 978-3-933761-82-8

179 Laux, Patrick: *Statistical Modeling of Precipitation for Agricultural Planning in the Volta Basin of West Africa,* 2009, ISBN 978-3-933761-83-5

180 Ehsan, Saqib: *Evaluation of Life Safety Risks Related to Severe Flooding,* 2009, ISBN 978-3-933761-84-2

181 Prohaska, Sandra: *Development and Application of a 1D Multi-Strip Fine Sediment Transport Model for Regulated Rivers,* 2009, ISBN 978-3-933761-85-9

182 Kopp, Andreas: *Evaluation of CO_2 Injection Processes in Geological Formations for Site Screening,* 2009, ISBN 978-3-933761-86-6

183 Ebigbo, Anozie: *Modelling of biofilm growth and its influence on CO_2 and water (two-phase) flow in porous media,* 2009, ISBN 978-3-933761-87-3

184 Freiboth, Sandra: *A phenomenological model for the numerical simulation of multiphase multicomponent processes considering structural alterations of porous media*, 2009, ISBN 978-3-933761-88-0

185 Zöllner, Frank: *Implementierung und Anwendung netzfreier Methoden im Konstruktiven Wasserbau und in der Hydromechanik*, 2009, ISBN 978-3-933761-89-7

186 Vasin, Milos: *Influence of the soil structure and property contrast on flow and transport in the unsaturated zone*, 2010, ISBN 978-3-933761-90-3

187 Li, Jing: *Application of Copulas as a New Geostatistical Tool*, 2010, ISBN 978-3-933761-91-0

188 AghaKouchak, Amir: *Simulation of Remotely Sensed Rainfall Fields Using Copulas*, 2010, ISBN 978-3-933761-92-7

189 Thapa, Pawan Kumar: *Physically-based spatially distributed rainfall runoff modelling for soil erosion estimation*, 2010, ISBN 978-3-933761-93-4

190 Wurms, Sven: *Numerische Modellierung der Sedimentationsprozesse in Retentionsanlagen zur Steuerung von Stoffströmen bei extremen Hochwasserabflussereignissen*, 2011, ISBN 978-3-933761-94-1

191 Merkel, Uwe: *Unsicherheitsanalyse hydraulischer Einwirkungen auf Hochwasserschutzdeiche und Steigerung der Leistungsfähigkeit durch adaptive Strömungsmodellierung*, 2011, ISBN 978-3-933761-95-8

192 Fritz, Jochen: *A Decoupled Model for Compositional Non-Isothermal Multiphase Flow in Porous Media and Multiphysics Approaches for Two-Phase Flow*, 2010, ISBN 978-3-933761-96-5

193 Weber, Karolin (Hrsg.): *12. Treffen junger WissenschaftlerInnen an Wasserbauinstituten*, 2010, ISBN 978-3-933761-97-2

194 Bliefernicht, Jan-Geert: *Probability Forecasts of Daily Areal Precipitation for Small River Basins,* 2011, ISBN 978-3-933761-98-9

195 Hrsg.: Koschitzky, Hans-Peter; Braun, Jürgen: *VEGAS-Kolloquium 2010 In-situ-Sanierung - Stand und Entwicklung Nano und ISCO -,* Tagungsband zur Veranstaltung am 07. Oktober 2010 an der Universität Stuttgart, Campus Stuttgart-Vaihingen*,* 2010*,* ISBN 978-3-933761-99-6

196 Gafurov, Abror: *Water Balance Modeling Using Remote Sensing Information - Focus on Central Asia,* 2010, ISBN 978-3-942036-00-9

197 Mackenberg, Sylvia: *Die Quellstärke in der Sickerwasserprognose: Möglichkeiten und Grenzen von Labor- und Freilanduntersuchungen,* 2010, ISBN 978-3-942036-01-6

198 Singh, Shailesh Kumar: *Robust Parameter Estimation in Gauged and Ungauged Basins,* 2010, ISBN 978-3-942036-02-3

199 Doğan, Mehmet Onur: *Coupling of porous media flow with pipe flow,* 2011, ISBN 978-3-942036-03-0

200 Liu, Min: *Study of Topographic Effects on Hydrological Patterns and the Implication on Hydrological Modeling and Data Interpolation,* 2011, ISBN 978-3-942036-04-7

201 Geleta, Habtamu Itefa: *Watershed Sediment Yield Modeling for Data Scarce Areas,* 2011, ISBN 978-3-942036-05-4

202 Franke, Jörg: *Einfluss der Überwachung auf die Versagenswahrscheinlichkeit von Staustufen,* 2011, ISBN 978-3-942036-06-1

203 Bakimchandra, Oinam: *Integrated Fuzzy-GIS approach for assessing regional soil erosion risks,* 2011, ISBN 978-3-942036-07-8

204 Alam, Muhammad Mahboob: *Statistical Downscaling of Extremes of Precipitation in Mesoscale Catchments from Different RCMs and Their Effects on Local Hydrology,* 2011, ISBN 978-3-942036-08-5

205 Hrsg.: Koschitzky, Hans-Peter; Braun, Jürgen: *VEGAS-Kolloquium 2011 Flache Geothermie - Perspektiven und Risiken,* Tagungsband zur Veranstaltung am 06. Oktober 2011 an der Universität Stuttgart, Campus Stuttgart-Vaihingen, 2011, ISBN 978-3-933761-09-2

206 Haslauer, Claus: *Analysis of Real-World Spatial Dependence of Subsurface Hydraulic Properties Using Copulas with a Focus on Solute Transport Behaviour,* 2011, ISBN 978-3-942036-10-8

207 Dung, Nguyen Viet: *Multi-objective automatic calibration of hydrodynamic models – development of the concept and an application in the Mekong Delta,* 2011, ISBN 978-3-942036-11-5

208 Hung, Nguyen Nghia: *Sediment dynamics in the floodplain of the Mekong Delta, Vietnam,* 2011, ISBN 978-3-942036-12-2

209 Kuhlmann, Anna: *Influence of soil structure and root water uptake on flow in the unsaturated zone,* 2012, ISBN 978-3-942036-13-9

210 Tuhtan, Jeffrey Andrew: *Including the Second Law Inequality in Aquatic Ecodynamics: A Modeling Approach for Alpine Rivers Impacted by Hydropeaking,* 2012, ISBN 978-3-942036-14-6

211 Tolossa, Habtamu: *Sediment Transport Computation Using a Data-Driven Adaptive Neuro-Fuzzy Modelling Approach,* 2012, ISBN 978-3-942036-15-3

212 Tatomir, Alexandru-Bodgan: *From Discrete to Continuum Concepts of Flow in Fractured Porous Media,* 2012, ISBN 978-3-942036-16-0

213 Erbertseder, Karin: *A Multi-Scale Model for Describing Cancer-Therapeutic Transport in the Human Lung,* 2012, ISBN 978-3-942036-17-7

214 Noack, Markus: *Modelling Approach for Interstitial Sediment Dynamics and Reproduction of Gravel Spawning Fish,* 2012, ISBN 978-3-942036-18-4

215 De Boer, Cjestmir Volkert: *Transport of Nano Sized Zero Valent Iron Colloids during Injection into the Subsurface*, 2012, ISBN 978-3-942036-19-1

216 Pfaff, Thomas: *Processing and Analysis of Weather Radar Data for Use in Hydrology*, 2013, ISBN 978-3-942036-20-7

217 Lebrenz, Hans-Henning: *Addressing the Input Uncertainty for Hydrological Modeling by a New Geostatistical Method*, 2013, ISBN 978-3-942036-21-4

218 Darcis, Melanie Yvonne: *Coupling Models of Different Complexity for the Simulation of CO_2 Storage in Deep Saline Aquifers*, 2013, ISBN 978-3-942036-22-1

219 Beck, Ferdinand: *Generation of Spatially Correlated Synthetic Rainfall Time Series in High Temporal Resolution - A Data Driven Approach*, 2013, ISBN 978-3-942036-23-8

220 Guthke, Philipp: *Non-multi-Gaussian spatial structures: Process-driven natural genesis, manifestation, modeling approaches, and influences on dependent processes*, 2013, ISBN 978-3-942036-24-5

221 Walter, Lena: *Uncertainty studies and risk assessment for CO_2 storage in geological formations*, 2013, ISBN 978-3-942036-25-2

222 Wolff, Markus: *Multi-scale modeling of two-phase flow in porous media including capillary pressure effects,* 2013, ISBN 978-3-942036-26-9

223 Mosthaf, Klaus Roland: *Modeling and analysis of coupled porous-medium and free flow with application to evaporation processes,* 2014, ISBN 978-3-942036-27-6

224 Leube, Philipp Christoph: *Methods for Physically-Based Model Reduction in Time: Analysis, Comparison of Methods and Application*, 2013, ISBN 978-3-942036-28-3

225 Rodríguez Fernández, Jhan Ignacio: *High Order Interactions among environmental variables: Diagnostics and initial steps towards modeling*, 2013, ISBN 978-3-942036-29-0

226 Eder, Maria Magdalena: *Climate Sensitivity of a Large Lake*, 2013, ISBN 978-3-942036-30-6

227 Greiner, Philipp: *Alkoholinjektion zur In-situ-Sanierung von CKW Schadensherden in Grundwasserleitern: Charakterisierung der relevanten Prozesse auf unterschiedlichen Skalen*, 2014, ISBN 978-3-942036-31-3

228 Lauser, Andreas: *Theory and Numerical Applications of Compositional Multi-Phase Flow in Porous Media*, 2014, ISBN 978-3-942036-32-0

Die Mitteilungshefte ab der Nr. 134 (Jg. 2005) stehen als pdf-Datei über die Homepage des Instituts: www.iws.uni-stuttgart.de zur Verfügung.